# ICE COLLISION EXPERIMENTS WITH A PENDULUM IMPACT APPARATUS

GEOFF CLARKE

# Ice Collision Experiments with a Pendulum Impact Apparatus

by

© Geoff Clarke

A Thesis submitted to the School of Graduate Studies

in partial fulfillment of the requirements for the degree of

Masters of Engineering

**Faculty of Engineering and Applied Science**

Memorial University of Newfoundland

**December 2012**

St. John's Newfoundland Canada

# ABSTRACT

This thesis examines the interaction of ice and structures under simplified dynamic impact conditions, where the compliance of the structure and geometry of the ice was varied. Laboratory ice and iceberg ice conical specimens were impacted with a simply supported steel plate in a pendulum impact apparatus. The geometry of the ice cone was varied from 20 to 40 degrees and the thickness of the steel plate was varied from 0.25" to 0.75". Initial potential energy remained constant for each experiment. Forces, nominal pressures and specific energies were analyzed using response surface methodology. The compliance of the plate and cone angle of the ice specimen showed significant influence on the peak forces and nominal pressures. However, the specific energy was found to be only dependent on the compliance of the plate. Four iceberg specimens were also tested and significantly lower peak forces, nominal pressures, and specific energy was observed in the iceberg samples.

# ACKNOWLEDGEMENTS

This research could not be possible without the support and guidance of the STePS$^2$ research team. I owe particular thanks to Dr. Bruce Colbourne my graduate supervisor and Dr. Claude Daley my graduate co-supervisor for their guidance and financial support provided.

I would like to Mr. Matt Curtis for assistance with the experimental setup in the structures lab. Also special thanks to the work term students which include Mr. Edward Moakler, Mr. Goubin Zhuang, and Mr. Mathew Davison. I couldn't have completed the experiments without their help.

I would also like to thank Dr. Steve Bruneau, Dr. Shah Alam, Dr. Suresh Reddy, Dr. John Wang, and Dr. Bob Gagnon, members of STePS$^2$ who all offered assistance during my two years of graduate studies at Memorial university. Furthermore, Dr. Leonard Lye for guidance using Design of Experiments Methodology. Also I would like to mention John Dolny, a fellow graduate student during my research.

Finally, I would like to thank all of my family for their encouragement and support. Including my mother Jayne Clarke and father Glenn Clarke for all the support they have provided, I dedicate this thesis to you.

# Table of Contents

# List of Tables

# List of Figures

## List of Symbols, Nomenclature or Abbreviations

| | |
|---|---|
| $STePS^2$ | Sustainable Technology for Polar Ships and Structures |
| RSM | Response Surface Methodology |
| DOE | Design of Experiments Methodology |
| CCD | Central Composite Design |
| FIR | Finite Impulse Response |
| FFT | Fast Fourier Transform |
| LPF | Low Pass Filter |
| ANOVA | Analysis of Variance |
| SS | Sum of Squares |
| $SS_A$ | Sum of squares of factor A |
| $SS_B$ | Sum of squares of factor B |
| $SS_T$ | Sum of squares total |
| $SS_{Subtotal}$ | Sum of squares sub-total |
| DOF | Degree of Freedom |
| MS | Mean of Squares |
| $MS_A$ | Mean of Squares of factor A |
| $MS_E$ | Mean of Squares of Error |
| | |
| $\alpha$ | Angle of ice specimen referenced from the base |
| | Distance to axle design point in response surface methodology |
| | Significance level used in ANOVA to reject the null hypothesis |

| | |
|---|---|
| $K$ | Number of factors in factorial design |
| $r$ | Radius of ice specimen base |
| $h_i$ | Height of ice specimen measured from base to tip of cone |
| $x_i$ | Initial ice specimen height |
| $x_f$ | Finial ice specimen height |
| $D_i$ | Displacement from center of rotation to tip of ice specimen |
| $\theta_i$ | Angle of pendulum arms attached to ice specimen referenced from horizontal |
| $D_g$ | Displacement from center of rotation to surface of impact plate (impact face) |
| $D_p$ | Displacement of plate |
| $\theta_g$ | Angle of pendulum arms attached to impact plate referenced from horizontal |
| $x$ | Ice crushing displacement starting at tip of ice specimen |
| $x_{max}$ | Maximum ice crushing displacement |
| $f(x)$ | Filtered force as a function of ice crushing displacement |
| $A(x)$ | Nominal contact area as a function of ice crushing displacement |
| $P$ | Nominal pressure |
| $C$ | Nominal pressure at 1 $m^2$ of ice of process area curve |
| $e$ | Pressure exponent of process area curve |
| $R^2$ | Correlation coefficient |

| | |
|---|---|
| $E_p$ | Energy of plate consisting of both recoverable (elastic) and plastic (non-recoverable) |
| $E_c$ | Crushing energy of ice |
| $E_s$ | Specific energy absorbed |
| P | Density of ice (900 kg/m$^3$) |
| A | Factor A, impact plate thickness |
| B | Factor B, specimen cone angle |
| AB | Interaction between factor A and factor B |
| $A^2$ | Curvature of factor A |
| $B^2$ | Curvature of factor B |
| $\epsilon$ | Experimental error |
| $x_1, x_{2\ldots} x_j$ | Factors 1 and 2 of experiment |
| y | Measured response of experiment |
| $\eta$ | Response surface of experiment |
| $\beta_o, \beta_{1\ldots} \beta_j$ | Regression coefficients |
| n | Number of experimental replications |

# List of Appendices

# 1 INTRODUCTION

Limited oil resources elsewhere in the world and new technological advances are making the Arctic an attractive location for oil exploration. The United States Geological Survey estimates that 30 percent of the world's undiscovered gas and 13 percent of undiscovered oil maybe found offshore in water depths of less than 500 m in the Arctic (Gautier 2009). Also the possibility of opening up a northwest passage from the Atlantic to Pacific may increase Arctic shipping traffic.

Dynamic ice-structure interaction is an important consideration for the safety of offshore structures and ships. People, and the environment, can be at risk if ice loads experienced by a ship or offshore structure exceed the designed capacity. Current design rules are limited in their estimations of the ice loading effects in dynamic ice-structure interactions (Kärnä 1999). Relatively little research has been completed to investigate dynamic ice-structure interaction.

Dynamic ice interactions are important in the design of both Polar Class Ships and Arctic offshore structures. Dynamic loads are generated when drifting ice impacts against offshore structures or when ships collide with drifting ice. Long slender structures exhibit dynamic behavior from such impacts. In these cases, the stiffness, mass and damping effects are apparent in the ice interaction phenomena. Such analysis requires that the time dependent loading be known. Problems arise when solving dynamic ice loads since there is inadequate knowledge of the dynamic ice forces (Cammaert & Muggeridge, 1988).

Sustainable Technology for Polar Ships and Structures (STePS$^2$) is research project at Memorial University which is aimed at studying ice-structure interactions using experiments and numerical models. Dynamic ice and structure interaction on deformable structural grillages is one of the topics of the research. A dynamic impact apparatus consisting of two-pendulums has been developed for investigating this topic. This apparatus includes a frame with dimensions of 1 m x 1 m x 1 m with a pendulum arm length of 0.5 m and is shown in Figure 1-1.

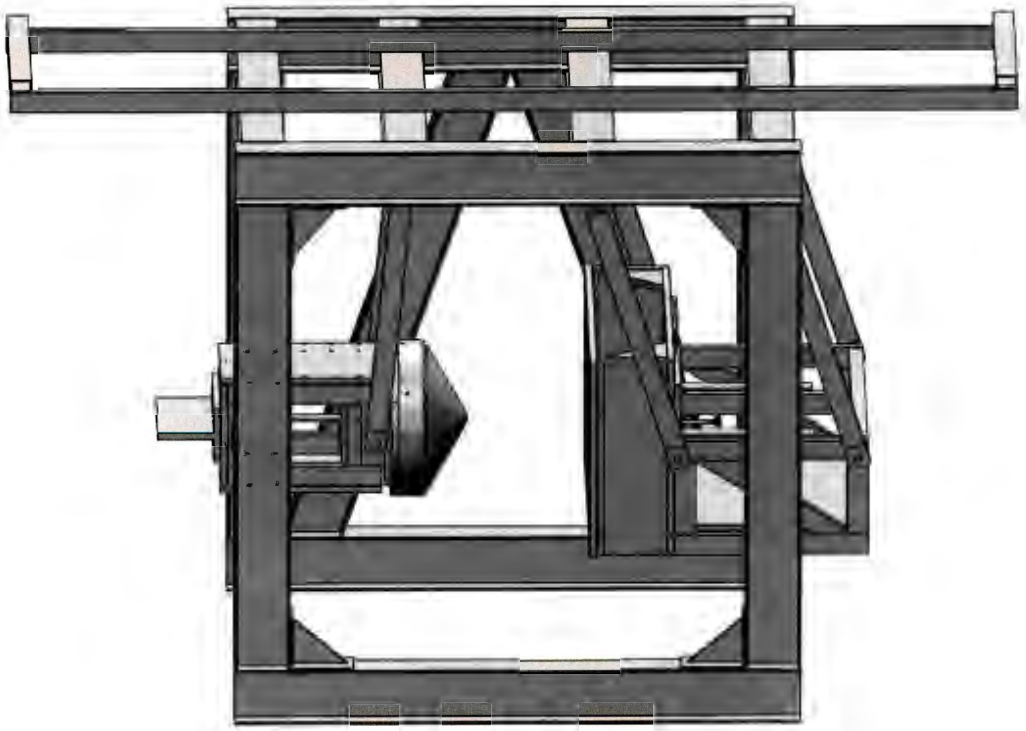

**Figure 1-1: Small pendulum impact apparatus**

The two-pendulum apparatus consists of a single simply supported plate (left) and a 0.25 m diameter ice cone specimen (right), each side containing a mass of approximately 101 kg.

## 1.1 Scope and Objectives

The goal of this thesis is to investigate the dynamic interaction between a steel plate and an ice specimen. The dynamic ice impact scenario consists of a simply supported steel plate and a conical ice specimen. This simplified geometry is intended to provide insight into the important parameters of ice-structure interactions where the ice and structure are deforming. The compliance of the impact plate and angle of ice specimens is varied to investigate the ice to structure interaction. The stiffness of the ice specimen can effectively be varied by cone angle. A stiffer ice specimen has a lower cone angle (blunter) which implies more ice crushing volume for equal ice crushing displacement.

The Design of Experiments Methodology (DOE) is used as a tool for planning test programs and analyzing the results and supporting the conclusions from the impact experiments. Response Surface Methodology (RSM) is applied to predict the ice-structure interaction experimental results.

The following items were analyzed with DOE from the experimental results to study structure and ice interaction effects:

- Peak forces
- Nominal pressure at 1 $m^2$ from process pressure area curves
- Specific energy

The deviation of each of these quantities is discussed in later sections.

## 1.2 Literature Review

One of the earliest ice impact experiments that concluded that ice pulverized from impacts was completed in Russia by Khesin and Kurdymov (1976). A steel ball was dropped onto an ice plate where accelerations were measured to predict force. A model was generated from these tests to predict ice loads, but it presumed the ice pulverized at a uniform thickness with uniform pressures.

Ice impact tests were later conducted during ship-ice rams. The Canadian Coast Guard ice breaker Louis S. St-Laurent (1977) and the Canmar Kigoriak ice breaker (1980) were outfitted with hull pressure sensors and impacted with ice floes. The results from these tests indicated localized high pressure zones that disagreed with the Khesin-Kurdymov model. Also the Kigoriak tests indicated that the ice loading was dependent on velocity (Ghoneim Keinonen 1983). In another study, a 9 $m^2$ load panel comprised of strain gages was outfitted on the USCGC Polar Sea vessel (1987). The data was processed and the pressure area effects are presented in the following form (Sanderson 1988):

$$P = CA^{-0.5} \qquad [1\text{-}1]$$

Where the C value is around 8 Mpa,

P is the nominal pressure

Many ice impact tests have been completed by means of dropped projectiles on top of ice sheets. Jordaan and Mckenna (1988) provide a literature review of the tests completed in

the 1960's to 1980's. Specific energy, the ratio of kinetic energy to the volume of damaged material was used by many of the researchers as a fundamental index for measuring the resistance of the ice to impact. Table 1-1 below, from Jordaan and Mckenna (1988), summarizes the results from impact tests on ice in terms of specific energy. This shows that the damaged volume used to calculate specific energy is dependent on the geometry of the projectile. Also it was found that temperature, whether the ice was fixed or floating and the energy dissipated from friction were significant factors in determining the specific energy from ice pulverization. Many of the experimenters only measured penetration depth. Penetration depths are often only valid for the specific experimental indenter geometry and ice conditions (Jordaan and Mckenna, 1988).

**Table 1-1: Ice Impact experiments specific energy (Jordaan and Mckenna 1988)**

| Author | Ice Conditions | Test | Impact Energy | Specific Energy ($MJ/m^3$) |
|---|---|---|---|---|
| Itagaki and Sabourin (1980) | Freshwater -32 to -2 °C | Standard charpy | 0.035-0.5 | 0.006-0.1 |
| Kheisin and Likhamanov (1973) | Floating fresh water 30 °C | Dropped ball | 1-2400 | 3-13 |
| Garcia et al. (1983) | Freshwater -5°C | Dropped weight projectile | 1-800 | 1-20 |
| Kawakami et al. (1983) | Freshwater -8°C | Projectile | 2-2000<br>20-500 | 3-20<br>0.045 |
| Ross (1967) | Floating fresh and sea water | Dropped weight | 7-20 | 0.01-0.4 |

| Author | Ice Conditions | Test | Impact Energy | Specific Energy ($MJ/m^3$) |
|---|---|---|---|---|
| Comfort and Menon (1981) | Sea ice -25 to 0 °C | Dropped weight pendulum | 2000-15000 | 1-3 |
| Timco and Martin (1979) | Floating river ice | Dropped weight | 2-15 | 1-5 |
| El-Tahan et al. (1984) | Freshwater | Dropped weight | 120 | 1 |
| Gerard (1970) | Freshwater -10 to -1 °C | Projectile | 250-900 | Penetration only |
| Yen et al (1970) | Freshwater -10 to -1 °C | Dropped ball | 0.0025-2.5 | Coefficients of restitution |
| Ross (1969) | Floating sea ice -15 to 0 °C | Dropped weight projectile | 200-8000 | Perforation depth |
| Brooks (1975) | Freshwater | Projectile | 200-4000 | Penetration depth |
| Mcintosh et al. (1973) | Floating sea ice -20 to -5 °C | Dropped projectile | $0.05*10^6$ to $25*10^6$ | Penetration depth |
| Young (1973) | Floating sea ice | Dropped projectile | $0.05*10^6$ to $15*10^6$ | Penetration depth |
| Rychnovsky (1987) | Floating sea ice | Dropped projectile | $0.2*10^6$ to $1.5*10^6$ | Penetration depth |

Measurement of forces and accelerations were also used for impact experiments. These measurements were preferred over specific energy for engineering applications and for explaining the ice impact phenomena. Some of the early measurements of ice impacts with accelerometers were Ross (1967), Rychnovsky (1987), Likhomanov and Kheisin (1971), Mcintosh et al. (1973), and Comfort and Menon (1981). In the summary paper

decelerations of the projectiles were shown to be dependent on the confinement of the ice sample and the stiffness of the supports (Jordaan and Mckenna, 1988).

Glen and Comfort (1983) used a pendulum impact apparatus that consisted of a steel plate attached to a 2 m pendulum arm that impacts with a stationary grown ice sample. The ice sample was a wedge shape with an apex angle of 153 degrees. The pendulum masses were 650 kg and 1160 kg. Local pressures were measured with 25 custom built strain gauged diaphragm pressure transducers, forces were calculated from strain gauge and accelerometer measurements on the plate and the kinetic energy was calculated from impact speed which was measured with a rotary potentiometer connected to the pendulum arm. The ice thickness, salinity and temperature were varied in the experiments. Glen and Comfort (1983) observed that the mean and maximum pressure was inversely proportional to contact area. Also pressure ranged from 2 Mpa (areas of 800 - 1000$cm^2$ ) to 20 Mpa (area of 200 $cm^2$). Glen and Comfort (1983) reported problems with the strain gauge force and acceleration transducers. They noted errors up to 100 % from discrepancies between integrated pressure over contact area and measured force.

A more recent impact experiment was conducted by Timco and Frederking (1993), where an accelerometer and pressure transducer mounted on a projectile and dropped on fresh water ice. The projectile shape (spherical, flat and wedge) and the thickness of the ice were varied. The maximum force ($F_m$) was found to be related to the average loading rate ($\dot{F}_m$) by

$$F_m = 0.9\,\dot{F}_m^{\,0.4} \qquad [1\text{-}2]$$

Gagnon (1996) conducted similar drop tests on an iceberg. Impact velocity (1.8 to 3.9 m/s) temperature (-0.5 to -13.5 °C) and mass (155 – 510 kg) were varied. Specific energy, peak force and nominal pressure were analyzed. Gagnon (1996) observed that there was no correlation between peak pressure and projectile mass or velocity. Specific energy was observed to decrease with increased impact energy and crater volume. Also the peak pressures were found to be independent of the impact energy and velocity, which agrees with the results observed by Timco and Frederking (1993).

Recently, Gagnon (2008) has developed a 1m x 1m x 0.46 m acrylic block impact panel for measuring impact loads and pressure distribution. The sensor uses optical-mechanical technology to measure the pressures and a high speed camera is used to capture the data. Preliminary drop tests have been completed with the impact panel (Gagnon 2009) to show the sensor is capable of measuring rapid changing pressures from impact loads. Plans are currently in place to use the pressure panel in the large pendulum impact apparatus as part of STePS$^2$.

The pendulum impact experiments presented in this thesis are similar to those of Glen and Comfort (1983). However, the current work consists of two pendulums which allow both objects to rebound, similar to the scenario of a ship to iceberg collision. Also the thickness of the impact plate is varied to change the effective compliance of the structure. This scenario has not been previously investigated, although other authors have noted the effects of changing the compliance of the indenter due to the boundary conditions. The

current experiments will expand the knowledge of ice impacts by investigating the relationship between compliance of the structure / ice and loads.

# 2 EXPERIMENTAL DESIGN

The following sections detail the design of the experiment. The goal of the experimental design was to use a robust statistical approach to determine the ice – structure interaction as a function of the response parameters. Response Surface Methodology (RSM) has been implemented for setting up the experimental design. This method is more efficient than using a one factor at a time approach, where only one factor is varied and the others are held constant (Czitrom, 2009). The statistical design approach requires less resources, effects of factors are more precise, and interaction between factors can be estimated.

## 2.1 Experiment Factors and Levels

Ice specimen cone angle and plate thickness of the impact plate have been varied with three levels for the laboratory ice impact experiments. Altering the cone angle ($\alpha$) of the ice specimen changes the effective ice crushing "stiffness" and implementing plates of various different thicknesses will change the structural stiffness. The levels of the experiments cannot cover too large an area over the entire design space for RSM. The response surface must be fitted over a relatively small area to provide a reasonable representation. Table 2-1 presents the factors and levels of the pendulum impact experiment.

**Table 2-1: Experiment factors and levels**

| Factor | Name | Low Level (-1) | Middle Level (0) | High Level (+1) |
|---|---|---|---|---|
| A | Plate Thickness (inches) | 0.25 | 0.5 | 0.75 |
| B | Cone Angle (degrees) | 20 | 30 | 40 |

## 2.2 Responses

The sampling rate of 4.5 kHz was a limitation of the data acquisition system. This was shown to be adequate in preliminary tests. The following responses were sampled in the pendulum impact tests:

- Force
- Acceleration of Ice Holder
- Accelerations of Impact Plate
- Deflection of Plate
- Angle of one pendulum arm attached to ice specimen
- Angle of one pendulum arm attached to impact plate

## 2.3 Response Surface Design

A central composite design (CCD) was chosen to fit a second-order model. This is the most popular RSM design and was introduced by Box and Wilson (1951). The CCD contains $2^k$ design points, the same as a factorial experiment, where $k$ is the number of

factors. But the CCD also contains $2k$ axial points and center points that allow the second order terms to be estimated.

Figure 2-1 below shows the CCD points with two factors.

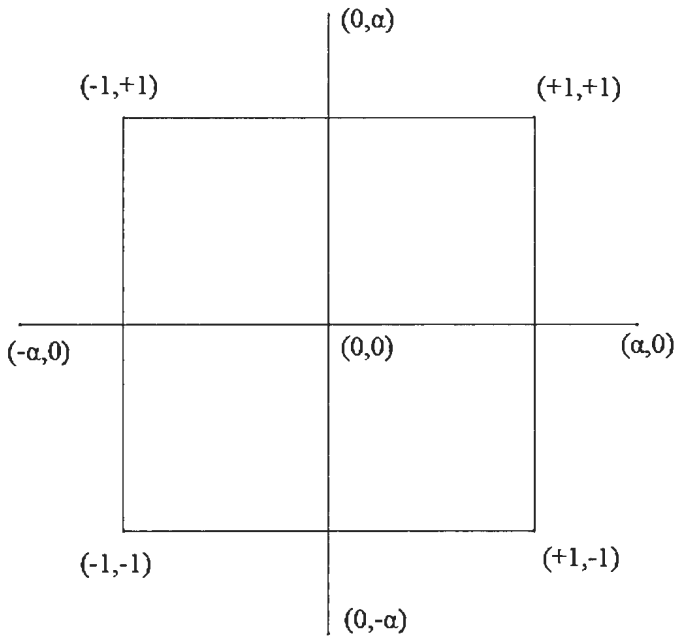


**Figure 2-1: Two factor (k=2) Central Composite Design (CCD)**

The axial points are $(0,\pm\alpha)$ and $(\pm\alpha,0)$ ,the center point is (0,0) and the factorial points are $(\pm1,1)$ and $(1,\pm1)$. The $\pm1$ values are the minimum and maximum levels of the factors. The value of alpha ($\alpha$) determines the distance to the axial design points. A common value for $\alpha$ is $\sqrt{2}$. This value maintains rotatability, which maintains constant variance among the predicted response due to the fact all points are equal distance from the center point.

The experimental design was chosen as a face centered CCD. A face centered CCD only requires a three level design opposed to a five level design for a rotatable design. A face centered design was more convenient since the steel impact plates could only be purchased at standard thickness to meet the three levels of the experiment. Table 2-2 below summarizes the CCD design.

**Table 2-2: CCD design parameters**

| Parameter | Value |
|---|---|
| Number Factors | 2 |
| Replication of Factorial Points | 2 |
| Replication of Axial Points | 2 |
| Center Points | 5 |

## 2.4 Experimental Test Plan

The experimental test plan for the impact experimentation of ice specimens grown in the lab is provided in Table 2-3. The test plan developed from the CCD consists of 21 experiment runs.

**Table 2-3: Experimental test plan**

| Run # | Factor A: Plate Thickness (inches) | Factor B: Cone Angle (degrees) |
|---|---|---|
| 1 | 0.75 | 20 |
| 2 | 0.25 | 30 |
| 3 | 0.75 | 30 |
| 4 | 0.75 | 30 |
| 5 | 0.25 | 40 |

| Run # | Factor A: Plate Thickness (inches) | Factor B: Cone Angle (degrees) |
|---|---|---|
| 6 | 0.5 | 30 |
| 7 | 0.5 | 40 |
| 8 | 0.25 | 20 |
| 9 | 0.25 | 20 |
| 10 | 0.5 | 40 |
| 11 | 0.75 | 40 |
| 12 | 0.25 | 30 |
| 13 | 0.5 | 20 |
| 14 | 0.25 | 40 |
| 15 | 0.5 | 20 |
| 16 | 0.5 | 30 |
| 17 | 0.75 | 20 |
| 18 | 0.5 | 30 |
| 19 | 0.5 | 30 |
| 20 | 0.75 | 40 |
| 21 | 0.5 | 30 |

# 3 EXPERIMENTAL APPARATUS

The following section describes the experimental apparatus. The frame was not developed specifically for this experiment. The frame was designed for small scale experiments and to provide a model of a larger 4 m x 4 m x 4 m device to be built and used as a part of STePS$^2$. The experimental impact apparatus consists of a small dynamic impact pendulum frame. The apparatus, shown in Figure 3-1, consists of two colliding pendulums. One side (left) contains a frame supporting an ice holder and ice cone specimen. The opposite side (right) contains a frame supporting a steel plate simply supported near the vertical edges. The frame was constructed out of aluminum and the overall dimensions are approximately 1 m x 1 m x 1 m.

**Figure 3-1: Dynamic impact pendulum apparatus**

Table 3.1 summarizes the pendulum properties,

**Table 3-1: Pendulum impact apparatus properties**

| Parameter | Value |
|---|---|
| Mass of Pendulums | 101 kg |
| Combined Theoretical Impact Speed | 4.4 m/s |
| Pendulum Arm Length | 0.5 m |
| Vertical Center of Gravity[1] | 0.5 m |
| Dimensions of Frame | 1x1x1 m |
| Pendulum Release Angle[2] | 60° |

[1] Measured vertically from center of rotation
[2] Measured from vertical resting position

The center of gravity of both pendulums was carefully balanced to place it at the center of the cone. This was to reduce any possible eccentricity which may complicate results. The center of gravity and arm length are both measured from the center of rotation at the top of the frame. The impact speed in Table 3.1 is the theoretical impact speed based on potential energy. Actual impact speeds will be slightly less due to frictional forces in bearings, air resistance, and slight distance changes that occur when changing the height of ice and thickness of the impact plates.

The pendulums were raised by electric winches to 60 degrees with respect to the resting position (vertical). Figure 3-2 shows the electric winch and pulleys used to pull the pendulum arms.

**Figure 3-2: Mechanical system to raise pendulum arms**

Electromagnets hold each side in position and were disengaged simultaneously to release the two pendulums and initiate the impact. Figure 3-3 shows the electromagnetic on the left and the automatic release rectifier controller on the right. The automatic release rectifier incorporates a provision for reverse current that insures instantaneous release even though the steel plate was magnetically retentive. It was important to reduce the delay between the releases of both pendulums.

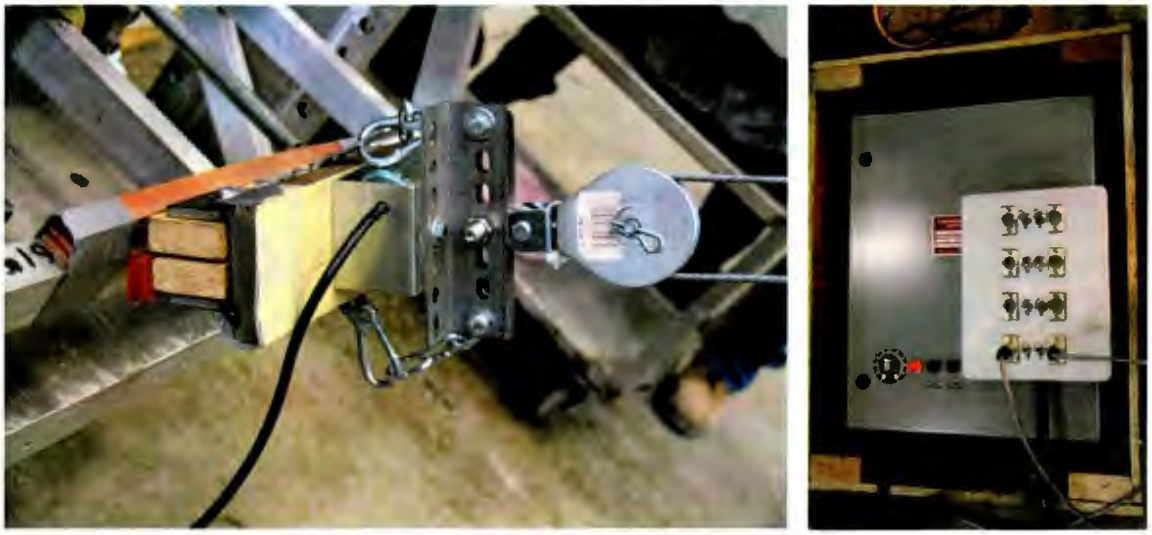

**Figure 3-3: Electromagnetic release system**

Ballast weights (steel plates) were added behind the ice holder and/or impact plate supports depending on the test conditions to ensure a potential energy balance before starting each experiment.

## 3.1 Sensors

Table 3-2 presents the sensors used in the pendulum impact tests.

**Table 3-2: Impact pendulum sensors summary**

| Sensor | Manufacture | Model Number |
|---|---|---|
| 10 000 lbs. Ring Type LIVM Force Sensor | Dytran | 1203V |
| 5000 g K-Shear Accelerometer | Kislter | 8704B5000 |
| 500 g K-Shear Accelerometer | Kistler | 8702B500 |
| PiezoSmart Power Supply Coupler | Kistler | 5134B |
| Analog Output Dura Coder | AMCI | DC25 |
| 100 mm Linear Potentiometer | Celesco | MLP-100 |

### 3.1.1 Force Sensors

Piezoelectric washer-style ring force sensors were chosen for measuring the forces. These sensors use quartz crystals as the sensing elements. When placed under a changing mechanical load they produce electrical charges. These sensors are unique compared with strain gauge based sensors, because they are very stiff and they only produce a charge when there is a change in load and this makes them suitable for dynamic measurements. The advantages of the piezoelectric sensors are:

- Compact compared to strain gauge based sensors
- A high overload capacity which is normally 50 percent
- Practically negligible displacements
- Very rigid and have a high natural frequency

Three piezoelectric force sensors were located behind the ice holder. The force sensors were placed at equal radial distance from center of the ice impact and 120 degrees apart. Figure 3-4 shows the configuration of the force sensors. A 0.5" aluminum plate with three bolts (left) is bolted on top of 1" steel plate (right). The loads cells are sandwiched and preloaded between the steel and aluminum plates. Since the force sensors were preloaded with a bolt, the sensitivity of the sensors differed from the original calibration. This is due to the influence of the bolt stiffness on the sensitivity of the sensors. The ratio of the stiffness of the bolt to the stiffness of the force sensor has to be taken into account. To maintain accuracy, the force sensors were recalibrated after the preloading.

The center stud (bottom) in Figure 3-4 extending out of the aluminum plate is for attaching the ice holder. This entire assembly was attached to the pendulum frame after the preloading process was completed.

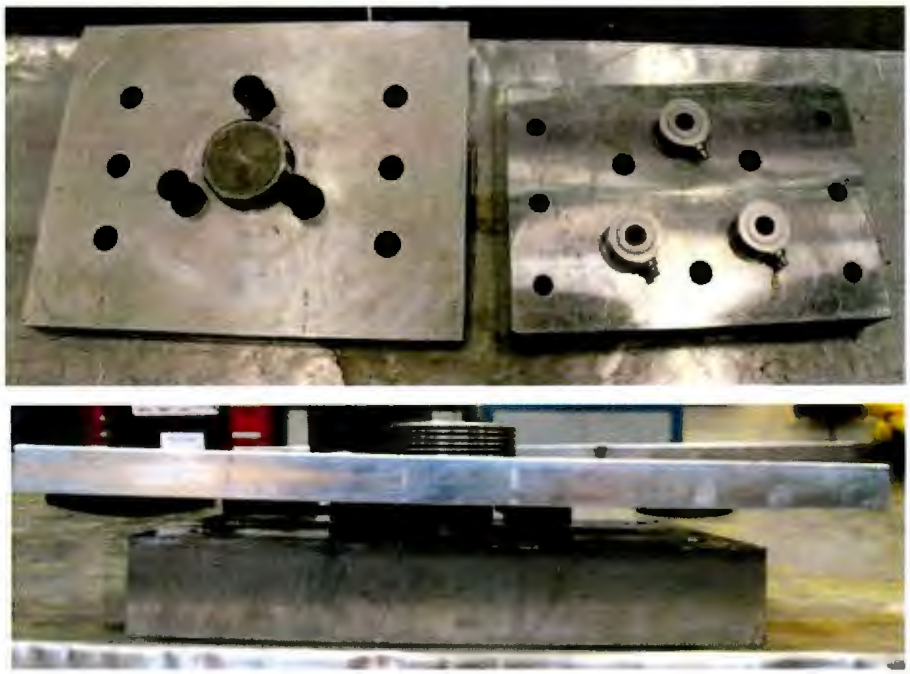

**Figure 3-4: Force sensor configuration**

### 3.1.2 Linear Potentiometer

The impact plate displacements are measured with a linear potentiometer. The linear potentiometer was screwed into tack welded bolts at the back of the impact plate. Figure 3-5 below shows the bolts attached to the back of the impact plate. This was an alternative to drilling a hole and tapping the plate, which could potentially alter the plate stiffness.

**Figure 3-5: Impact plate sensor arrangement**

The larger bolt (top) was placed at the geometric center of the plate. This was where an accelerometer was attached. The linear potentiometer was attached to the smaller bolt (bottom). There was approximately 2 cm offset between the bolts. Figure 3-6 displays the accelerometer and linear potentiometer attached to the back of the impact plate.

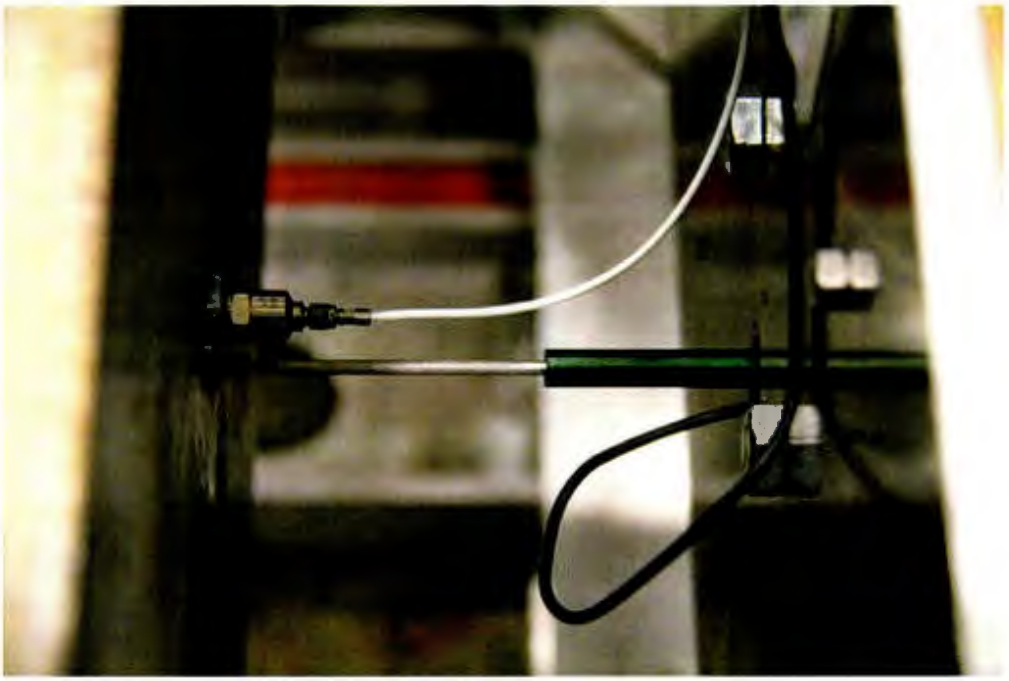

**Figure 3-6: Sensors attached to impact plate**

### 3.1.3 Accelerometers

A piezoelectric accelerometer was attached to the ice holder to measure accelerations of the boundary support of the ice specimen. Figure 3-7 displays the attachment of the accelerometer to the ice holder. The second piezoelectric accelerometer was attached to the back of the impact plate (Figure 3-6).

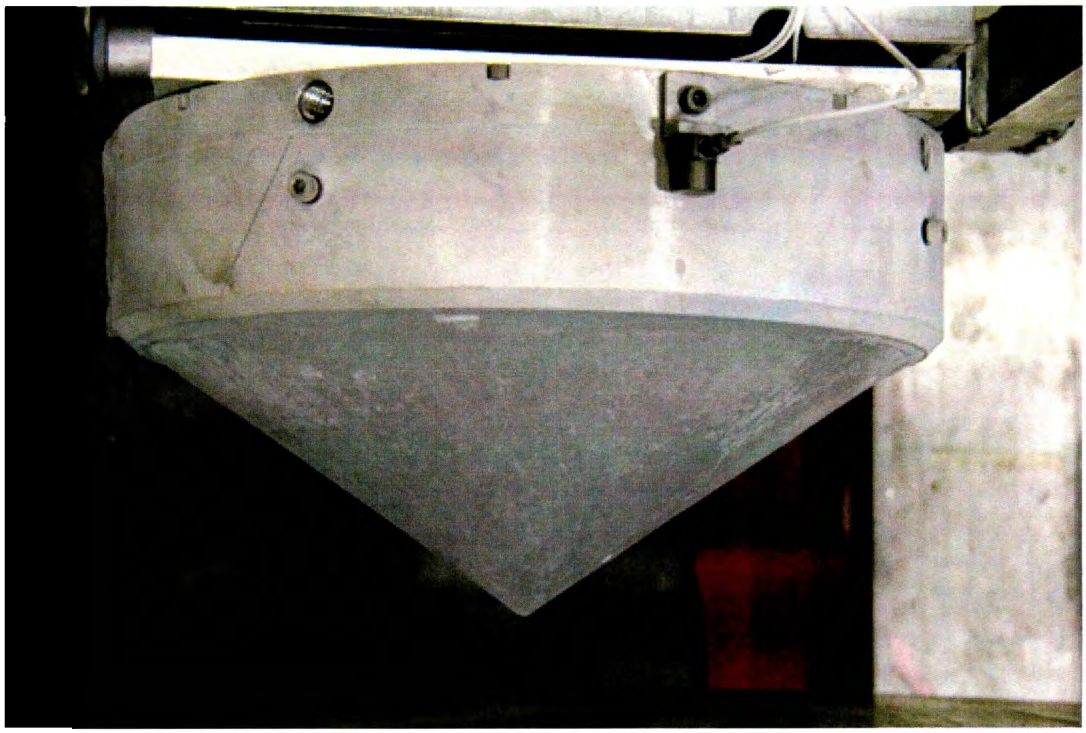

**Figure 3-7: Ice holder and accelerometer**

### 3.1.4 Rotary Encoder

Two digital rotary encoders with built-in analog converters were installed at the centers of rotation of the ice-pendulum arm and the plate-pendulum arm. The rotary encoders, shown in Figure 3-8, measure the relative angular position of the arms during the experiment. The rotary encoder data and linear potentiometer was used to derive the ice crushing displacements.

**Figure 3-8: Rotary encoder**

## 3.2 Boundary Conditions

Three quarter inch (¾") 44w grade steel plates were attached to the pendulum frame to impact with the ice specimen. The supports of the plate were rounded to provide a simply supported plate boundary condition. A slot was cut in the plate to allow free rotation at the fixed end without interference from the bolt. Figure 3-9 shows the impact plate setup attached to the pendulum frame and Figure 3-10 presents the dimensions of the impact plate. A new steel plate was attached to the pendulum after each experimental run if permanent plate deformations occurred. This was to eliminate potential strain hardening effects from a previous test.

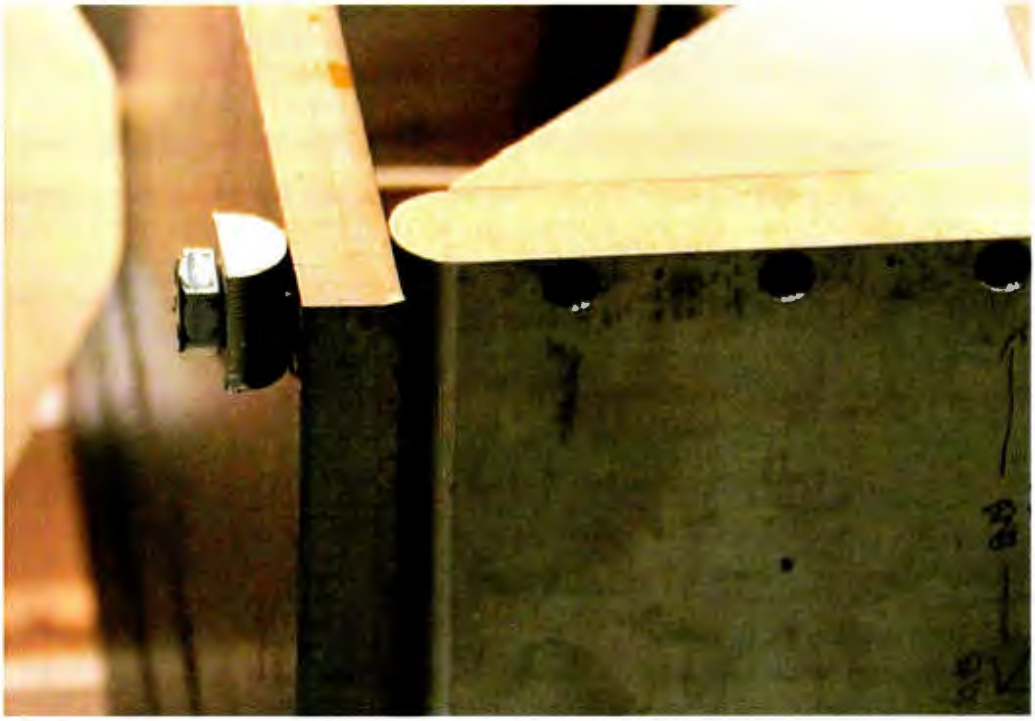

**Figure 3-9: Simple plate edge supports**

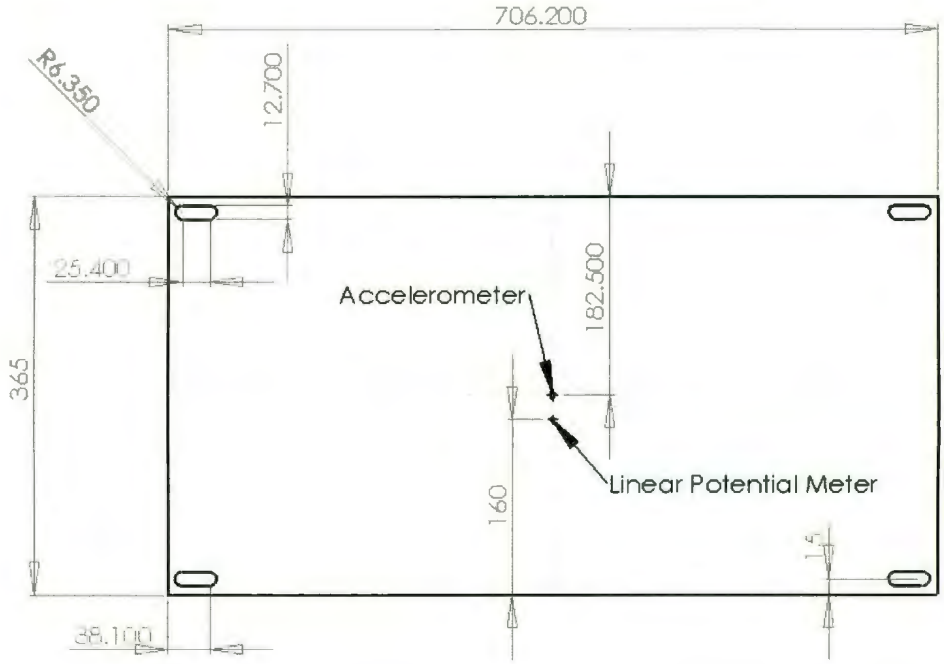


**Figure 3-10: Dimensions of impact plate**

## 3.3 Data Acquisition System

All 9 channels of data from the sensors were recorded on a common data acquisition system. It was very important to have all the data synchronized for post processing. The data sampling was limited to a frequency of 4.5 KHz by the equipment. Figure 3-11 shows the National Instruments NICDAQ-9178 data acquisition system with multiple NI 9239 4 channel, 24 Bit Analog Input Modules logging data for the ice impact experiments.

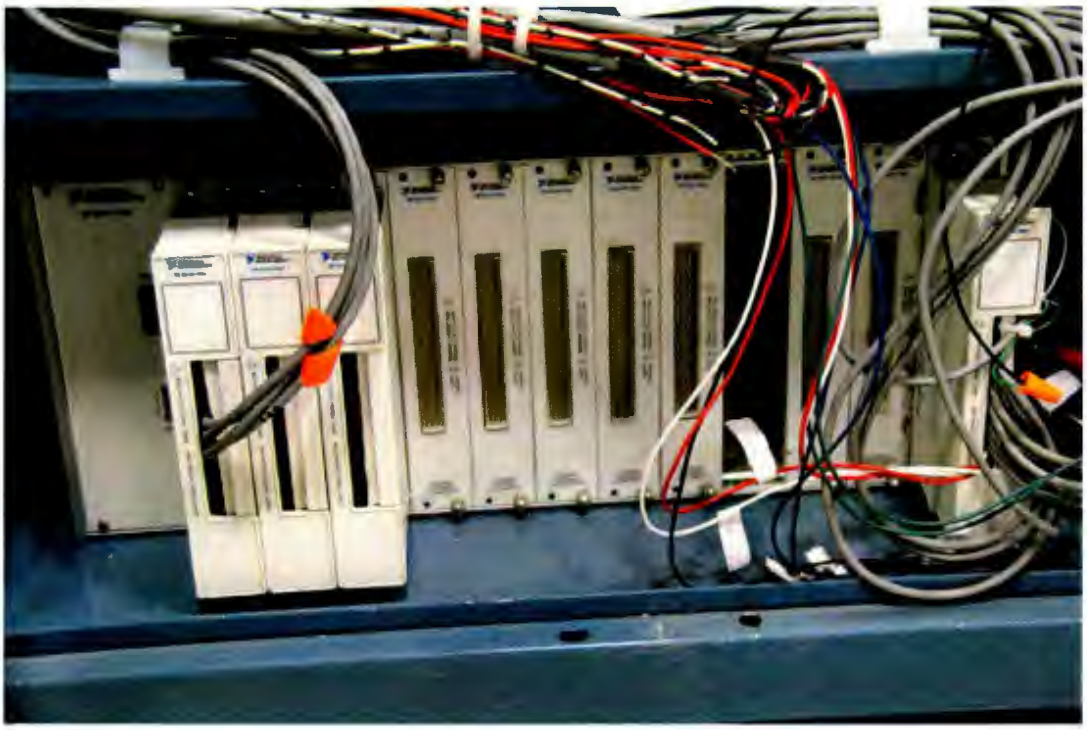

**Figure 3-11: National Instruments data acquisition system**

## 3.4 High Speed Camera

Experiments were filmed with a high speed video camera positioned on the side of the pendulum impact apparatus to record ice failure during impact. To capture the ice crushing event, a high frame rate, and high light intensities were required. Figure 3-12 below displays the high speed camera setup. The camera was located behind a frame supporting a number of 75 W halogen light bulbs (right). This allowed adequate lighting while eliminating glare from light projecting directly at the high speed camera.

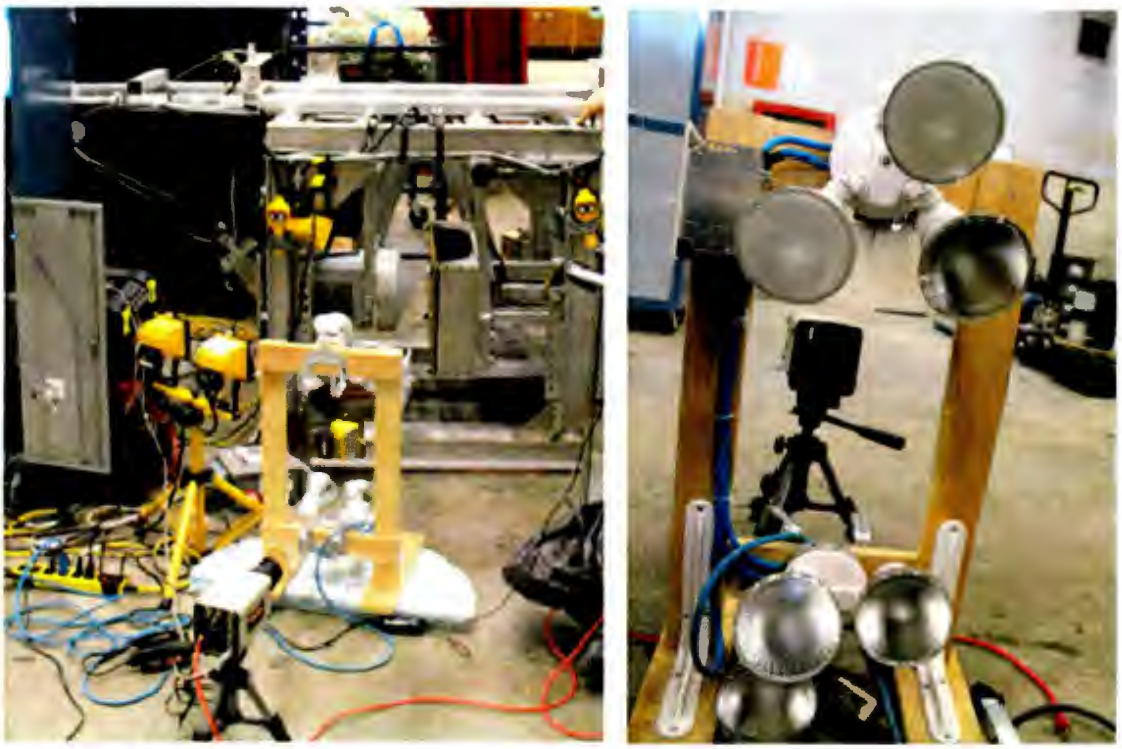

**Figure 3-12: High speed camera arrangement**

The High Speed Camera used to film the impacts was a black and white Mega Speed 55K. This camera was limited by both capture rate and resolution. The camera was not able to operate simultaneously at maximum frame capture rate and at maximum resolution. A resolution of 592 x 450 pixels with a frame capture rate of 2.25 KHz was selected.

## 3.5 Preparation of Ice Specimens

Ice specimens were grown and shaped in the lab using a modified freezer and a custom built ice shaping apparatus. This process followed experimental and ice generation procedures developed by Bruneau et al (2011). The lab ice is a controlled and consistent polycrystalline ice with high strength levels.

### 3.5.1 Growing Ice Specimen

Distilled and deionized water was used to remove impurities which can influence the crystal growth. The water was then routed through a deaeration system, to remove any dissolved gasses, and chilled to zero degrees. Figure 3-13 below displays the vacuum pump (left) and the vacuum vessel (right). The vacuum vessel was brought to an absolute pressure of 1.6 kPa and the impeller at the bottom of the vessel induces cavitation to remove the gases in the water.


**Figure 3-13: Water dearation system**

An industrial ice chipping machine (Clawson Hail Queen, Model HQ-C) was used to produce ice chips of consistent sizes ranging from 3 mm to 10 mm. The ice crushing machine is displayed in Figure 3-14. The ice cubes supplied for the ice chipping machine were provided in bulk from commercial ice production facility.

**Figure 3-14: Hail Queen ice chipping machine**

The ice chips were flooded with the purified, deaerated water in plastic buckets (1.2 m x 0.5 m x 0.75 m) fitted with a steel ice-holder ring. The steel rings contain a flange which was used for securing the specimens during the shaping the specimen. The bucket and steel ring were placed in a modified freezer cover shown in Figure 3-15. The plastic buckets were insulated with foam around the cylindrical surface to allow the ice to grow in one direction (from the bottom up). Figure 3-16 presents a cross section view of the ice specimen mold.

**Figure 3-15: Modified freezer cover with ice specimen molds**


**Figure 3-16: Cross section of ice specimen mold (Bruneau et al 2011)**

The ice seeds and deaerated chilled water were added to the mold in layers approximately 5 cm thick. To avoid air pockets in the ice specimens, after each layer the mixture was stirred with a plastic rod to provide a homogenous mixture of the ice seeds and water. The ice chip seeding process predetermines the ice grain size, effectively removing the dependence on freezing rate.

**Figure 3-17: Preparing seeded ice specimen in freezer mold**

An insulated cover was placed over the specimen and the freezer was set at a temperature of minus 20 degree Celsius for 48 hours to allow the specimens to freeze adequately.

### 3.5.2 Shaping Ice Specimen

Once the freezing process was finished, the ice specimens were removed from the buckets and shaped into conical ice specimens using a custom built shaping device. The shaping device, pictured in Figure 3-18 contains a turntable which rotates the specimens at 300 revolutions per minute with a planer blade that was lowered onto the specimen. The cone geometry is displayed in Figure 3-19, where cone angle ($\alpha$), the radius (r) and cone height ($h_i$) are defined. The height and inner radius of the steel ring were 50.8 and 130 mm respectively.

**Figure 3-18: Ice shaping apparatus**

The arm of the shaping device was initially set to shape ice specimens at angle (α) of 30 degrees. Cone angles of 20 and 40 degrees were also shaped with the apparatus by adjusting the pitch of the planer blade with applied wedges.

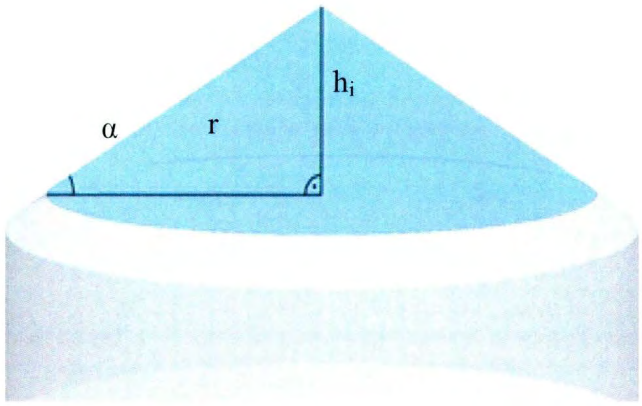


**Figure 3-19: Ice cone geometry**

After the specimens were shaped to the desired cone angles, they were removed from the steel ring and frozen into an aluminum ice holder, shown in Figure 3-20. The aluminum ice holder had a slightly larger diameter than the steel ring the specimen was grown in. This was to allow room to add water at near freezing temperature between the ice holder and ice specimen. Also, four #10 bolts with rubber gaskets on the head of the bolts to prevent leakage were inserted through the 10-24 tapped holes in the ice holder. The bolts were only long enough to fill the gap between the ice specimen and ice holder, since penetration may cause unwanted cracks in the ice specimen. The bolts in the ice holder assisted in securing the ice sample during impact. Once this process was complete, the ice specimen was frozen in the ice holder for 24 hours at -20 Degrees Celsius in a freezer

located in close proximity to the pendulum impact apparatus. Figure 3-21 shows 20, 30 and 40 degree ice specimens frozen in the aluminum ice holder.

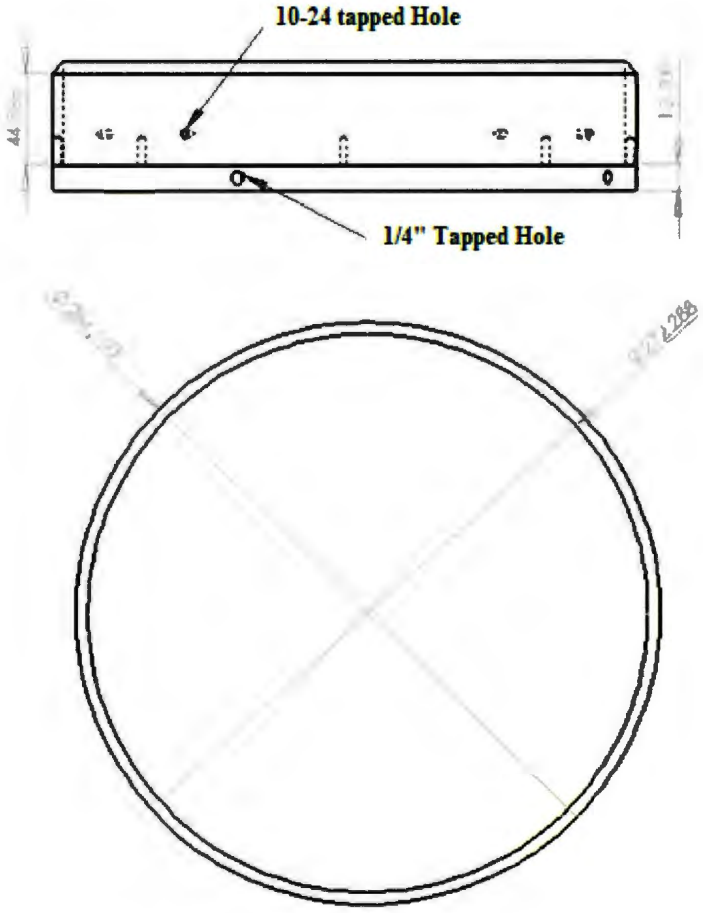


**Figure 3-20: Aluminum ice holder dimensions (mm)**

**Figure 3-21: 20, 30 and 40 degree ice specimens in aluminum ice holder**

## 3.6 Experiments

The ice specimens were stored in air tight plastic bags in a freezer that was in close proximity to impact apparatus before testing. Figure 3-22 shows the experimental setup of the pendulum impact apparatus.

**Figure 3-22: Experimental test setup**

The procedure used for all experiments with the pendulum impact apparatus is as follows:

1. The mass of both pendulums were carefully balanced to a tolerance of 0.1 kg. The ice specimen and steel impact plate were weighed with a digital scale.
2. The high speed camera and lighting was setup on the side of the pendulum impact apparatus.

3. The impact plate was attached to the pendulum frame and the accelerometer and linear potentiometer are attached to the back of the impact plate.
4. Before attaching the ice specimen to the pendulum frame, the initial height ($x_i$) of the cone was measured using a digital caliper and level.
5. Next, the ice specimen was attached to the pendulum frame. The ice holder was bolted to the 2" diameter stud that extends from the load cell mounting plate shown in Figure 3-4. A ¼" steel rod was attached to the 1/4" tapped hole in the ice holder shown in Figure 3-4. This allows the ice holder to be securely attached to the pendulum and reduces the chance of the ice holder becoming loose during impact.
6. After the ice specimen was attached to the pendulum, the electro-magnets and a safety mechanism consisting of two chains were attached to the pendulums. The electromagnets and safety chains are shown in Figure 3-3. The arms of the pendulum were raised to 30 degrees using the electric winches and an electronic digital inclinometer used to ensure both sides of the pendulum are at 30 degrees. The surface temperature of the ice specimen was recorded.
7. Once the arms were in position, the safety mechanisms were removed. The data acquisition system was initiated with the computer system to start sampling data at 4.5 kHz and the high speed camera was started. Then the electromagnets were released.
8. Second impact was prevented by securing one of the pendulum arms with a strap after impact.
9. After the impact, the ice holder and specimen mass was recorded.

See Table 2-3 in Chapter 2 for test plan showing summary with a matrix.

# 4 ANALYSIS OF DATA

This chapter provides the basis for the calculation of forces, displacements of ice crushing, pressures and energy. Details of Filtering and RSM are also provided.

## 4.1 Total Force

Three outputs of force were logged in the data acquisition system through the three load cells. The force from each load cell was added to produce total force. It was desirable to plot the individual forces from the three load cells to observe if the ice loads were eccentric. Figure 4-1 presents the non-summed force trace for Run # 7. The summed force signal for Run #7 can be found in Appendix A3.

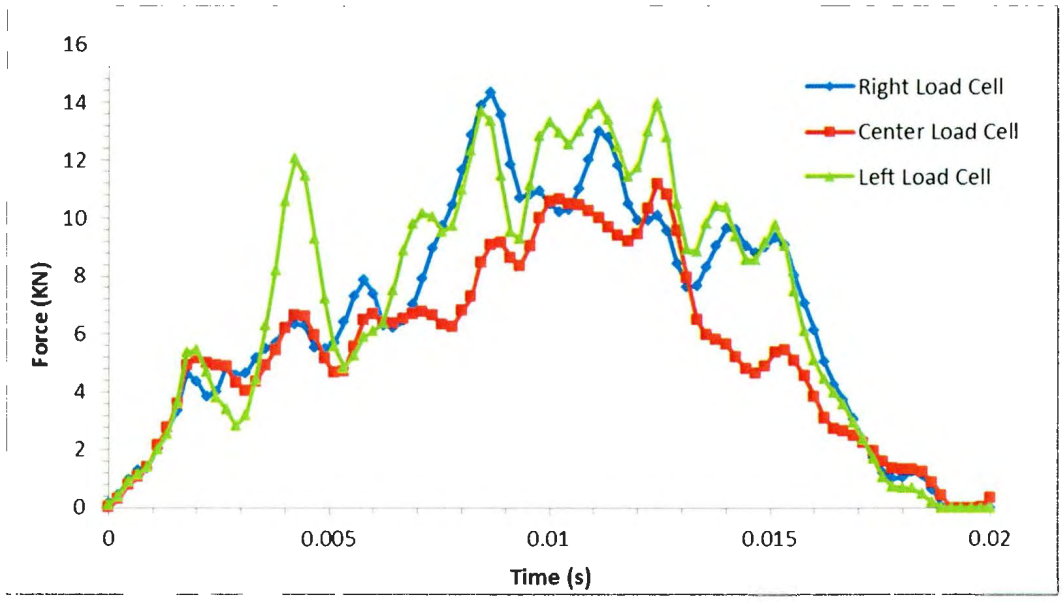


**Figure 4-1: Example of non-summed force data for Run #7**

## 4.2 Filtering

The total force was filtered to eliminate noise and structural vibrations from the output signal of the load cells. Overall the amplitude of the vibration was relatively small compared to the total force. Figure 4-2 compares the filtered peak force with the unfiltered peak force. Although the filtering reduces the peak force, the reduction in most cases is small and the higher peaks were judged to be associated with vibration or ringing in the system rather than the impact load. The unfiltered force data is presented in Appendix A.

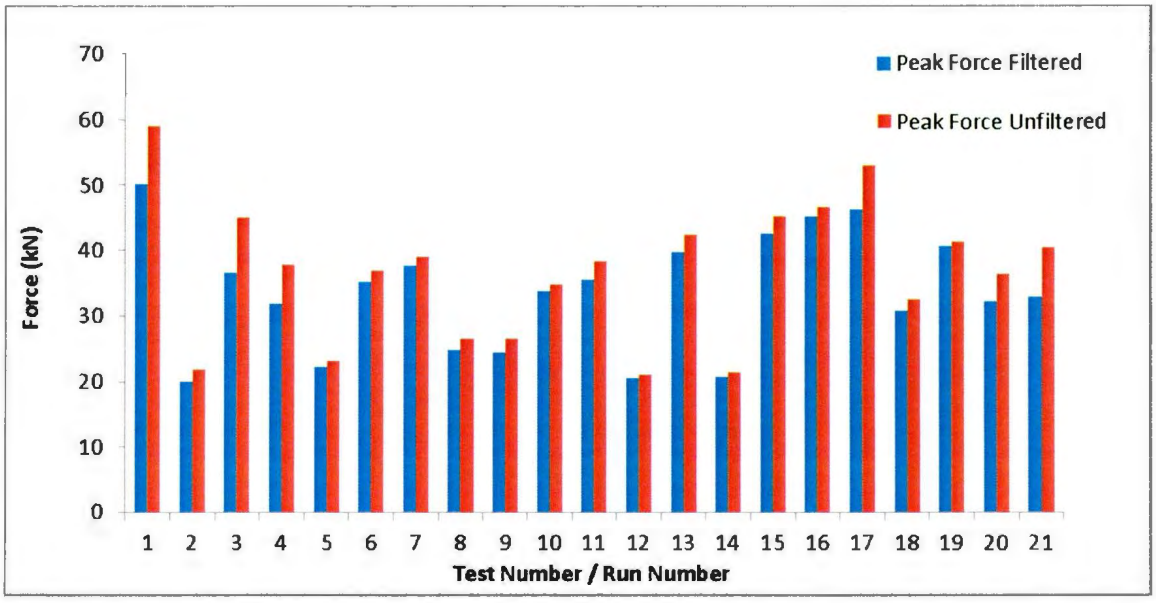


**Figure 4-2: Filtered peak force vs. unfiltered peak force**

The data was filtered using IGOR Pro by Wave Metrics. A Finite Impulse Response (FIR) filtered was applied to the total force data for all the experimental runs. A FIR filter will execute linear phase shift between all frequencies, thus steps between all the frequencies of the input signal were not disturbed.

A Fast Fourier Transform (FFT) of Force was completed of the total force ice data. Figure 4- 3 contains an example of a FFT for Run 11. The FFT did not show discrete spikes in frequency. However, the majority of the frequencies were in the lower range of the spectrum.

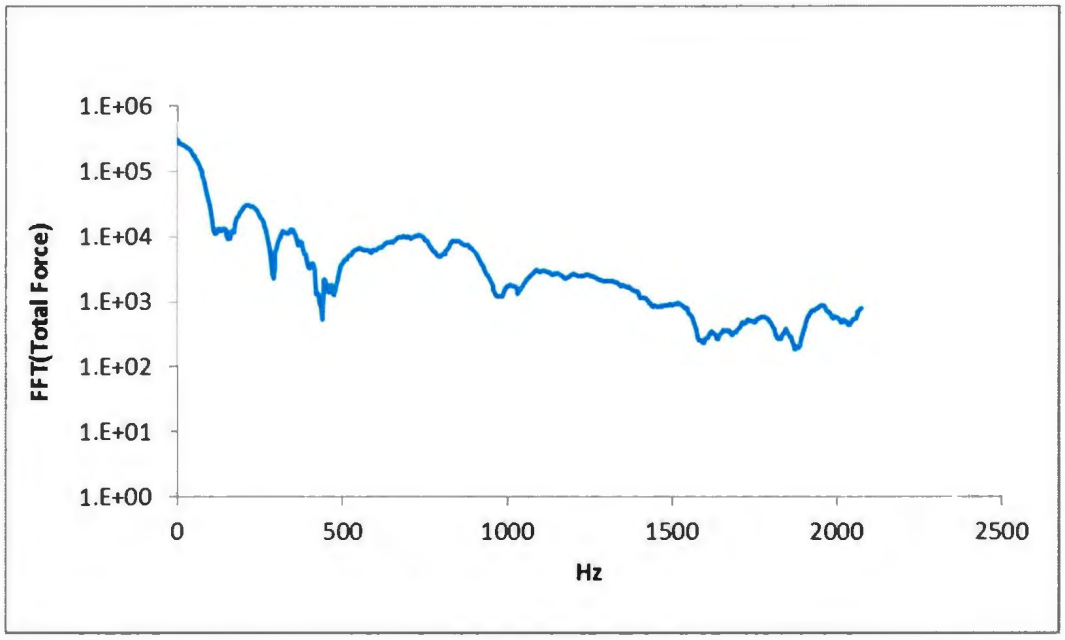


**Figure 4-3: Example of Fourier Transform of total force trace for Run 11**

A Low-Pass Filter (LPF) of 350 HZ was applied to the total force to smooth the force trace curve. Figure 4-4 presents the unfiltered and filtered results of a sample force trace. A Hanning Window function was chosen for the filter design. Apparent noise and structural vibrations were removed adequately after applying the filter. The unfiltered force traces for all 21 runs are presented Appendix A indexed by the angle of ice specimen.

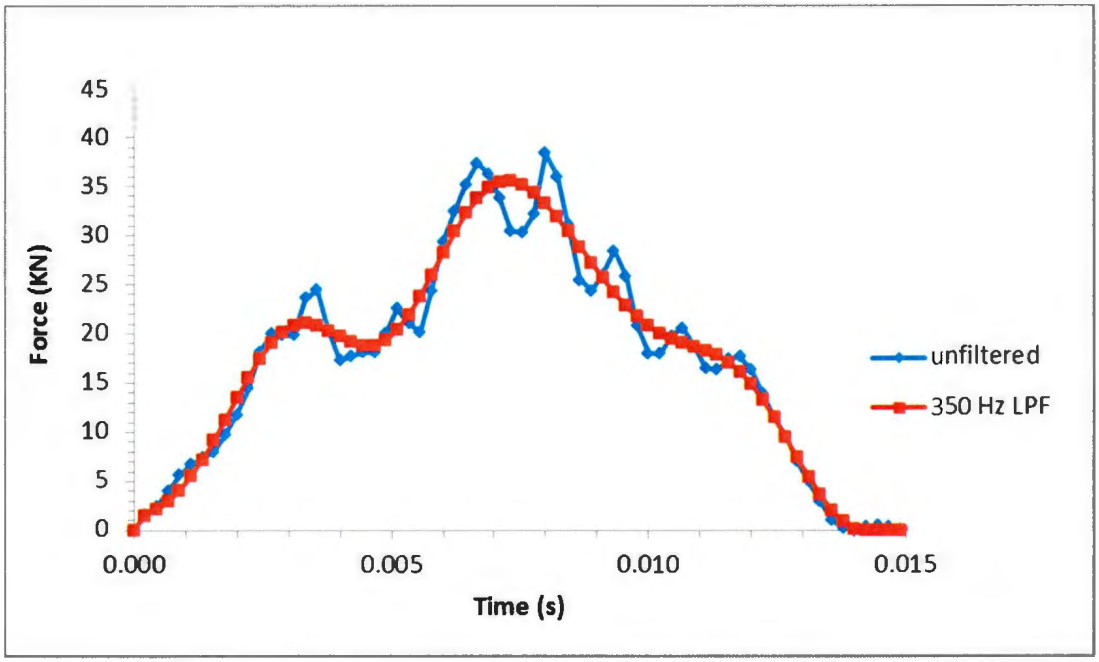


**Figure 4-4: Filtered and unfiltered force trace Run 11**

## 4.3 Displacements

To calculate the displacements of the ice crushing during the impact, two rotary encoders attached to the arms of the pendulum and the linear potentiometer attached to the back of the plate were used to calculate the relative displacement of the ice to the plate surface.

The ice carriage displacement from the center of rotation tip of ice specimen ($D_i$) is calculated by:

$$D_i = -500(\cos\theta_i) + (h_i + 100.6) \qquad [4\text{-}1]$$

Where: $\theta_i$ is angle of the ice carriage arm

$h_i$ is the initial height of the ice cone

And for the Grillage Carriage, the displacement for the center of rotation to the surface of The impact plate ($D_g$) is calculated by:

$$\boldsymbol{D_g = -500(\cos\theta_g) + (t_p + 160.1) + D_p} \qquad \textbf{[4-2]}$$

Where $\theta_g$ is angle of the grillage carriage arm

$t_p$ is thickness of plate

$D_p$ is displacement of plate

Figure 4-5 provides the dimension used for calculating the ice crushing displacements. The two angles $\theta_i$ and $\theta_g$ were derived from the rotary encoder outputs. The 20, 30, and 40 degree cone angle contain different initial cone heights ($h_i$). All dimensions in Figure 4-5 are provided in millimeters.

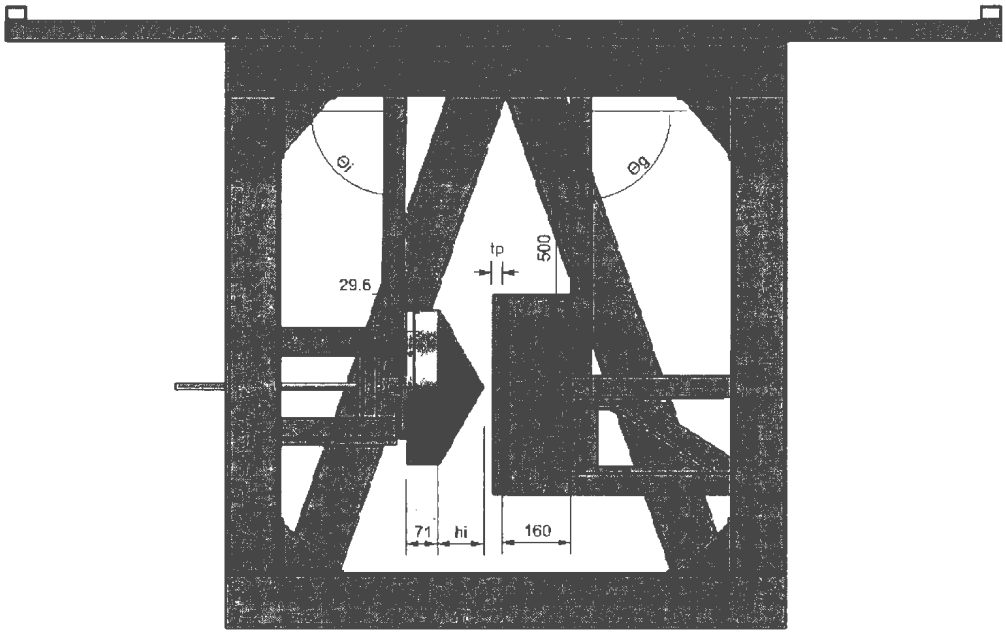


**Figure 4-5: Dimensions used to calculate ice crushing displacements (mm)**

The Ice Crushing Displacement is calculated from:

$$\mathbf{X} = \mathbf{340} - D_i - D_g \qquad \textbf{[4-3]}$$

A positive value represents a gap between the ice and surface of the impact plate and a negative value represents ice crushing displacement.

## 4.4 Pressure-Area Graphs

Pressure-area graphs are a common way of quantifying ice loads on ships and structures. The process pressure area curves show the relationship between the average pressure and the contact area, over the course of an ice collision. To calculate the process pressure-area curve for an ice crushing process, the average crushing pressure of the ice cone must be calculated.

The pressure (p(x)) is calculated:

$$\mathbf{p(x)} = \frac{\mathbf{F(x)}}{A(x)} \qquad \textbf{[4-4]}$$

Where: $F(x)$ is the force

$A(x)$ is the nominal contact area

The nominal contact area of the cone is dependent on the ice crushing displacement. The nominal contact area of the ice cone as a function of displacement A(x) is calculated by:

$$\mathbf{A(x)} = \pi\left(\frac{x}{tan(\alpha)}\right)^2 \qquad \textbf{[4-5]}$$

Where: $\alpha$ is the cone angle of the ice specimen (See Figure 3-19)

Daley (2004) provides the following relationship for pressure area distribution:

$$P = CA^e \quad [4\text{-}6]$$

Where: P is the nominal pressure

A is nominal contact area

C is the average pressure at 1 $m^2$

e is the pressure exponent ( dimensionless )

The average pressure is a function of force and nominal contact area, based on the ice crushing displacement. The ice crushing displacement data was calculated from the plate displacement and pendulum arm rotary displacements from Section 4.3. Forces were measured with the three piezoelectric load cells. The calculated process pressure-area curves were plotted and have been fitted with the pressure area distribution equation. The process area curve was taken over the relatively small contact areas of the collision which resulted in high pressures for some cases. The first significant change in force from the load cell data was used as the starting point of the pressure area curve. The pressure area distribution was somewhat dependent on the selection of the first data point and selecting one later or earlier could sometimes change the process area distribution.

Data at the end of the collision process was eliminated to reduce the skew and increase the correlation coefficient in the model ($R^2$). In general, the data after the first peak force

was eliminated, this data was influenced by the rebound and in some cases the elastic energy in the plate caused it to rebound and impact the ice a second time. Additionally, ice displaced after the first peak force was influenced by spalling.

## 4.5 Energy

This section provides the crushing energy, plate energy, and specific energy calculations from the ice-structure interaction.

### 4.5.1 Ice Impact Energy

Ice impact energy can be calculated from the integral of force as a function of displacement. The equation is expressed as (Daley 1999):

$$E_c = \int_0^{x_{max}} F(x) d_x \qquad [4\text{-}7]$$

Where: $x_{max}$ is the maximum ice crushing displacement

$d_x$ is the ice crushing displacement

$F(x)$ is the ice crushing force

The integration in the analyses was completed using the trapezoidal rule, this is an approximate method for calculating the definite integral.

### 4.5.2 Energy of the Plate

The energy of the plate was calculated from the work performed on the plate from the impact event.

$$E_p = f(x)D_p \qquad [4\text{-}8]$$

Where f(x) is the measured force

$D_p$ is the deformation at the center of the plate

## 4.6 Specific Energy Absorbed

The specific energy from the impact experiments is the ratio of input kinetic energy to the volume of damaged ice. Since all of the initial kinetic energy of the impact was not absorbed by the ice, specific energy was not a useful index for the pendulum impact experiments. An alternative index was to relate the volume of crushed ice to the ice impact energy (Jordaan 1988). This can be defined as the Specific Energy Absorbed ($E_s$). The crushing energy ($E_c$) was calculated from Equation 4 -7 and the mass was determined from the difference between measured weight of the ice sample before impact and the weight of the ice sample after the impact.

The Specific Energy Absorbed is given by

$$E_{sm} = \frac{E_c}{(m)\rho} \qquad [4\text{-}9]$$

Where $m$ is the mass loss during impact

$\rho$ is the density of ice (900 kg/m$^3$)

## 4.7 Response Surface Methodology

The response surface analysis was applied to the experimental results using DOE software, Design Expert-8. This section provides an introduction to the RSM analysis.

RSM applied to peak force, nominal pressure at 1 $m^2$ from the process area curve and specific energy.

### 4.7.1 General

RSM was used to develop the response surface model from the experimental results. This method uses statistical experimental design methods, regression analysis, and optimization methods to fit experimental data into a response surface model. Normally, preliminary experiments are completed using Design of Experiments Methodology (DOE) to screening factors and to assist in determining the range of the factors. Screening was not necessary for the ice impact experiments, since there were only two factors and the variables and the possibility of other factors such as impact speed and mass was limited by the apparatus.

### 4.7.2 Assumptions

The following assumptions were used in developing the Response Surface (Montgomery, 2009):

- Observations are independently distributed
- Normality of data
- Independence of variables and error
- Constant variance
- Sparsity of effects principle

The first four assumptions above are required by analysis of variance (ANOVA). These are validated with diagnostic plots presented in Appendix B and are discussed in Chapter 5 Results and Discussions. The following must verified with the diagnostic plots:

- The normal plot of residual should fall on a straight line
- Residuals versus predicted should show random scatter
- Residuals versus run should show no trends

The condition that observations are independently distributed requires the experimental runs to be randomized. This averages out factors that may have effects on the model that are assumed to be held constant.

The sparsity of effects principle was considered another important assumption in the analysis. This principle states that most systems are dominated by the low order interactions and high level interactions can be eliminated from the system (Montgomery, 2009). Thus the following terms interactions are only considered in the response surface model:

- A, B, AB, $A^2$ and $B^2$

### 4.7.3 Fitting a Second Order Model

Each individual response (y) from the experimentation analysis, including peak force, nominal pressure and specific energy can expressed as a function of factors ($x_1$) and ($x_2$). Where the two factors ($x_1$) and ($x_2$) are plate thickness and ice specimen angle.

These responses are represented in terms of the factors by (Montgomery, 2009)

$$y = f(x_1, x_2) + \in \quad \textbf{[4-10]}$$

Where $\in$ is the noise or error observed in the response

The response surface is represented by

$$\eta = f(x_1, x_2) \quad \textbf{[4-11]}$$

The levels of the experimental factors $x_1$ and $x_2$ can be plotted for the responses to produce a response surface graph. These responses can also be visualized in 2-D with contour plots.

The first approximation of the relationship between the response y and the independent variables $x_1$ and $x_2$ is approximated using the first order model (Montgomery, 2009)

$$y = \beta_o + \beta_1 x_1 + \beta_2 x_2 + \cdots + \beta_k x_k \quad \textbf{[4-12]}$$

If curvature is present in the response, the second order model can be used

$$y = \beta_o + \sum_{i=1}^{k} \beta_i x_i + \sum_{i=1}^{k} \beta_{ii} x_i^2 + \sum \sum_{i<j} \beta_{ij} x_i x_j + \epsilon \quad \textbf{[4-13]}$$

Where $\beta_{i,j} = 0,1 \ldots k$ are regression coefficients

## 4.7.4 Method of Least Squares

The regression coefficients are estimated using the method of least squares with Analysis of Variance (ANOVA). This method (Montgomery, 2009) can be used to determine the coefficients in Equations 4-12 and 4-13 that will minimize the error term $\epsilon$ in the model.

## 4.7.5 ANOVA

ANOVA tables for the peak force, nominal pressure and crushing energy are discussed in this section. ANOVA uses statistics to determine if the null hypothesis is valid. The null hypothesis states that the means of two or more factors are equal and the alternative hypothesis states that the means of the factors are not equal. The first column of the ANOVA table is the sum of squares (SS). This is the total variance of each term and each SS has a corresponding degree of freedom (DOF). All terms were initially included in the AOVA tables, the insignificant terms were eliminated after checking the P-values.

The Sum of Squares of the main effects of factor A and factor B from Myers and Montgomery 2008 are,

$$SS_A = \frac{1}{bn}\sum_{i=1}^{a} y_{i..}^{\ 2} - \frac{y^2_{...}}{abn} \qquad \textbf{[4-14]}$$

$$SS_B = \frac{1}{an}\sum_{i=1}^{a} y_{i..}^{\ 2} - \frac{y^2_{...}}{abn} \qquad \textbf{[4-15]}$$

Where: a and b are the levels of factor A and B

n is the number of replications

$y_{i..}$ and $y_{j..}$ are the total of all observations under the $i^{th}$ level of factor A and $j^{th}$ level of factor B

$y_{...}$ is the grand total of all the observations

Subtotal used to calculate the Sum of Squares for interaction effect,

$$SS_{Subtotal} = \frac{1}{n}\sum_{i=1}^{a}\sum_{j=1}^{b} y_{ij}^{\ 2} - \frac{y^2_{...}}{abn} \qquad \textbf{[4-16]}$$

Sum of Squares for the interaction effect,

$$SS_A = SS_{Subtotal} - SS_A - SS_B \quad [4\text{-}17]$$

The DOF for each term is,

$$DOF = n - 1 \quad [4\text{-}18]$$

Where n is the number of levels of the experiment

Dividing the $SS_T$ for each term by the DOF provides the mean square (MS),

$$MS_T = \frac{SS_T}{DOF} \quad [4\text{-}19]$$

The F-value is the "test statistic" for the null hypothesis for ANOVA. The F-value is calculated by

$$MS_{T=\frac{MS_T}{MS_E}} \quad [4\text{-}20]$$

Where $MS_E$ is the Mean Square for the Error Term

The F-value is compared with the F-distribution to compute the p-value. The p-value is the probability that the alternative hypothesis should be accepted. If the p-value is less than Alpha ($\alpha$), the null hypothesis should be rejected. Alpha was chosen as 5 percent in the present analysis.

# 5 RESULTS AND DISCUSSIONS

The following Chapter provides the results of the pendulum impact experiments. Force history, force versus ice crushing displacement, and pressure area curves are presented. Maximum impact plate thicknesses, plate accelerations, spall weight and ice crushing energy were also calculated and are shown in this section. These results are analyzed with design of experiments methodology for the peak forces, nominal pressure term from the process area curve and the specific energy.

## 5.1 Forces

The unfiltered force trace plots are presented in Appendix A. This section contains plots of the filtered force grouped by specimen cone angle.

### 5.1.1 20 Degree Ice Specimen Results

The force traces from the 20 degree cones impacting with 0.25" plate, 0.5" plate and 0.75" plate are presented in Figure 5-1. Two replications of impact force with each plate thickness are presented. The highest peak force occurred with the 0.75" impact plate. The results showed reasonable repeatability between each replication. Also the collision duration decreased with plate thickness.

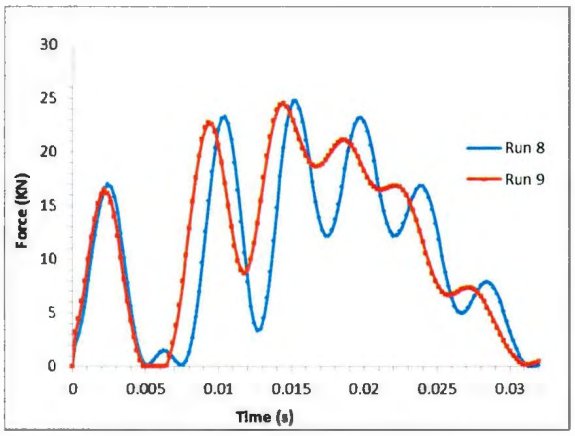


(A) 0.25" Thick Plate

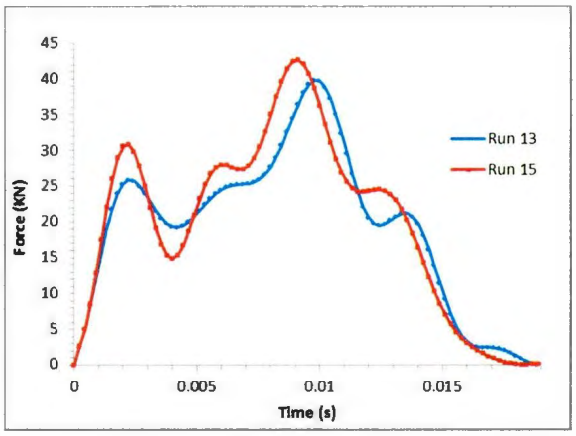


(B) 0.5" Thick Plate

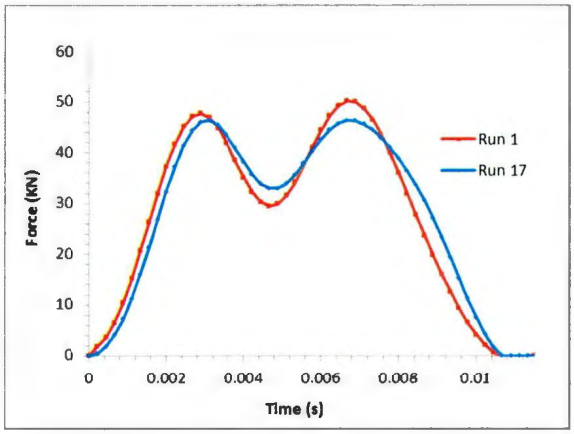


(C) 0.75" Thick Plate

**Figure 5-1: Force trace of 20 degree ice specimens impacted with various plate thicknesses**

### 5.1.2 30 Degree Ice Specimen Results

Figure 5-2 presents the force trace of the 30 degree ice cones impacted with the 0.25", 0.5" and 0.75" impact plates. The same trend was observed in this case, the stiffer 0.5" and 0.75" plates produced higher peak forces.

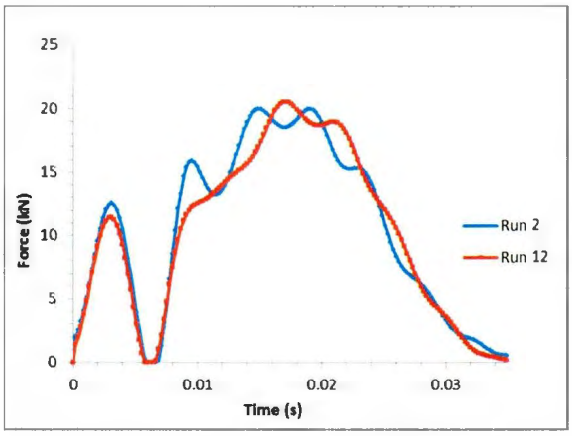


(A) 0.25" Thick Plate

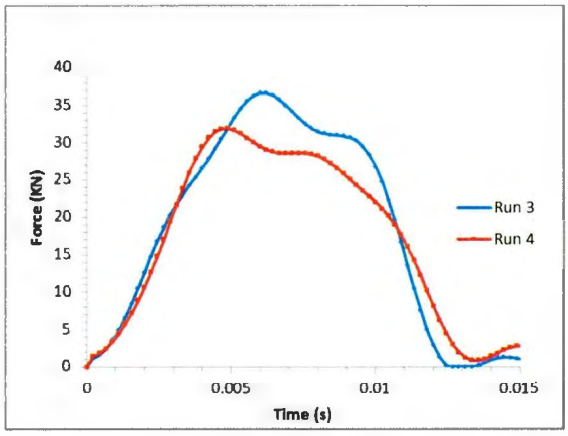


(B) 0.75" Thick Plate

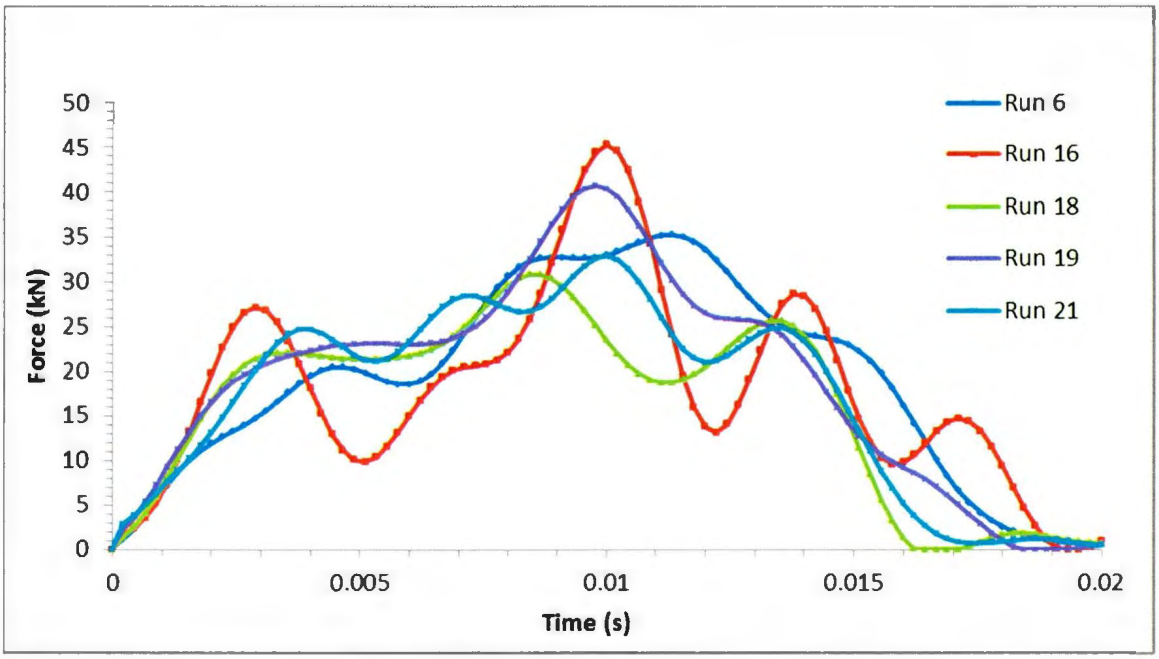


(C) 0.5" Thick Plate

**Figure 5-2: Force trace of 30 degree ice cones impacted with various plate thicknesses**

### 5.1.3 40 Degree Ice Specimen Results

In Figure 5-3, the force traces of the 40 degree cones impacted with the 0.25", 0.5" and 0.75" plate are presented. The peak forces from the ice impacts with the 0.5" plate and the 0.75" plate was observed to be significantly higher than the impact of the 40 degree ice cone with the 0.25" plate. Similar peak forces were exhibited with the 0.5" and 0.75" impact plate.

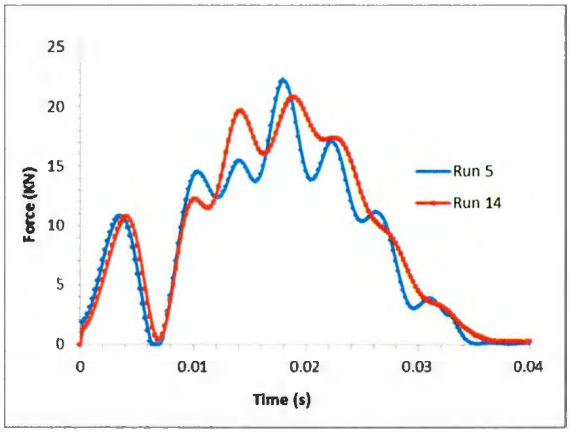


(A) 0.25" Thick Plate

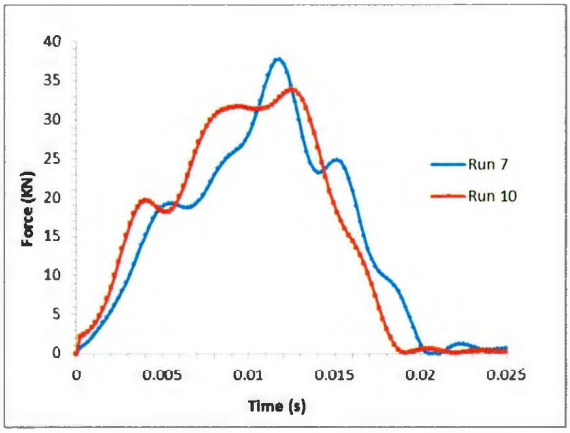


(B) 0.5" Thick Plate

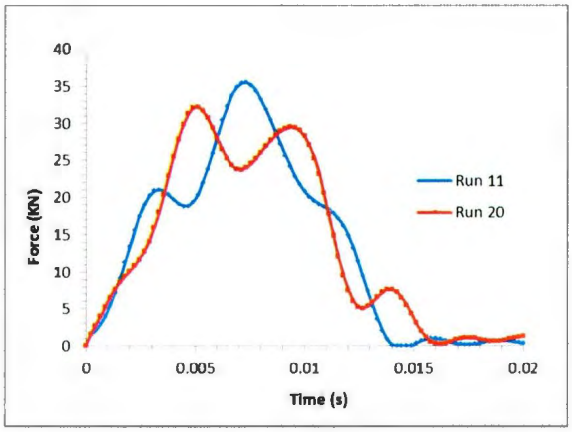


(C) 0.75" Thick Plate

**Figure 5-3: Force trace of 40 degree ice cones impacted with various plate thickness plate**

### 5.1.4 Summary of Results

Table 5-1 summarizes the peak force of the 20, 30 and 40 degree ice cones colliding with the 0.25", 0.5" and 0.75" steel plates. In general, the 20 degree ice specimens showed an increase in peak force as plate thickness increased. Both the 30 degree and 40 degree cones showed an increase in peak force from the 0.25" plate to the 0.5" plate. However, this relationship was not observed when comparing the 0.5" plate and 0.75" plate.

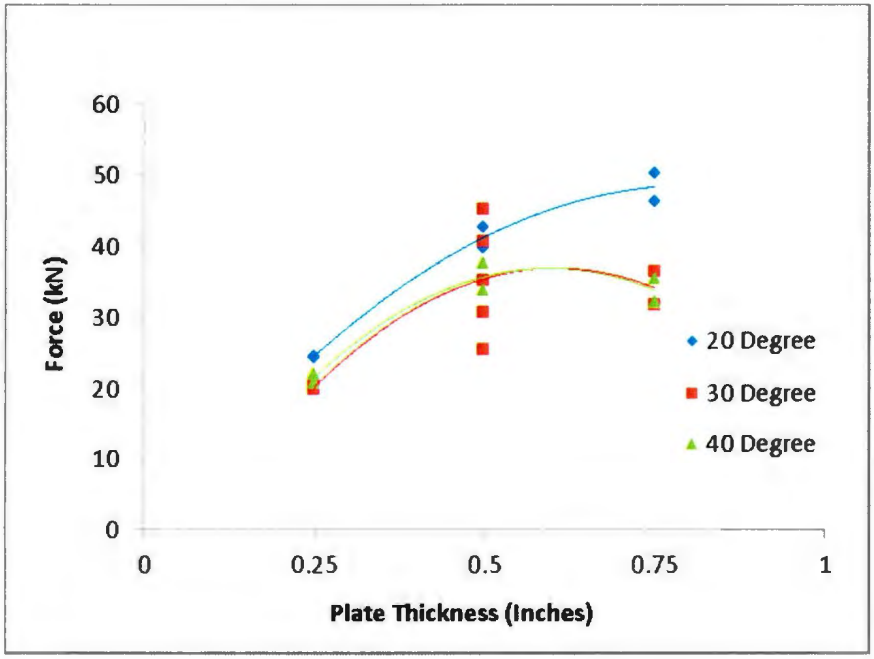


**Figure 5-4: Peak force vs. plate thickness**

**Table 5-1: Peak force summary**

| Run # | Cone Angle (degrees) | Plate Thickness (inches) | Peak Force (kN) |
|---|---|---|---|
| 8 | 20 | 0.25 | 24.76 |
| 9 | 20 | 0.25 | 24.52 |
| 13 | 20 | 0.5 | 39.80 |
| 15 | 20 | 0.5 | 42.63 |
| 1 | 20 | 0.75 | 50.20 |
| 17 | 20 | 0.75 | 46.34 |
| 2 | 30 | 0.25 | 19.99 |
| 12 | 30 | 0.25 | 20.54 |
| 6 | 30 | 0.5 | 35.23 |
| 16 | 30 | 0.5 | 45.20 |
| 18 | 30 | 0.5 | 30.82 |
| 19 | 30 | 0.5 | 40.63 |
| 21 | 30 | 0.5 | 32.8 |
| 3 | 30 | 0.75 | 36.61 |
| 4 | 30 | 0.75 | 31.92 |
| 5 | 40 | 0.25 | 22.22 |
| 14 | 40 | 0.25 | 20.81 |
| 7 | 40 | 0.5 | 37.70 |
| 10 | 40 | 0.5 | 33.78 |
| 11 | 40 | 0.75 | 35.49 |
| 20 | 40 | 0.75 | 32.22 |

### 5.1.5 Response Surface Model

Table 5-2 below presents the ANOVA table for the Peak Force Model. All main terms are significant in the Peak Force Model since the P-values are less than 0.05. The interaction term AB was significant, thus this indicates there was interaction between plate thickness and the ice specimen angle. $A^2$ and $B^2$ indicated curvature was present and the $2^{nd}$ order model is fitted with a quadratic model. The lack of fit term was also not significant which implied that the lack of fit was not significant relative to the pure error.

All terms remain in the response surface model.

- A, B, AB, $A^2$ and $B^2$

**Table 5-2: Analysis of variance table for peak force model**

| Source of Variation | Sum of Squares | Degrees of Freedom | Mean Square | F Value | P Value |
|---|---|---|---|---|---|
| A: Plate Thickness | 832.11 | 1 | 832.11 | 101.57 | <0.0001 |
| B: Cone Angle | 176.60 | 1 | 176.60 | 21.56 | <0.0005 |
| AB | 63.79 | 1 | 63.79 | 7.79 | 0.0153 |
| $A^2$ | 223.83 | 1 | 223.83 | 27.32 | 0.0002 |
| $B^2$ | 72.49 | 1 | 72.49 | 8.85 | 0.0108 |
| Error | 106.51 | 13 | 8.19 | | |
| Lack of Fit | 2.94 | 5 | 5 | 1.73 | 0.2021 |
| Pure Error | 4.08 | 12 | 12 | | |
| Total | 1453.56 | 18 | | | |

Figure 5-5 contains the interaction plot of the average peak force values from the ice impact experiments. Interaction between cone angle and plate thickness was evident from

the plot. The plot indicates that the peak force was higher with an ice specimen cone angle of 20 degrees compared with the 40 degree cone. The peak force for the 40 degree ice cone specimen did not peak with the 0.75" plate.

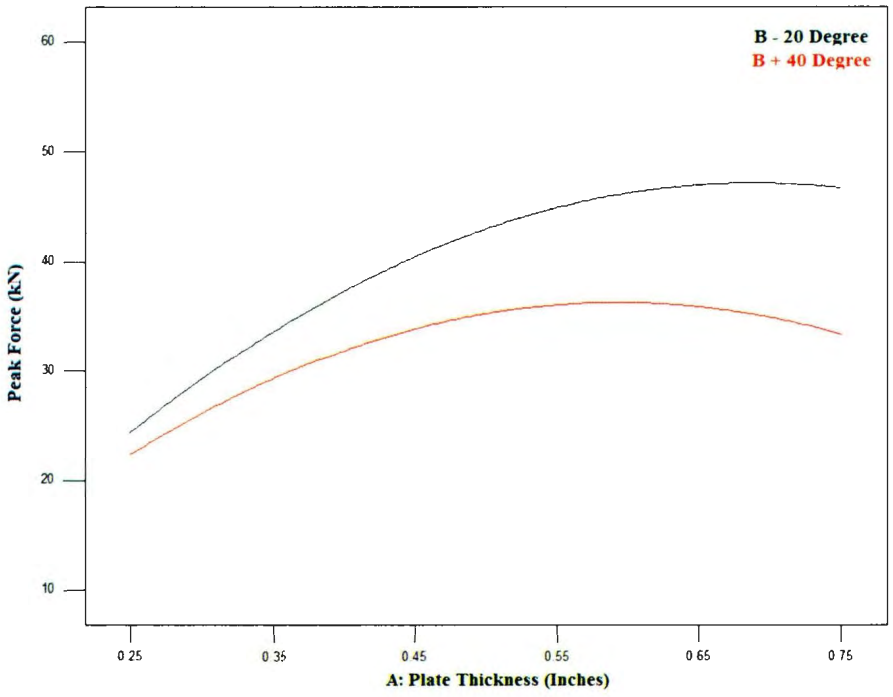


**Figure 5-5: Interaction plot of peak force**

The diagnostic plots are found in Appendix B1 to verify the model meets the assumptions of ANOVA. The diagnostic plots validated these assumptions.

Table 5-3 below contains the statistics of the peak force response surface model. The adjusted R-squared parameter is adjusted according to the number of terms in the model.

If terms are included in the models that are not adding value, the Adjusted-R-Squared value will decrease. The predicted R-Squared measures the variation in the new data from the model. In this case the adjusted R-squared and predicted R-squared were adequately close which indicates agreement between the two terms. The adequate precision term contains the signal to noise ratio. This compares the range of predicted values with the design points to the average prediction error. In this case the ratio is greater than 4 (Design Expert-8). This indicates the model was adequate within the design space.

**Table 5-3: Statistics of peak force response surface model**

| Parameter | Value |
|---|---|
| R-Squared | 0.90 |
| Adjusted R-Squared | 0.87 |
| Predicted R-Squared | 0.84 |
| Adequate Precision | 16.31 |
| Standard Deviation | 3.11 |
| Mean | 33.29 |
| Coefficient of Variation | 9.34 |

The following equation was fitted by Design Expert from the regression analysis.

$$\textbf{Peak Force} = 17.70 + 185.98A - 2.09B - 1.13AB - 118.78A^2 - 0.04B^2 \qquad [5\text{-}1]$$

Figure 5-6 below presents the response surface plot of the peak force model. The optimum condition for maximum ice force is found on the right hand side of the plot with the cone angle of the ice specimen at the lowest level (20 degrees) and plate thickness at the highest level (0.75").

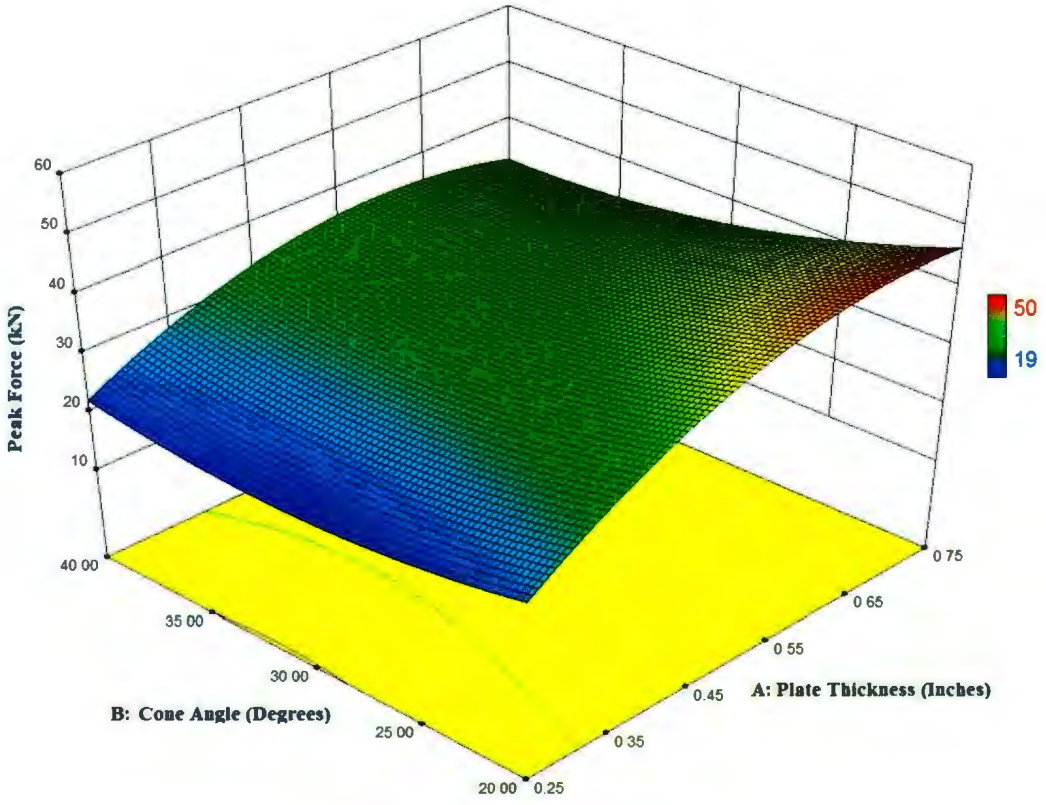


**Figure 5-6: Response surface model of peak force**

## 5.2 Force versus Displacement Curves

The force versus displacements curves were derived from the force traces, pendulum arm angle data and impact plate displacement. This data was all logged simultaneously during the ice impact event. The force vs. displacement curves are presented in Appendix C.

The maximum peak forces did not occur at the maximum ice crushing displacement due to large spalls, which may have dislocated from the ice at the end of the impact and due to

the plate rebounding after maximum deflection and causing a second impact. This plate rebound is evident in the 0.75" plate impacts in Appendix C. The second peak in the plot may have been a result of this phenomenon. Spalling also led to rapid force drops as the impact proceeded. These force drops are more pronounced for the thinner plates but are evident in almost all experiments.

## 5.3 Pressure-Area Curves

This section contains the process pressure-area curves calculated from the average pressures derived from the force trace and ice crushing displacements during the impact. The pressure area curves are grouped by ice specimen angle.

### 5.3.1 20 Degree Ice Specimen Results

Figure 5-7 below presents the pressure area curves for 20 degree ice cone crushed against a 0.25" impact plate. The initial impacts contain high pressures due to the very small surface area.

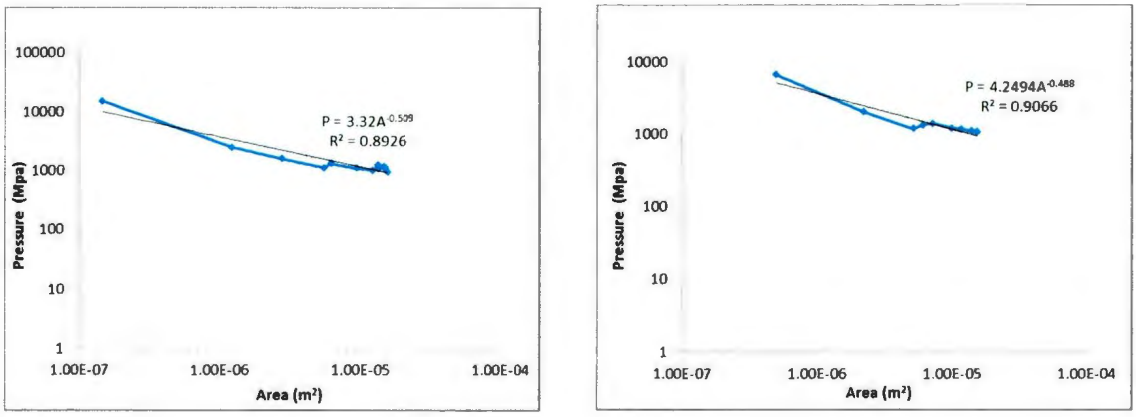


(A) Run 8 (B) Run 9

**Figure 5-7: Pressure-area curve of 20 degree ice specimens impacted with 0.25" thick impact plates**

Figure 5-8 displays the pressure-area curve of a 20 degree ice cone impacting with the 0.5" thick impact plate and Figure 5-9 displays the 20 degree cone impacting with a 0.75" plate. The nominal pressure coefficient increased significantly with the 20 degree ice specimens when plate thickness increased. This is evident in Figure 5-7 to Figure 5-9.

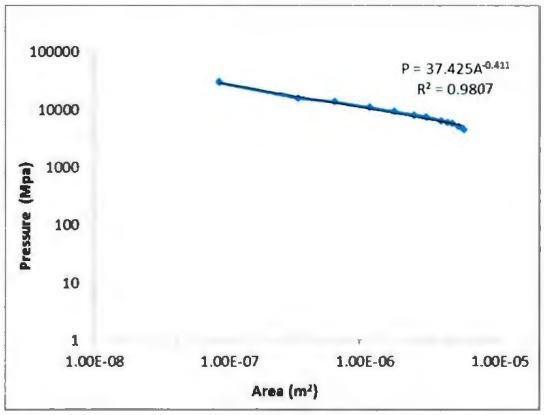


(A) Run 13

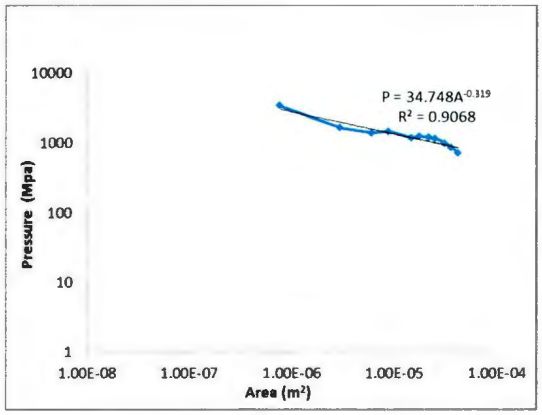


(B) Run 15

**Figure 5-8: Pressure-area curve of 20 degree ice specimen impacted with 0.5" thick impact plates**

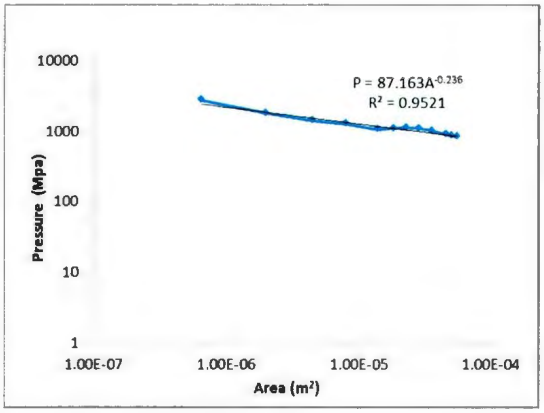


(A) Run 1

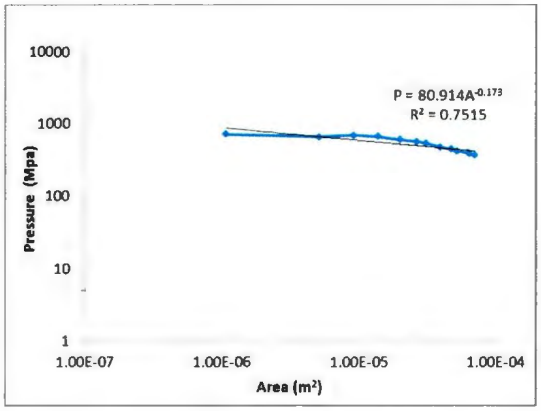


(B) Run 17

**Figure 5-9: Pressure-area curve of 20 degree ice specimens impacted with 0.75" thick impact plates**

### 5.3.2 30 Degree Ice Specimen Results

Figure 5-10 and Figure 5-11 below contain the pressure-area curves for 2 replications of 30 degree ice cones impacted with the 0.25" impact plate and 5 replications of 30 degree cone specimens impacted with the 0.5" impact plates.

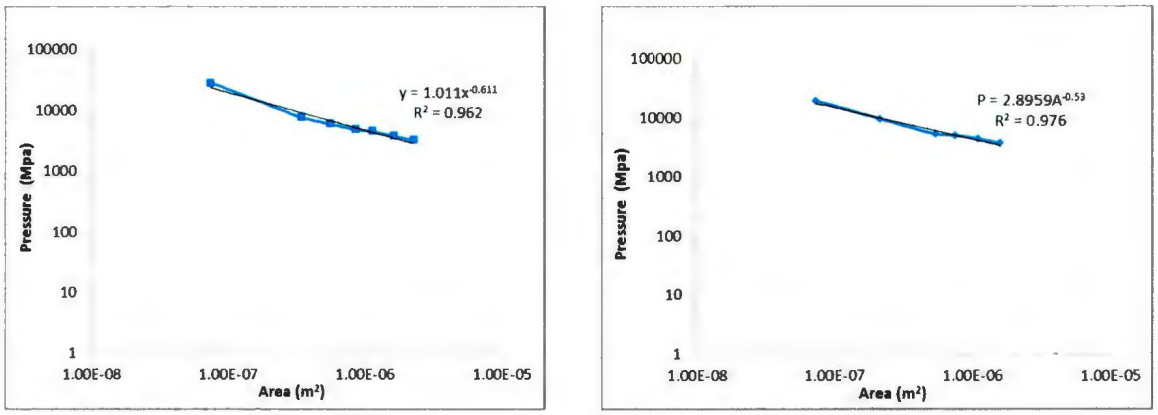


(A) Run 2 (B) Run 12

**Figure 5-10: Pressure-area curves of 30 degree ice specimens impacted with 0.25" thick impact plates**

Figure 5-11 displayed scatter in the nominal pressure terms. These varied from 1.0 Mpa in (A) to 13.7 Mpa in (C).

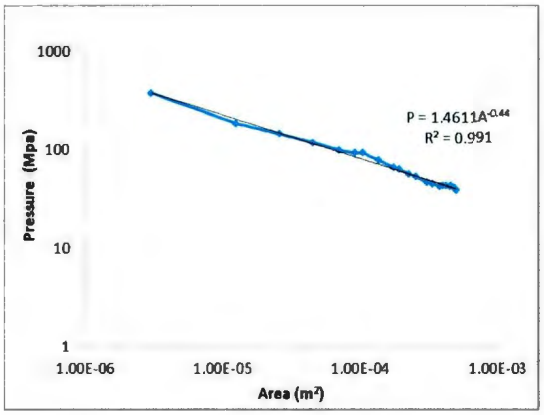


(A) Run 6

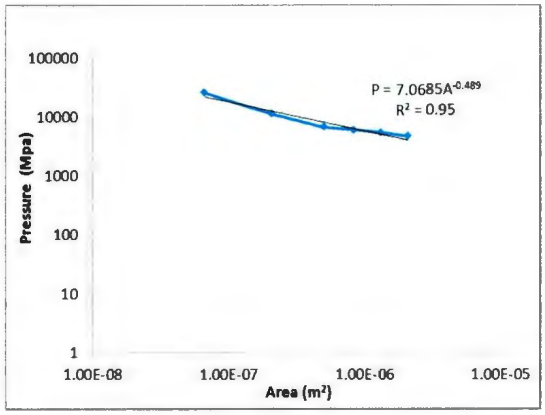


(B) Run 16

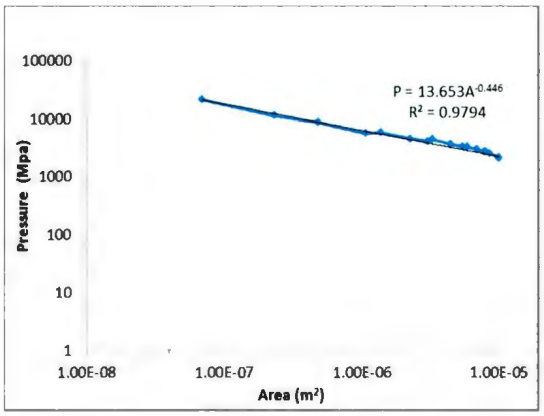


(C) Run 18

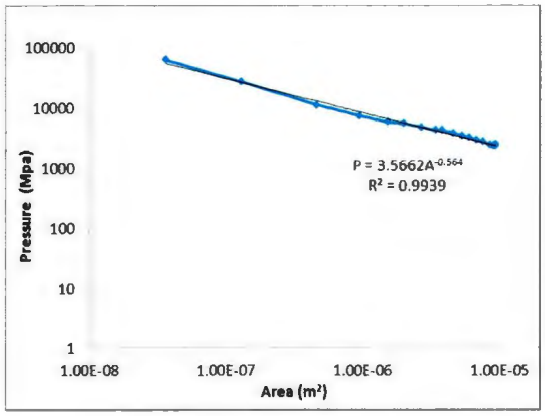


(D) Run 19

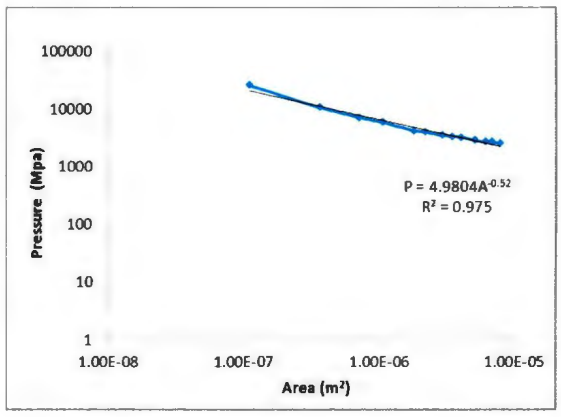


(E) Run 21

**Figure 5-11: Pressure-area curves of 30 degree ice cones impacted with 0.5" thick impact plate**

Figure 5-12 presents the pressure-area curves for the 30 degree cone specimens impacted with the 0.75" impact places. Overall the nominal pressure term for the 30 degree ice specimens increased with plate thickness.

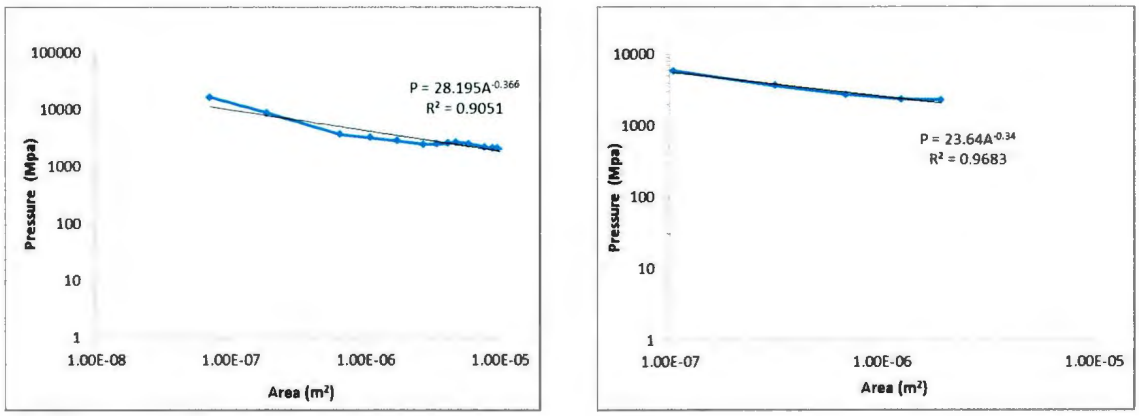


(A) Run 3 (B) Run 4

**Figure 5-12: Pressure-area curves of 30 degree ice specimen impacted with 0.75" thick impact plates**

### 5.3.3 40 Degree Ice Specimen Results

The following figures contain the pressure-area curves for the 40 degree ice cones impacted with the 0.25" plate in Figure 5-13 and 0.5" plate in Figure 5-14. The nominal pressure terms did not show an apparent increase when the impact plate thickness was increased from 0.25" to 0.5".

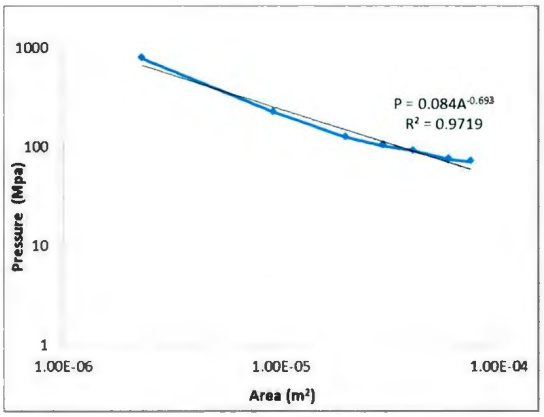


(A) Run 5

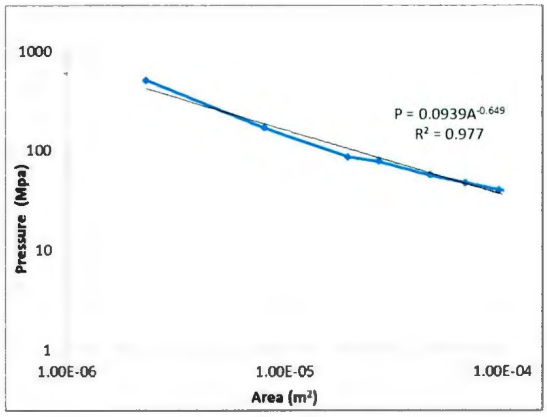


(B) Run 14

**Figure 5-13: Pressure-area curve of 40 degree ice specimens impacted with 0.25" thick impact plates**

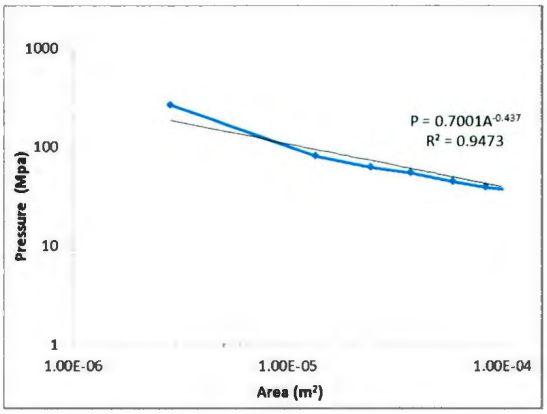


(A) Run 7

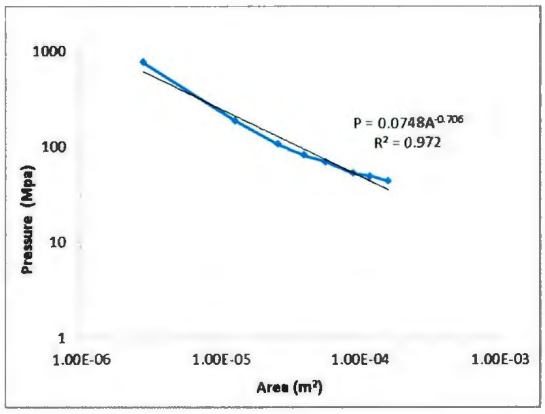


(B) Run 10

**Figure 5-14: Pressure-area curves of 40 degree ice specimens impacted with 0.5" thick impact plates**

Figure 5-15 presents the 40 degree ice specimens pressure-area curve impacted with the 0.75" impact plate.

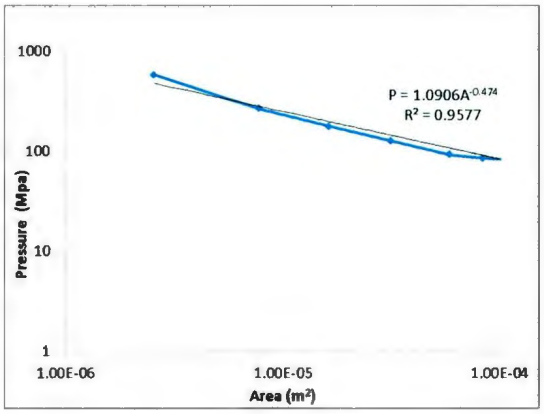


(A) Run 11

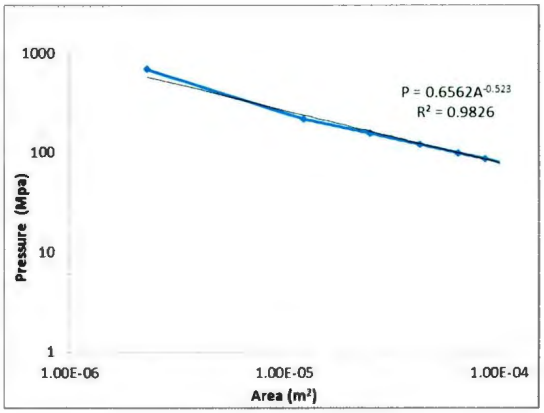


(B) Run 20

**Figure 5-15: Pressure-area curve of 40 degree ice specimens impacted with 0.75" thick impact plates**

## 5.3.4 Summary of Results

The nominal pressure constants from the pressure area distribution curves are plotted in Figure 5-16 as a function of plate thickness.

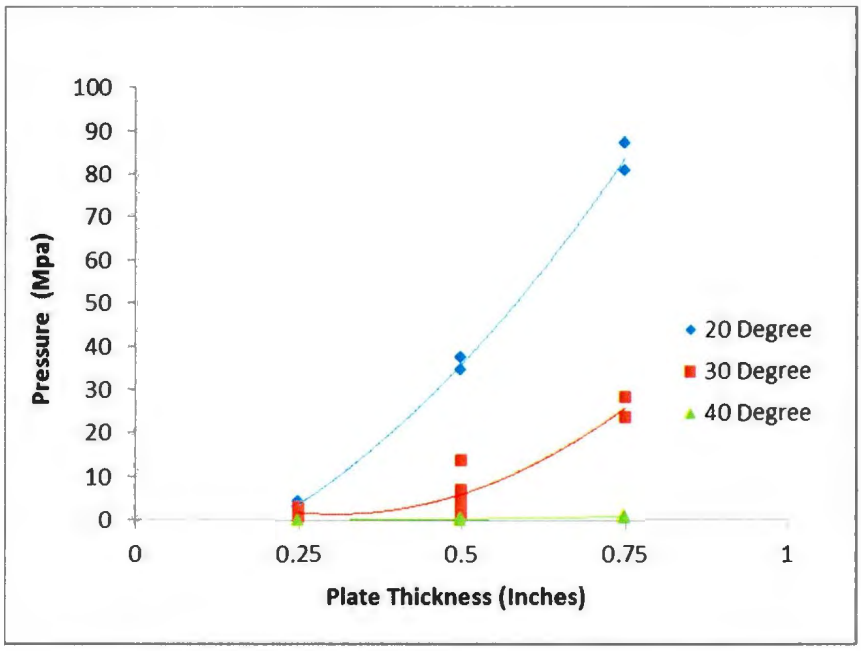


**Figure 5-16: Nominal pressure (C) vs. plate thickness**

Figure 5-16 summarizes the nominal pressure terms (C) and exponent terms (t) for process pressure distribution curve. The average nominal pressure at $1m^2$ ranged from 0.08 Mpa to 87.16 Mpa. The average exponent terms were -0.45, which demonstrates that when the contact area increases the pressure falls. Other authors have declared both declining and rising tends in their work (Daley, 2004). The results presented in Table 5-4 showed consistent declining trends.

**Table 5-4: Pressure-area curve parameter summary**

| Run # | Cone Angle (degrees) | Plate Thickness (inches) | Nominal Pressure C (Mpa) | Exponent Term (t) | Correlation Coefficient ($R^2$) |
|---|---|---|---|---|---|
| 8 | 20 | 0.25 | 3.32 | -0.509 | 0.89 |
| 9 | 20 | 0.25 | 4.24 | -0.488 | 0.906 |
| 13 | 20 | 0.5 | 37.42 | -0.411 | 0.98 |
| 15 | 20 | 0.5 | 34.75 | -0.319 | 0.9 |
| 1 | 20 | 0.75 | 87.16 | -0.236 | 0.95 |
| 17 | 20 | 0.75 | 80.91 | -0.173 | 0.76 |
| 2 | 30 | 0.25 | 1.01 | -0.611 | 0.96 |
| 12 | 30 | 0.25 | 2.89 | -0.53 | 0.98 |
| 6 | 30 | 0.5 | 1.46 | -0.44 | 0.92 |
| 16 | 30 | 0.5 | 7.07 | -0.489 | 0.95 |
| 18 | 30 | 0.5 | 13.65 | -0.446 | 0.97 |
| 19 | 30 | 0.5 | 3.56 | -0.564 | 0.99 |
| 21 | 30 | 0.5 | 4.98 | -0.452 | 0.97 |
| 3 | 30 | 0.75 | 28.19 | -0.366 | 0.91 |
| 4 | 30 | 0.75 | 23.64 | -0.34 | 0.97 |
| 5 | 40 | 0.25 | 0.08 | -0.693 | 0.97 |
| 14 | 40 | 0.25 | 0.09 | -0.649 | 0.97 |
| 7 | 40 | 0.5 | 0.70 | -0.437 | 0.95 |

### 5.3.5 Response Surface Model

Table 5-5 below presents the ANOVA table for the nominal pressure model. The main effects and interaction effects all are significant in the model. Curvature $A^2$ and $B^2$ are both insignificant, which indicates the model will be best fitted with a linear 2 factor interaction, first order model with an interaction term. The lack of fit is also not significant which implies the model fits the results.

The following terms are used in the response surface model:

- A, B, AB

**Table 5-5: Analysis of variance table for nominal pressure model**

| Source of Variation | Sum of Squares | Degrees of Freedom | Mean Square | F Value | P Value |
|---|---|---|---|---|---|
| A: Plate Thickness | 44.75 | 1 | 44.75 | 117.98 | <0.0001 |
| B: Cone Angle | 78.40 | 1 | 78.40 | 206.68 | <0.0001 |
| AB | 21.75 | 1 | 21.75 | 57.35 | <0.0001 |
| $A^2$ | 0.42 | 1 | 0.42 | 1.12 | 0.3067 |
| $B^2$ | 0.61 | 1 | 0.61 | 1.61 | 0.2232 |
| Error | 5.69 | 15 | 0.38 | | |
| Lack of Fit | 2.94 | 5 | 0.59 | 1.73 | 0.2021 |
| Pure Error | 4.08 | 12 | 0.34 | | |
| Total | 151.93 | 20 | | | |

Figure 5-17 presents the interaction plot of Nominal Pressure. This plot suggests there was a very large interaction effect between plate thickness and ice specimen angle. Plate thickness had no significant effect on nominal pressure when Factor B, ice specimen

angle was set to 40 degrees. However, when the angle of the ice specimen was 20 degrees, the peak force exhibited a positive effect on the nominal pressure.

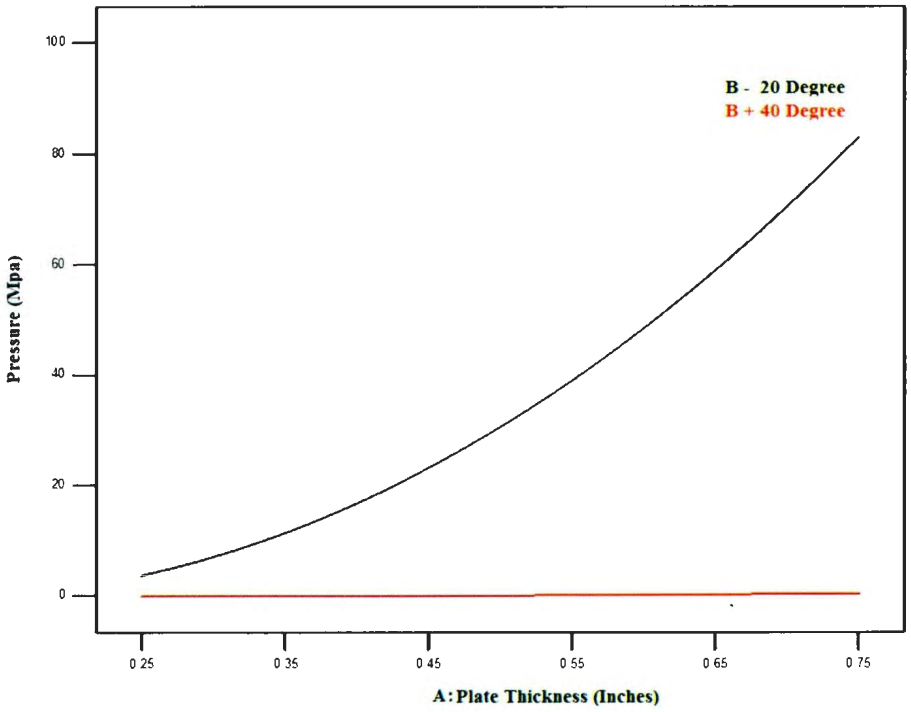


**Figure 5-17: Interaction plot of nominal pressure**

Appendix B contains the diagnostic plots for the nominal pressure model. The plots did not indicate any major concerns. A square root transform was performed on the response variable, this improved the model fit and stabilized the variance of the response. The Box Cox method was implemented by Design Expert-8 to select the appropriate transformation. Figure 5-18 below presents the Box-Cox plot. The 95 percent confidence interval in the Box-Cox plot did not include $\gamma$ equal to 1, thus a value of 0.5 was justified. The power transformation of the response is expressed in terms of lambda($\lambda$) by,

$$y' = y^{\lambda} \qquad [5\text{-}2]$$

Where y' is the transformed response

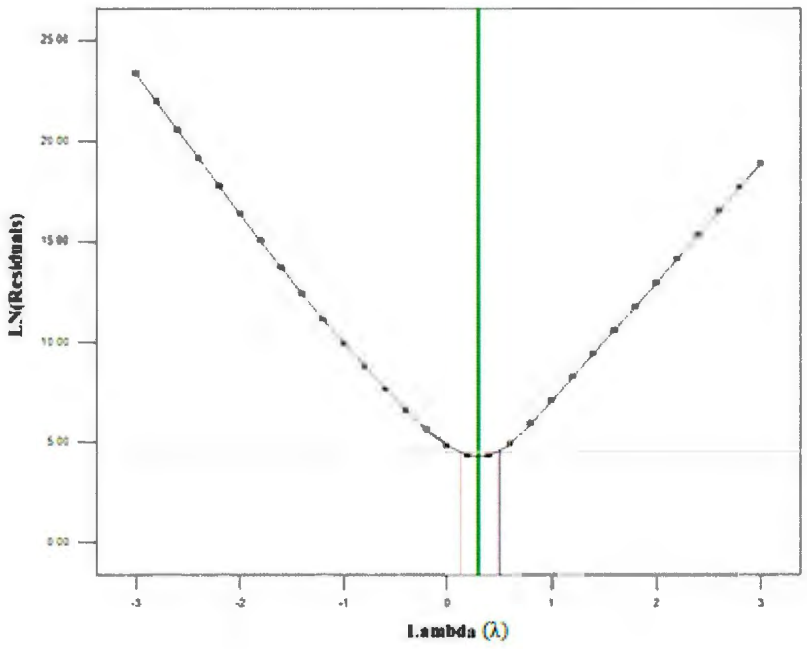


**Figure 5-18: Box Cox plot for nominal pressure model**

Table 5-6 summarizes the statistics for the nominal pressure response surface model. The adjusted- R-squared value is in full agreement with the predicted R-squared value. Also the adequate precision value is greater than 4, this indicates the model is adequate within the design space.

**Table 5-6: Statistics of nominal pressure response surface model**

| Parameter | Value |
|---|---|
| R-Squared | 0.95 |
| Adjusted R-Squared | 0.94 |
| Predicted R-Squared | 0.94 |
| Adequate Precision | 32.00 |
| Standard Deviation | 0.64 |
| Mean | 2.97 |
| Coefficient of Variation | 21.65 |

*All values are based on transformed response

The following equation was generated by Design Expert through linear regression analysis.

$$\boldsymbol{Nominal\ Pressure} = (-3.12 + 27.51A + 0.074B - 0.66AB)^2 \qquad [5\text{-}3]$$

Figure 5-19 presents the response surface plot of nominal pressure. The maximum ice pressure occurs when Factor A (plate thickness) was at high level and Factor B (ice specimen angle) was at the low level. Similarly, this optimum value occurred at the same factor levels as the peak force response model.

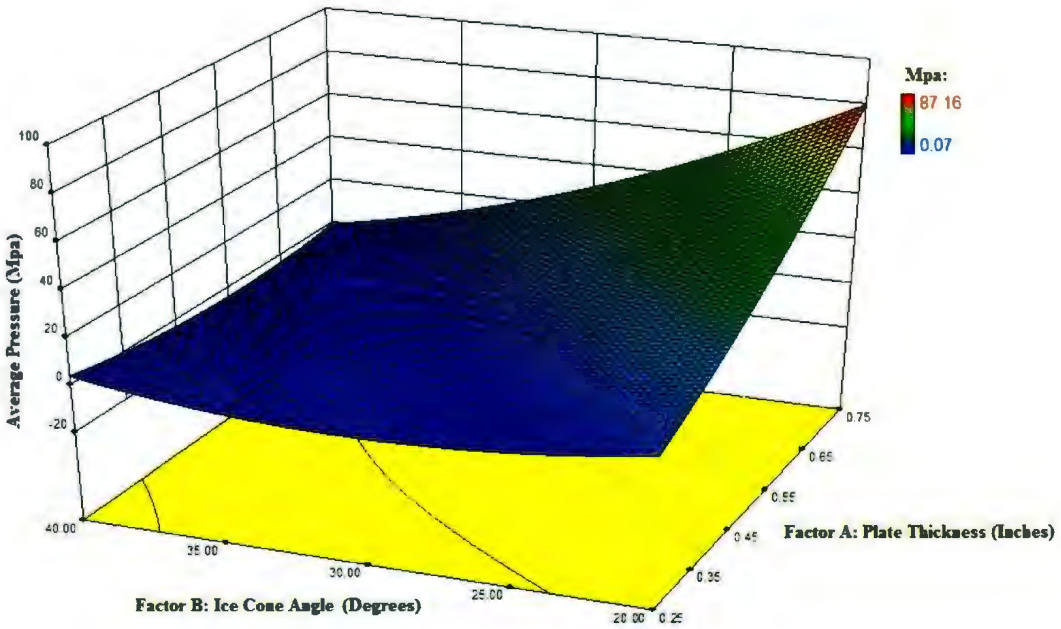


**Figure 5-19: Response surface model of nominal pressure**

## 5.4 Accelerations

Table 5-7 presents the peak accelerations measured from the ice holder and impact plate accelerometers. Some problems arose with the accelerometers, signals that peaked from the acceleration data were missing in some cases and the output signal became completely saturated in Runs 5 and 8.

**Table 5-7: Measured peak accelerations of ice holder and impact plate**

| Run # | Cone Angle (degrees) | Plate Thickness (inches) | Plate Acceleration (g) | Ice Acceleration (g) |
|---|---|---|---|---|
| 8 | 20 | 0.25 | -[1] | 228.43 |
| 9 | 20 | 0.25 | 699.60 | 226.18 |
| 13 | 20 | 0.5 | 1260.70 | 150.82 |
| 15 | 20 | 0.5 | 327.08 | 162.13 |
| 1 | 20 | 0.75 | 224.35 | 351.00 |
| 17 | 20 | 0.75 | 189.50 | 224.31 |
| 2 | 30 | 0.25 | 1480.63 | 126.59 |
| 12 | 30 | 0.25 | 565.83 | 181.20 |
| 6 | 30 | 0.5 | 743.30 | 148.72 |
| 16 | 30 | 0.5 | 274.50 | 146.96 |
| 18 | 30 | 0.5 | 318.08 | 170.50 |
| 19 | 30 | 0.5 | 294.80 | 70.41 |
| 21 | 30 | 0.5 | 304.30 | 132.13 |
| 3 | 30 | 0.75 | 202.82 | 235.64 |
| 4 | 30 | 0.75 | 712.14 | 350.21 |
| 5 | 40 | 0.25 | -[1] | 129.18 |
| 14 | 40 | 0.25 | 685.99 | 66.31 |
| 7 | 40 | 0.5 | 300.98 | 100.34 |
| 10 | 40 | 0.5 | 190.15 | 128.17 |
| 11 | 40 | 0.75 | 155.37 | 226.17 |
| 20 | 40 | 0.75 | 246.02 | 156.91 |

[1] Accelerometers signal became saturated

The accelerometer signal from the 0.75" plate for Runs 1 and 20 was multiplied by the mass of the plate to calculate the ice loads. The data was filtered, zeroed and compared with the measured force trace for Runs 1 and 20 (shown in Figure 5-20 and Figure 5-21). This was an attempt to see if the force varied on either side of the impact.

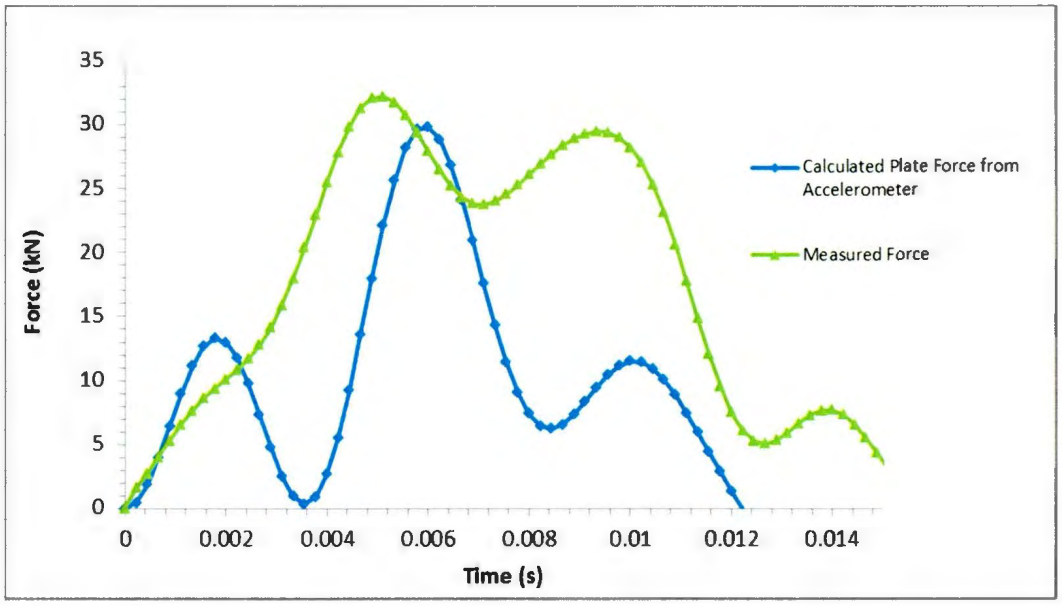


**Figure 5-20: Acceleration*mass vs. measured force for 0.75" plate and 20 degree ice specimen (Run1)**

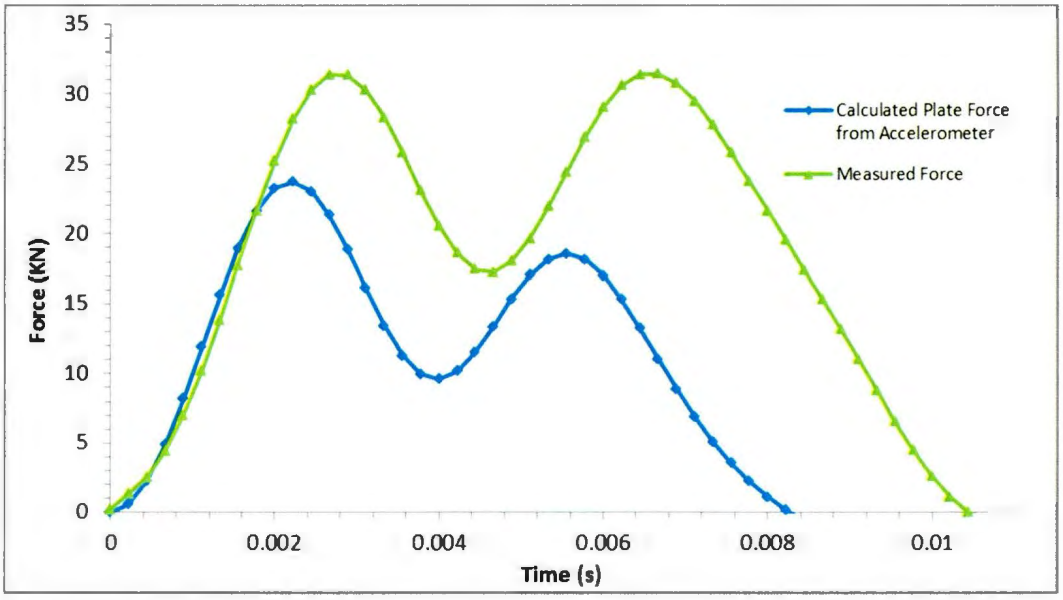


**Figure 5-21: Acceleration*mass vs. measured force for 0.75" plate and 40 degree ice specimen (Run 20)**

The force calculated from the accelerations in Run 1 deviated significantly from the measured values. The plate vibrations appeared to be out of phase with force measured behind the ice holder. However, the peak force values were close. Larger discrepancies existed between the peak values in Run 20 but both curves were similar in shape.

## 5.5 Impact Plate Deflections

The plate deflections were recorded at 4.5 KHz with a linear potentiometer. During the ice crushing process for all impact tests, the plate rebounded after reaching the maximum displacement. Figure 5-22 below displays the plate deflection over the full duration of the impact. The ice impact ended at approximately 0.03 seconds, this can be seen in the force plot for Run 8 in Appendix A-1.

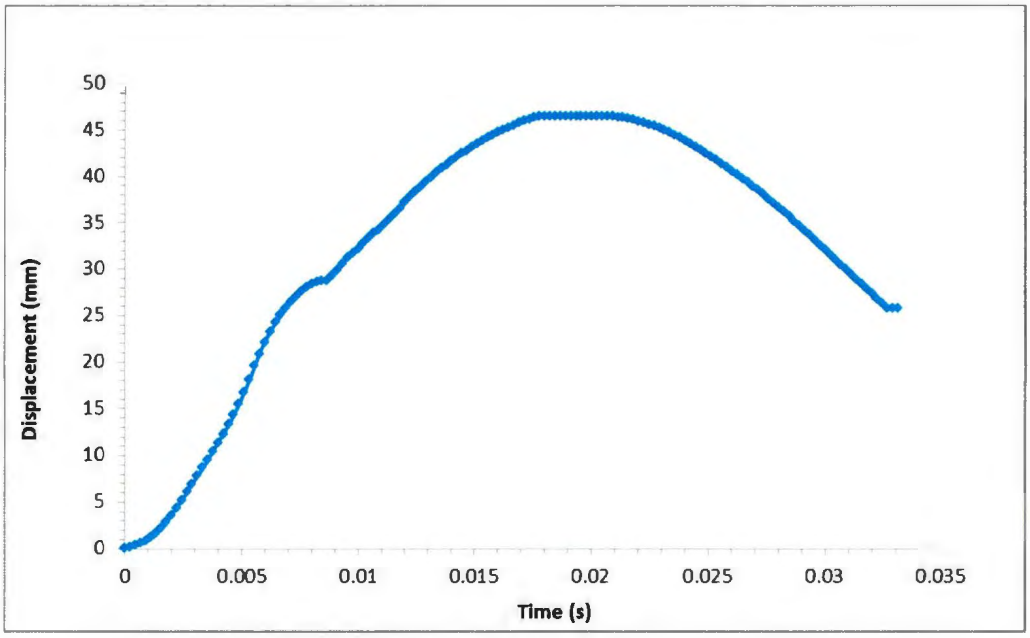


**Figure 5-22: 0.25" impact plate deflection of Run 8**

Figure 5-23 and Table 5-8 present the maximum plate defections observed for all the experimental runs. These deflections include both the elastic and plastic terms. As expected, the 0.25" plate showed the largest and the 0.75" plate showed the smallest deflections. Cone angle geometry did not appear to have a significant effect on the deflection of the plate.

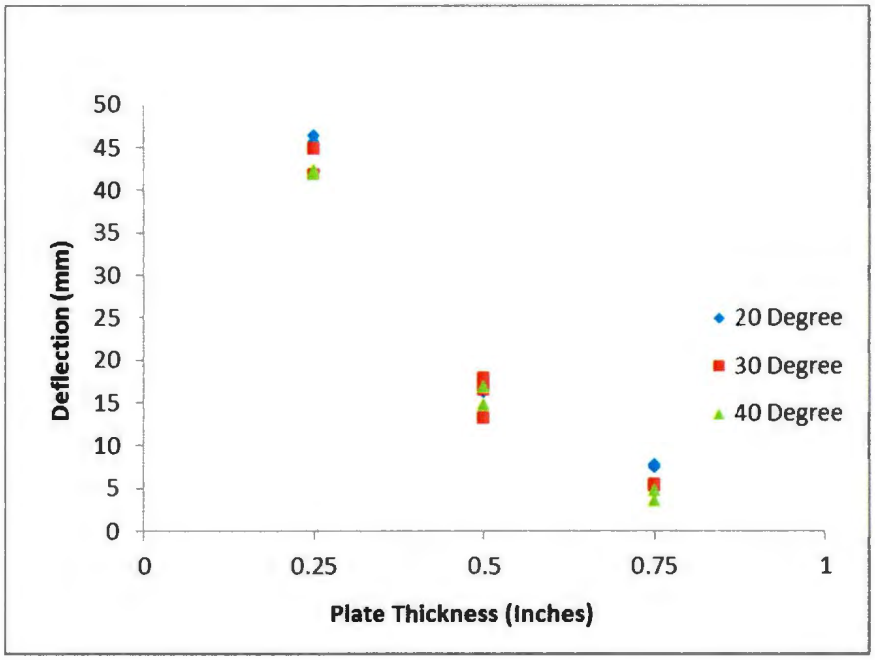


**Figure 5-23: Maximum plate deformation vs. plate thickness plot**

**Table 5-8: Maximum plate deflections values**

| Run # | Cone Angle (degrees) | Plate Thickness (inches) | Max. Plate Deflection (mm) |
|---|---|---|---|
| 8 | 20 | 0.25 | 46.39 |
| 9 | 20 | 0.25 | 45.61 |
| 13 | 20 | 0.5 | 16.17 |
| 15 | 20 | 0.5 | 16.64 |

| Run # | Cone Angle (degrees) | Plate Thickness (inches) | Max. Plate Deflection (mm) |
|---|---|---|---|
| 1 | 20 | 0.75 | 7.46 |
| 17 | 20 | 0.75 | 7.88 |
| 2 | 30 | 0.25 | 41.86 |
| 12 | 30 | 0.25 | 44.80 |
| 6 | 30 | 0.5 | 16.52 |
| 16 | 30 | 0.5 | 13.29 |
| 18 | 30 | 0.5 | 17.25 |
| 19 | 30 | 0.5 | 17.08 |
| 21 | 30 | 0.5 | 17.93 |
| 3 | 30 | 0.75 | 5.59 |
| 4 | 30 | 0.75 | 5.39 |
| 5 | 40 | 0.25 | 41.86 |
| 14 | 40 | 0.25 | 42.36 |
| 7 | 40 | 0.5 | 14.69 |
| 10 | 40 | 0.5 | 16.75 |
| 11 | 40 | 0.75 | 3.69 |
| 20 | 40 | 0.75 | 4.82 |

The data acquisition logged data for several seconds after each ice collision interaction with the steel plate to capture the final deflection of the plate. The difference between the initial and final deformation values determined the amount of plastic deformation in the impact plates. Plastic deformation was observed in the 0.25" and 0.5" steel plates. Figure 5-24 and Table 5-9 present the plastic plate deformation for each experiment containing impacts with a 0.25 or 0.75" thick steel plate. The result did not clearly show a relationship between cone angle geometry and the plastic deformation response of the plate. More scatter was evident for the 0.25" plate compared with the 0.5" plate.

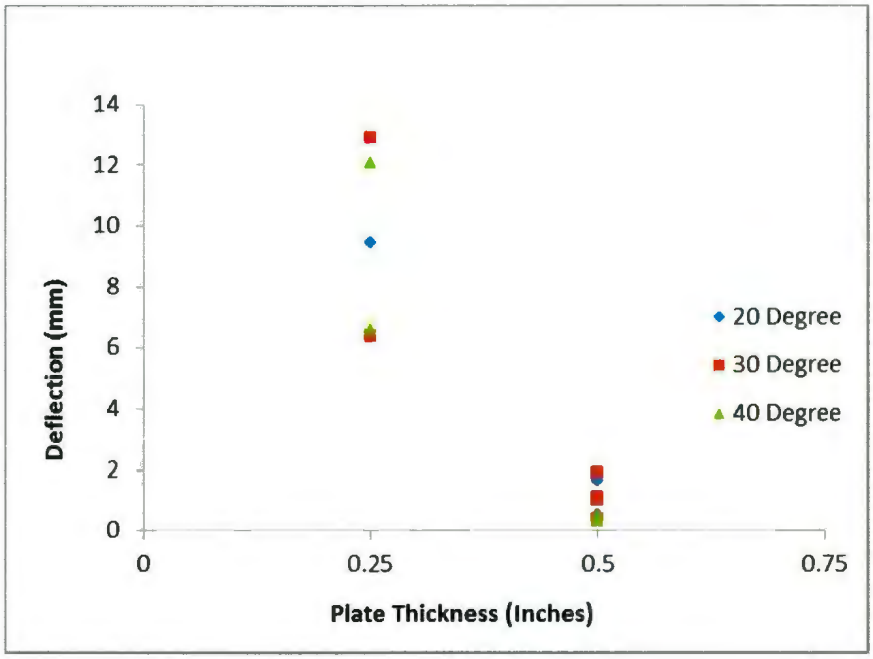


**Figure 5-24: Plate plastic deformations plot**

**Table 5-9: Plate plastic deformation values**

| Run # | Cone Angle (degrees) | Plate Thickness (inches) | Plastic Deformation (mm) |
|---|---|---|---|
| 8 | 20 | 0.25 | 16.00 |
| 9 | 20 | 0.25 | 9.41 |
| 13 | 20 | 0.5 | 1.62 |
| 15 | 20 | 0.5 | 0.47 |
| 1 | 20 | 0.75 | 0 |
| 17 | 20 | 0.75 | 0 |
| 2 | 30 | 0.25 | 6.40 |
| 12 | 30 | 0.25 | 12.91 |
| 6 | 30 | 0.5 | 0.40 |
| 16 | 30 | 0.5 | 0.34 |
| 18 | 30 | 0.5 | 1.90 |
| 19 | 30 | 0.5 | 1.02 |

| Run # | Cone Angle (degrees) | Plate Thickness (inches) | Plastic Deformation (mm) |
|---|---|---|---|
| 21 | 30 | 0.5 | 1.10 |
| 3 | 30 | 0.75 | 0 |
| 4 | 30 | 0.75 | 0 |
| 5 | 40 | 0.25 | 12.00 |
| 14 | 40 | 0.25 | 6.55 |
| 7 | 40 | 0.5 | 0.27 |
| 10 | 40 | 0.5 | 0.38 |
| 11 | 40 | 0.75 | 0 |
| 20 | 40 | 0.75 | 0 |

## 5.6 Energy

The following section presents the results from the plate energy, ice crushing energy and specific energy analysis. Appendix C contains the energy plots for each experimental run including the ice crushing energy and plate energy. The appendix is divided into three sections which include 20, 30 and 40 degree ice specimens. The plate energy for the 0.75" plates can be assumed to be the elastic energy during the impact. The 0.25" and 0.5" plates contained a combination of both elastic and plastic energy during the first collision. After the impact, energy was dissipated by rebound elastic energy and damping.

### 5.6.1 Kinetic Energy

Converting the total available potential energy into kinetic energy, the theoretical impact velocity was calculated to be 2.2 m/s for each pendulum. This provided a total closing velocity of 4.4 m/s. Table 5-10 below presents the initial combined kinetic energy of the

two pendulums pre-impact. The average impact speed was 4.30 m/s and the 0.1 m/s loss may have been due to friction and a small component of the velocity maybe lost due to gravity if the pendulums slightly exceeded 90 degrees before impact.

**Table 5-10: Initial kinetic energy values**

| Run # | Velocity (m/s) | Kinetic Energy (J) |
|---|---|---|
| 8 | 4.19 | 438.90 |
| 9 | 4.34 | 470.89 |
| 13 | 4.25 | 451.56 |
| 15 | 4.27 | 455.82 |
| 1 | 4.33 | 468.72 |
| 17 | 4.33 | 468.72 |
| 2 | 4.27 | 455.82 |
| 12 | 4.25 | 451.56 |
| 6 | 4.38 | 479.61 |
| 16 | 4.35 | 473.06 |
| 18 | 4.34 | 470.89 |
| 19 | 4.33 | 468.72 |
| 21 | 4.31 | 464.40 |
| 3 | 4.33 | 468.72 |
| 4 | 4.37 | 477.42 |
| 5 | 4.20 | 441.00 |
| 14 | 4.30 | 462.25 |
| 7 | 4.29 | 460.10 |
| 10 | 4.35 | 473.06 |
| 11 | 4.23 | 447.32 |
| 20 | 4.33 | 468.72 |

### 5.6.2 Crushing Energy

The crushing energy in the pendulum experiments was limited by the available kinetic energy. The amount of kinetic energy that was transformed into ice crushing energy varied in each experiment based on the structural stiffness of the structure and appeared to be independent of the ice specimen angle.

Figure 5-25 and Table 5-11 presents the crushing energy for each experimental run. These results were calculated with Equation 4-7. The ice interaction with the stiffer plates showed higher levels of crushing energy. This suggests that 0.25" plates absorbed deformation energy from the impact into deforming the plate compared with the 0.5" and 0.75" plates.

The calculated crushing energy exceeded the pre-impact kinetic energy in the denoted runs from Table 5-11. These runs were all of the experiments with the 0.75" plate. No reason could be clearly identified for this discrepancy. Filtering the force signal will have some influence on the crushing energy. In general, filtering should reduce the apparent crushing energy. Therefore, filtering the force data is unlikely to have caused the overestimate of crushing energy. Also the ice crushing displacements were calculated using relative displacements in Equation 4-3 and have incorporated both elastic and plastic components of the plate deformation using Equation 4-2. Results show evidence that the elastic energy in the plate caused a second impact. This effect is investigated in Section 5.6.3 and may have implications on the crushing energy calculations.

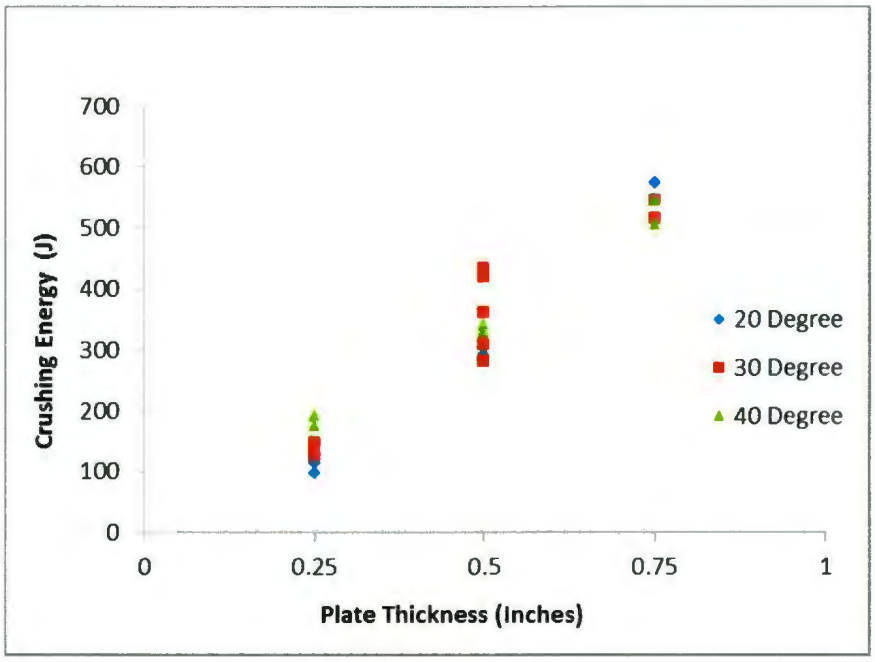


**Figure 5-25: Ice crushing energy**

**Table 5-11: Ice crushing energy values**

| Run # | Cone Angle (degrees) | Plate Thickness (inches) | Ice Crushing Energy (J) |
|---|---|---|---|
| 8 | 20 | 0.25 | 114.10 |
| 9 | 20 | 0.25 | 96.40 |
| 13 | 20 | 0.5 | 291.67 |
| 15 | 20 | 0.5 | 309.32 |
| 1 | 20 | 0.75 | 546.35[1] |
| 17 | 20 | 0.75 | 572.47[1] |
| 2 | 30 | 0.25 | 147.30 |
| 12 | 30 | 0.25 | 125.80 |
| 6 | 30 | 0.5 | 309.80 |
| 16 | 30 | 0.5 | 432.35 |
| 18 | 30 | 0.5 | 419.33 |
| 19 | 30 | 0.5 | 281.25 |

| Run # | Cone Angle (degrees) | Plate Thickness (inches) | Ice Crushing Energy (J) |
|---|---|---|---|
| 21 | 30 | 0.5 | 361.13 |
| 3 | 30 | 0.75 | 515.60[1] |
| 4 | 30 | 0.75 | 543.91[1] |
| 5 | 40 | 0.25 | 191.78 |
| 14 | 40 | 0.25 | 174.43 |
| 7 | 40 | 0.5 | 341.20 |
| 10 | 40 | 0.5 | 328.90 |
| 11 | 40 | 0.75 | 503.85[1] |
| 20 | 40 | 0.75 | 544.61[1] |

[1] Crushing energy exceed the pre-impact kinetic energy

### 5.6.2.1 Response Surface Model

Table 5-12 contains the ANOVA table for the ice crushing energy. The only term found to be significant was the plate thickness and it had a P-value less than 0.05. The interaction term AB indicates some slight interaction. Since term B was eliminated from the model, this interaction effect was excluded. Only term A remained in the response surface model.

**Table 5-12: Analysis of variance table for crushing energy**

| Source of Variation | Sum of Squares | Degrees of Freedom | Mean Square | F Value | P Value |
|---|---|---|---|---|---|
| A: Plate Thickness | 470800 | 1 | 470800 | 302.7 | <0.0001 |
| B: Cone Angle | 1988.15 | 1 | 1988.15 | 1.28 | <0.2760 |
| AB | 6388.44 | 1 | 6388.44 | 4.11 | 0.0609 |
| $A^2$ | 7.10 | 1 | 7.10 | 0.004 | 0.9470 |
| $B^2$ | 982.26 | 1 | 982.26 | 0.63 | 0.4392 |
| Error | 23331.45 | 15 | 1555.43 | | |
| Lack of Fit | 3514.63 | 3 | 1171.54 | 0.71 | 0.5647 |
| Pure Error | 19816.82 | 12 | 1651.40 | | |
| Total | 503500 | 20 | | | |

Figure 5-26 presents the main effect plot of crushing energy. Factor A produced a positive effect on crushing energy. No response surface plot was produced for the crushing energy response since only one factor was significant in the model. The diagnostic plots are shown in Appendix B3 and did not indicate any major concerns with the analysis.

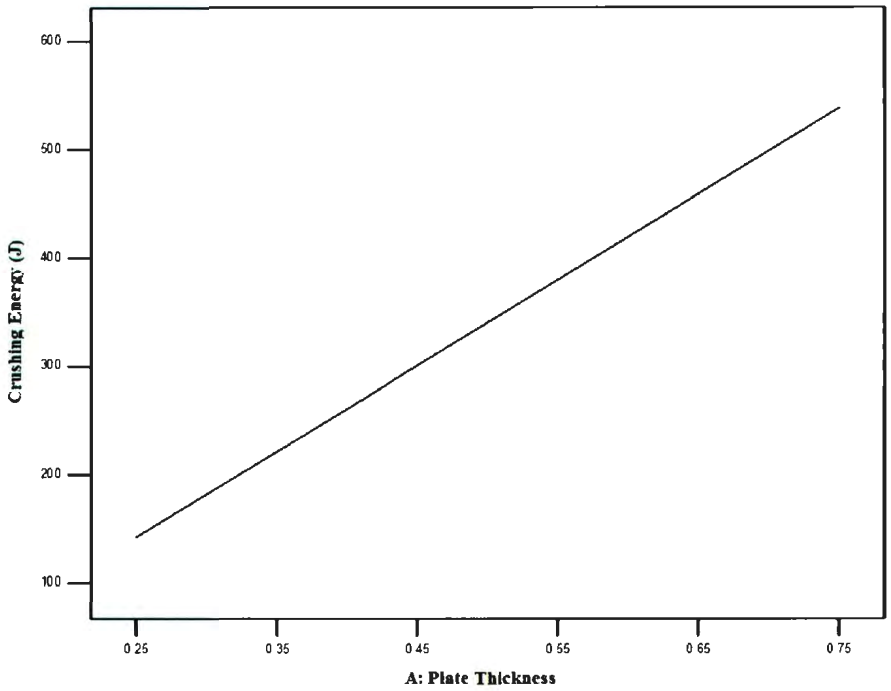


**Figure 5-26: Main effects plot of crushing energy**

Table 5-13 summarizes the statistics for the nominal pressure response surface model. The adjusted- R-squared value fully agreed with the predicted R-squared value. Also the adequate precision value was greater than 4, which indicated the model was adequate within the design space.

**Table 5-13: Statistics of crushing energy response surface model**

| Parameter | Value |
|---|---|
| R-Squared | 0.93 |
| Adjusted R-Squared | 0.93 |
| Predicted R-Squared | 0.92 |
| Adequate Precision | 30.94 |
| Standard Deviation | 41.49 |
| Mean | 340.55 |
| Coefficient of Variation | 12.18 |

The following linear regression equation was generated by Design Expert.

$$\boldsymbol{Crushing\ Energy = -55.61 + 792.32A} \qquad \textbf{[5-4]}$$

Where A is the plate thickness

### 5.6.3 Plate Energy

Figure 5-27 presents the maximum plate energy from the deflection of the plate due to the ice impact. The energy presented was combination of both elastic and plastic response of the plate. The negative trend suggests that the plate stiffness decreases the energy transfer.

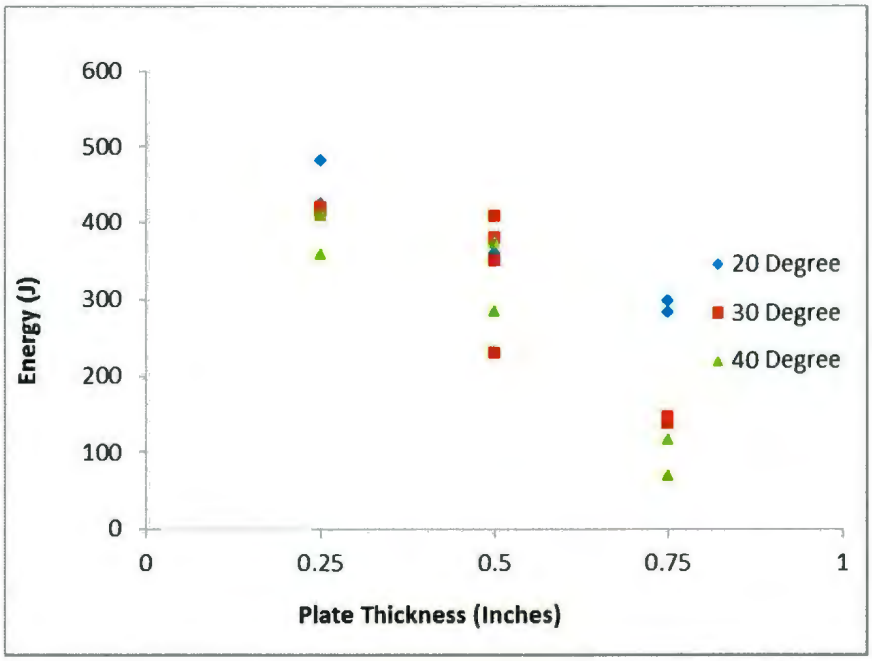


**Figure 5-27: Maximum plate energy plot**

**Table 5-14: Maximum plate energy values**

| Run # | Cone Angle (degrees) | Plate Thickness (inches) | Maximum Plate Energy (J) |
|---|---|---|---|
| 8 | 20 | 0.25 | 423.29 |
| 9 | 20 | 0.25 | 480.56 |
| 13 | 20 | 0.5 | 358.01 |
| 15 | 20 | 0.5 | 373.51 |
| 1 | 20 | 0.75 | 282.12 |
| 17 | 20 | 0.75 | 297.23 |
| 2 | 30 | 0.25 | 410.18 |
| 12 | 30 | 0.25 | 420.18 |
| 6 | 30 | 0.5 | 350.55 |
| 16 | 30 | 0.5 | 230.07 |
| 18 | 30 | 0.5 | 377.65 |
| 19 | 30 | 0.5 | 380.73 |

| Run # | Cone Angle (degrees) | Plate Thickness (inches) | Maximum Plate Energy (J) |
|---|---|---|---|
| 21 | 30 | 0.5 | 408.95 |
| 3 | 30 | 0.75 | 145.50 |
| 4 | 30 | 0.75 | 137.74 |
| 5 | 40 | 0.25 | 355.89 |
| 14 | 40 | 0.25 | 410.97 |
| 7 | 40 | 0.5 | 283.04 |
| 10 | 40 | 0.5 | 371.73 |
| 11 | 40 | 0.75 | 67.74 |
| 20 | 40 | 0.75 | 113.29 |

The elastic strain energy stored in the plate was observed to have a significant influence on responses of the ice-structure interaction, especially the forces, energy and ice crushing displacements. Figure 5-28 displays the strain energy effects during impact. After the plate reached maximum displacement, the force decayed and the ice crushing displacement remained unchanged. The force and ice crushing displacement increased as the plate deflected back to initial position due to elastic strain energy. These effects are evident from the energy plots in Appendix D for all experimental runs, the crushing energy increased as the elastic energy in the plate moved the plate back towards the ice specimen. As expected the effects appear to be greater on the experimental runs with the 0.75" and 0.5" impact plates compared with the 0.25" impact plates.

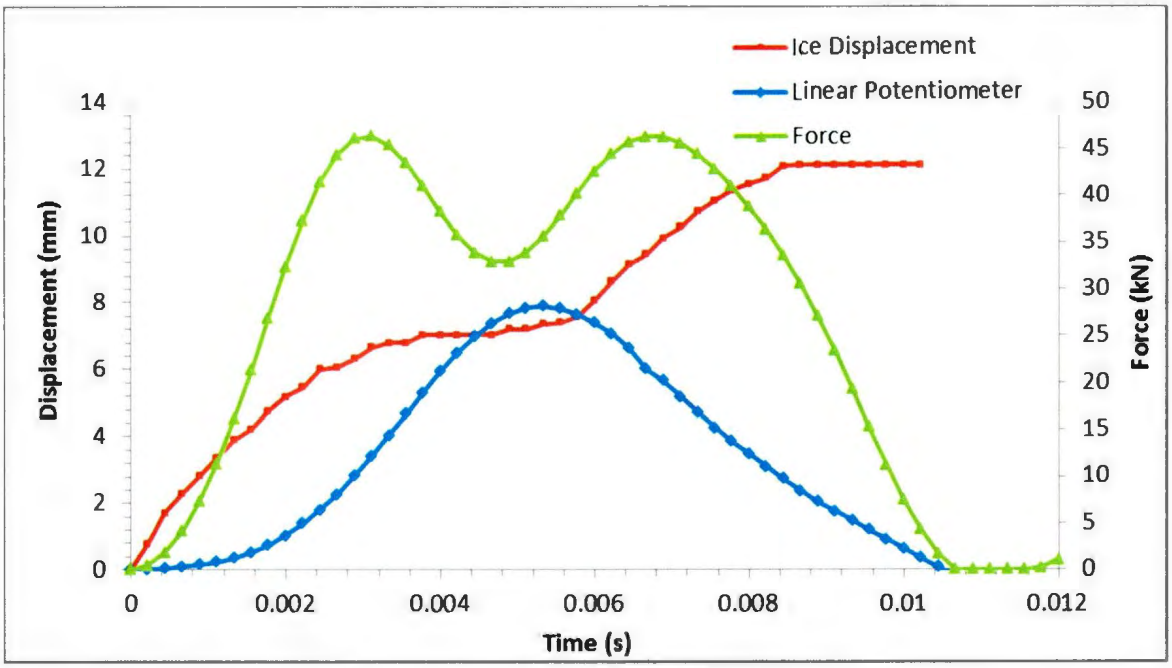


**Figure 5-28: Effects of strain energy (Run 17)**

### 5.6.3.1 Response Surface Model

Table 5-15 below contains the ANOVA table for the plate energy. Both experimental factors A and B were found to be significant, since the P value was less than 0.05. However, the interaction between A and B was found to be insignificant.

The following terms remain in the response surface model:

- A and B

**Table 5-15: Analysis of variance table for crushing energy**

| Source of Variation | Sum of Squares | Degrees of Freedom | Mean Square | F Value | P Value |
|---|---|---|---|---|---|
| A: Plate Thickness | 3.452E10 | 1 | 3.452E10 | 62.34 | <0.0001 |
| B: Cone Angle | 5.041E09 | 1 | 5.041E09 | 9.10 | 0.0087 |
| AB | 1.216E08 | 1 | 1.216E08 | 0.22 | 0.6461 |
| $A^2$ | 1.141E09 | 1 | 1.141E09 | 2.06 | 0.1717 |
| $B^2$ | 1.151E08 | 1 | 1.151E08 | 0.21 | 0.6550 |
| Error | 8.305E09 | 15 | 5.537E08 | | |
| Lack of Fit | 1.204E09 | 3 | 4.013E08 | 0.68 | 0.5820 |
| Pure Error | 7.101E09 | 12 | 5.918E08 | | |
| Total | 4.914E10 | 20 | | | |

Figures 5-29 and 5-30 below contain the main effect plot of plate energy for both Factor A and Factor B. The interaction plot is not included since interaction was considered insignificant by ANOVA. Factor A and B both produced a negative effect on crushing energy where Factor A had greater effects.

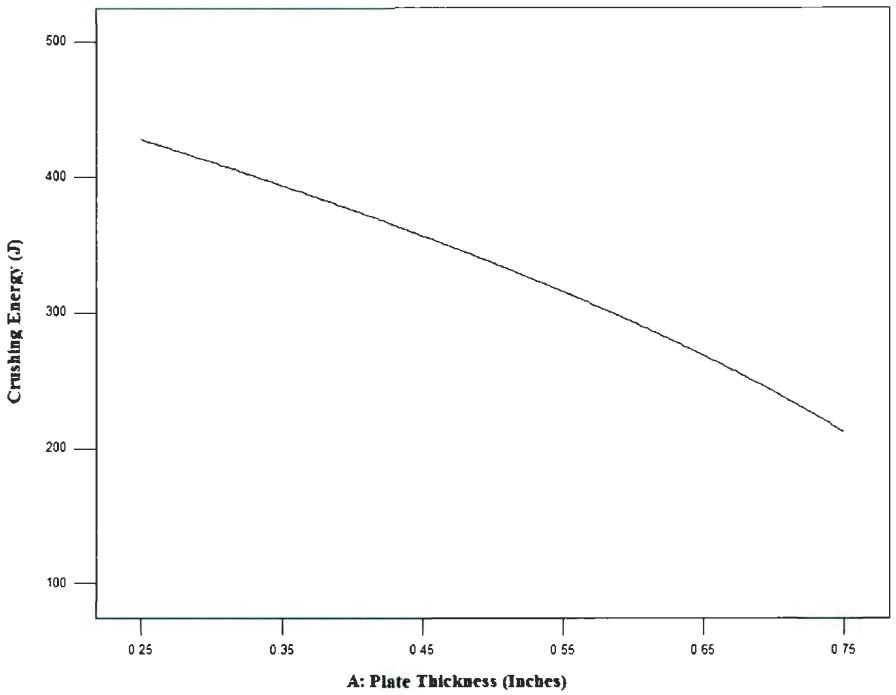


**Figure 5-29: Main effect plot for factor A for plate energy**

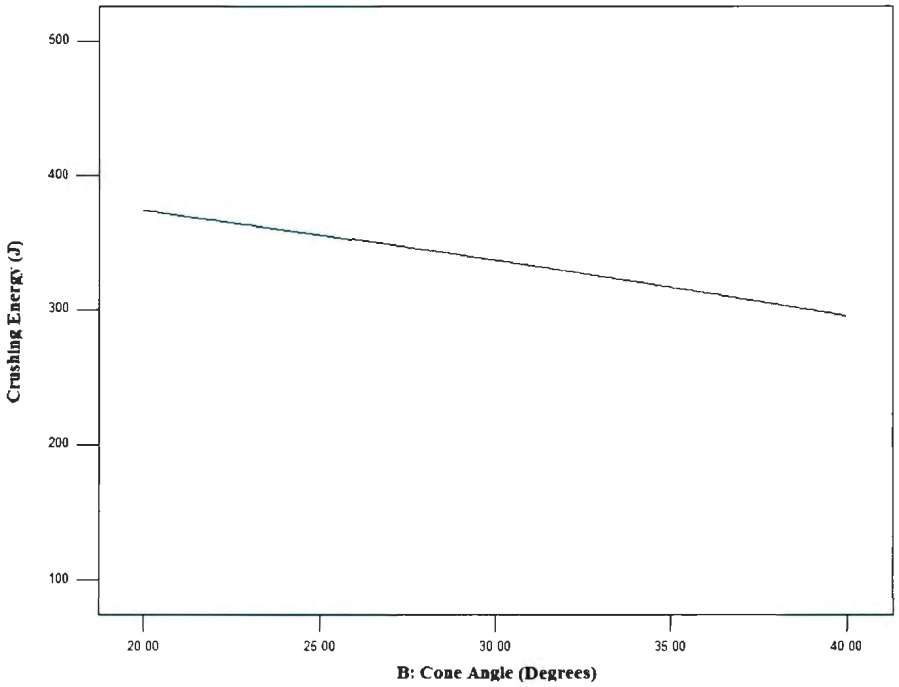


**Figure 5-30: Main effect plot for factor A for plate energy**

The diagnostic plots did not raise any concerns and are found in Appendix B. A power transform was implemented with lambda equal to 1.96 according to the Box-Cox plot shown in Figure 5-30.

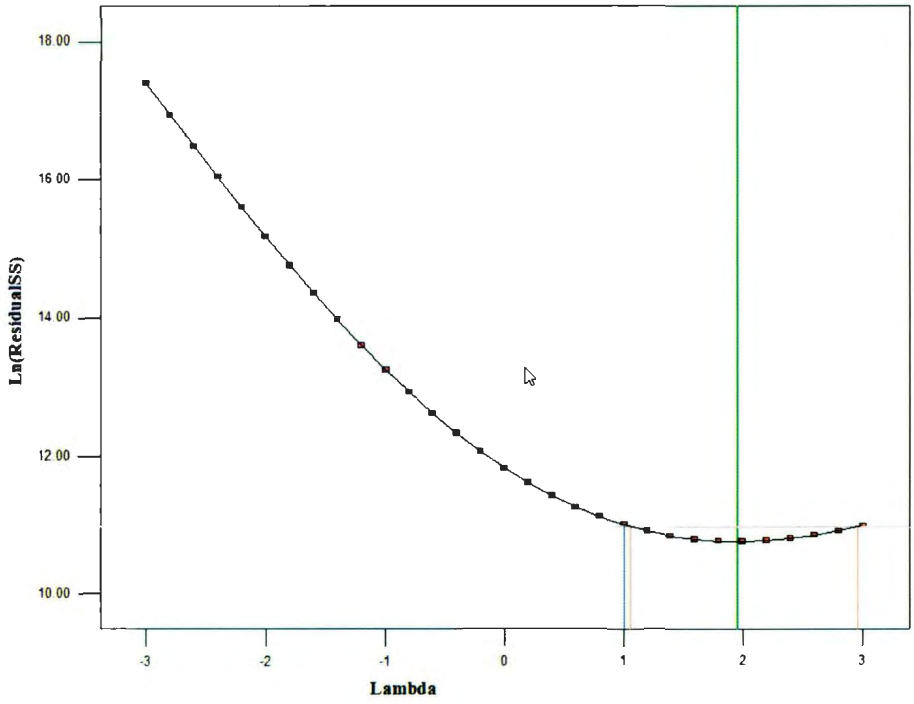


**Figure 5-31: Box Cox plot of plate energy**

Table 5-16 summarizes the statistics for the plate energy response surface model. The adjusted- R-squared value is in fully agreement with the predicted R-squared value. Also the adequate precision value is greater than 4, which indicated the model is adequate within the design space.

**Table 5-16: Statistics of crushing energy response surface model**

| Parameter | Value |
|---|---|
| R-Squared | 0.81 |
| Adjusted R-Squared | 0.78 |
| Predicted R-Squared | 0.75 |
| Adequate Precision | 17.00 |
| Standard Deviation | 23068.63 |
| Mean | 89932.17 |
| Coefficient of Variation | 25.65 |

*All values are based on transformed response

The following linear regression equation was generated by Design Expert.

$$\boldsymbol{Plate\ Energy} = (\boldsymbol{2.5868E05 - 2.1453E05 * A - 2049.59 * B})^{\frac{1}{1.96}} \quad \textbf{[5-5]}$$

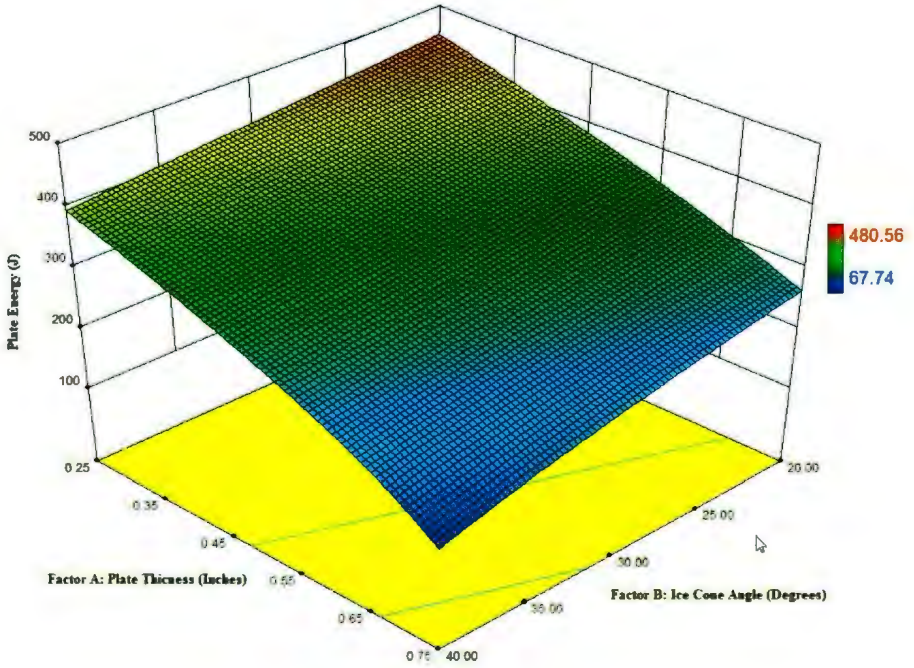


**Figure 5-32: Response surface of plate energy**

### 5.6.4 Specific Energy Absorbed

The specific energy absorbed during the pendulum impact tests is presented in Figure 5-33. The specific energy was calculated using Equation 4-9. Table 5-17 includes the data used to create Figure 5-33.

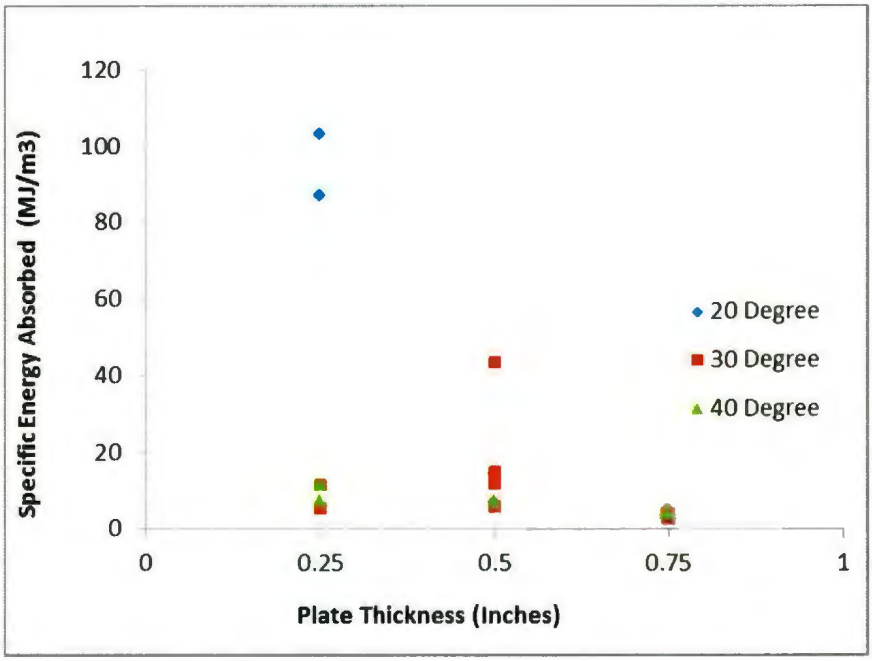


**Figure 5-33: Specific energy absorbed plot**

**Table 5-17: Specific energy absorbed values**

| Run # | Cone Angle (degrees) | Plate Thickness (inches) | Specific Energy Absorbed ($MJ/m^3$) |
|---|---|---|---|
| 8 | 20 | 0.25 | 102.69 |
| 9 | 20 | 0.25 | 86.76 |
| 13 | 20 | 0.5 | 6.56 |
| 15 | 20 | 0.5 | 13.92 |

| Run # | Cone Angle (degrees) | Plate Thickness (inches) | Specific Energy Absorbed ($MJ/m^3$) |
|---|---|---|---|
| 1 | 20 | 0.75 | 4.47 |
| 17 | 20 | 0.75 | 4.52 |
| 2 | 30 | 0.25 | 5.52 |
| 12 | 30 | 0.25 | 11.32 |
| 6 | 30 | 0.5 | 11.62 |
| 16 | 30 | 0.5 | 43.24 |
| 18 | 30 | 0.5 | 5.81 |
| 19 | 30 | 0.5 | 14.89 |
| 21 | 30 | 0.5 | 5.60 |
| 3 | 30 | 0.75 | 3.80 |
| 4 | 30 | 0.75 | 2.62 |
| 5 | 40 | 0.25 | 7.19 |
| 14 | 40 | 0.25 | 11.21 |
| 7 | 40 | 0.5 | 6.68 |
| 10 | 40 | 0.5 | 7.05 |
| 11 | 40 | 0.75 | 3.75 |
| 20 | 40 | 0.75 | 4.08 |

The mass loss during collision is presented in Table 5-18. The specific energy appears to be dependent on the angle of the ice specimen and the thickness of the plate. Smaller cone angles may provide higher specific energy. In general, the 20 degree ice specimens showed evidence of decreased loss of mass after collision and forces were larger relative to the 40 degree ice specimens (Figure 5-4).

**Table 5-18: Ice Specimen mass lost from impact**

| Run # | Cone Angle (degrees) | Plate Thickness (inches) | Ice Specimen mass Lost (g) |
|---|---|---|---|
| 8 | 20 | 0.25 | 1.00 |
| 9 | 20 | 0.25 | 1.00 |
| 13 | 20 | 0.5 | 40.00 |
| 15 | 20 | 0.5 | 20.00 |
| 1 | 20 | 0.75 | 110.00 |
| 17 | 20 | 0.75 | 114.00 |
| 2 | 30 | 0.25 | 24.00 |
| 12 | 30 | 0.25 | 10.00 |
| 6 | 30 | 0.5 | 24.00 |
| 16 | 30 | 0.5 | 9.00 |
| 18 | 30 | 0.5 | 65.00 |
| 19 | 30 | 0.5 | 17.00 |
| 21 | 30 | 0.5 | 58.00 |
| 3 | 30 | 0.75 | 122.00 |
| 4 | 30 | 0.75 | 187.00 |
| 5 | 40 | 0.25 | 24.00 |
| 14 | 40 | 0.25 | 14.00 |
| 7 | 40 | 0.5 | 46.00 |
| 10 | 40 | 0.5 | 42.00 |
| 11 | 40 | 0.75 | 121.00 |
| 20 | 40 | 0.75 | 120.00 |

### 5.6.4.1 Response Surface Model

Table 5-18 below presents the ANOVA table for specific energy. Plate thickness was the only term found to be significant in the response surface model. All other terms had a P

value greater than 0.05 except $A^2$. Due to the principle of hierarchy, term $A^2$ was removed from the model. Only term A is included in the response surface model.

**Table 5-19: Analysis of variance table for specific energy**

| Source of Variation | Sum of Squares | Degrees of Freedom | Mean Square | F Value | P Value |
|---|---|---|---|---|---|
| A: Plate Thickness | 0.098 | 1 | 0.098 | 30.59 | <0.0001 |
| B: Cone Angle | 9.697E-03 | 1 | 9.697E-03 | 3.04 | 0.1019 |
| AB | 2.460E-03 | 1 | 2.460E-03 | 0.77 | 0.3940 |
| $A^2$ | 0.023 | 1 | 0.023 | 7.05 | 0.0180 |
| $B^2$ | 4.921E-03 | 1 | 4.921E-03 | 1.54 | 0.2335 |
| Error | 0.048 | 15 | 3.193E-03 | | |
| Lack of Fit | 0.013 | 3 | 4.446E-03 | 1.54 | 0.2540 |
| Pure Error | 0.035 | 12 | 2.88-E-03 | | |
| Total | 0.18 | 20 | | | |

Figure 5-34 shows the effect plot of plate energy for Factor A, plate thickness. Plate thickness exhibited a negative impact on specific energy.

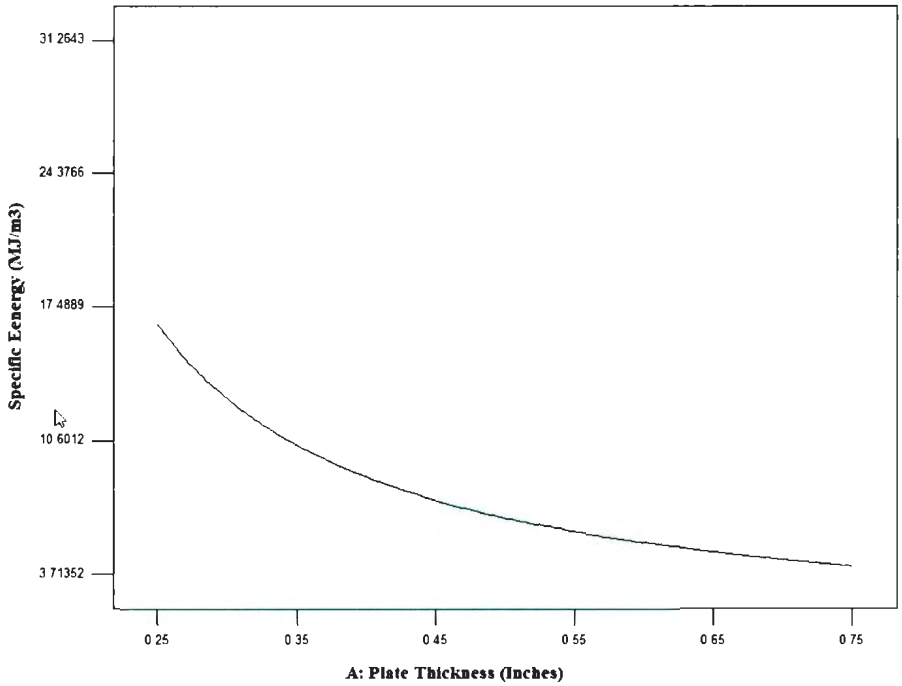


**Figure 5-34: Specific energy main effect plot for factor A**

The diagnostic can be found in Appendix B. An inverse transform was implemented with lambda equal to -1 according to the Box-Cox plot shown in Figure 5-35.

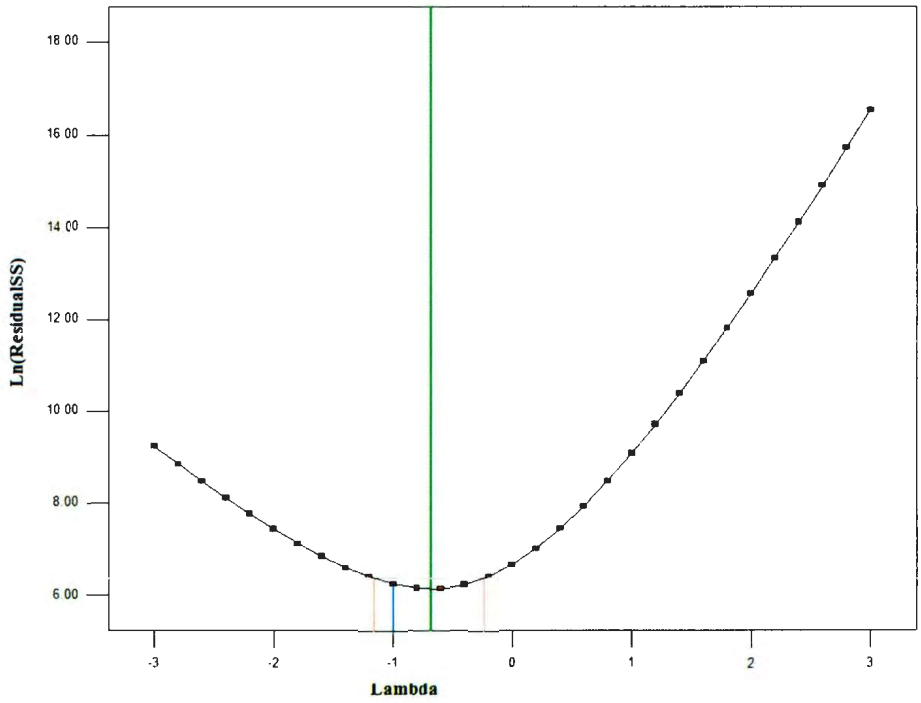


**Figure 5-35: Box Cox plot of specific energy**

The plots did not indicate any major concerns. Table 5-19 summarizes the statistics for the specific energy response surface model. The adjusted- R-squared value is in fully agreement with the predicted R-squared value. Also the adequate precision value is greater than 4, this indicate the model is adequate within the design space. However the R-squared values are very low due to scatter. This is present in the predicted versus actual plot in Appendix B5. However the specific energy trends determined through the analysis was proved significant by ANOVA.

**Table 5-20: Statistics of specific energy response surface model**

| Parameter | Value |
|---|---|
| R-Squared | 0.54 |
| Adjusted R-Squared | 0.51 |
| Predicted R-Squared | 0.43 |
| Adequate Precision | 8.79 |
| Standard Deviation | 0.066 |
| Mean | 0.15 |
| Coefficient of Variation | 44.14 |

*All values are based on transformed response

The following linear regression equation was generated by Design Expert.

$$\boldsymbol{Specific\ Energy} = (-\mathbf{0.0298} + \mathbf{0.361}\boldsymbol{A})^{-1} \qquad \textbf{[5-6]}$$

# 6 ICEBERG SPECIMEN TESTS

Ice berg specimens collected from the Northern Peninsula of Newfoundland in 2011 were shaped into 4 conical specimens for testing in the pendulum impact apparatus. These tests results were compared with the laboratory specimens in terms of force traces, crushing energy, and nominal pressures.

## 6.1 Preparation of Iceberg Specimens

Iceberg samples were wrapped in plastic and stored in a refrigerated shipping container before experimentation. Figure 6-1 presents the original iceberg sample used in the pendulum impact experiments.

**Figure 6-1: Iceberg sample prior to shaping into conical specimens**

The iceberg samples were cut into four 26cm diameter by approximately 20 cm high cylindrical specimens. Then the 4 cylindrical iceberg specimens were frozen into an aluminum ice holder and shaped into 30 degree ($\alpha=30^{o}$) samples using the procedure for shaping the laboratory ice samples. Figure 6-2 below presents a cylindrical iceberg specimens before (left) and after (right) shaping.

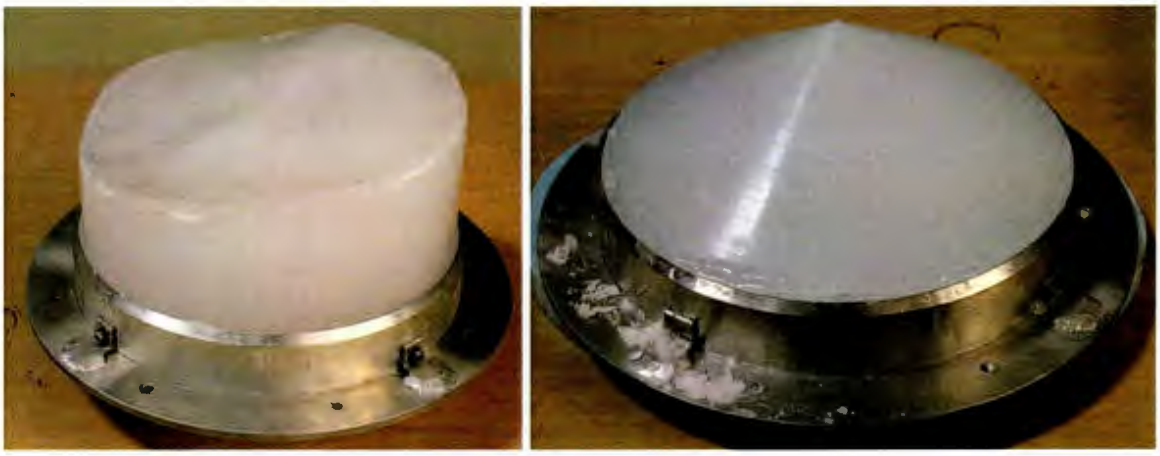

**Figure 6-2: Iceberg specimen before and after shaping into 30 degrees cone**

## 6.2 Testing of Iceberg Specimens

Test procedures were the same as the laboratory ice impact tests in all aspects. Table 6-1 contains the experimental test plan used in testing the iceberg specimens. A 0.75" steel impact plate was selected to avoid plastic deformation in the plate, due to the limited number of impact plates available.

**Table 6-1: Experiment test plan for iceberg specimen tests**

| Run # | Cone Angle (degrees) | Plate Thickness (inches) |
|---|---|---|
| 001 | 30 | 0.75 |
| 002 | 30 | 0.75 |
| 003 | 30 | 0.75 |
| 004 | 30 | 0.75 |

## 6.3 Results and Discussion

The forces traces, pressure area curves and energy analysis results are presented in this section. Figure 6-3 below presents pictures of a laboratory ice specimen Run 4 (left) and iceberg specimen test 004 (right) after the impact tests. The iceberg specimen displayed more spalling than the laboratory ice specimen. This may have been due to the larger grain size of the iceberg specimen.

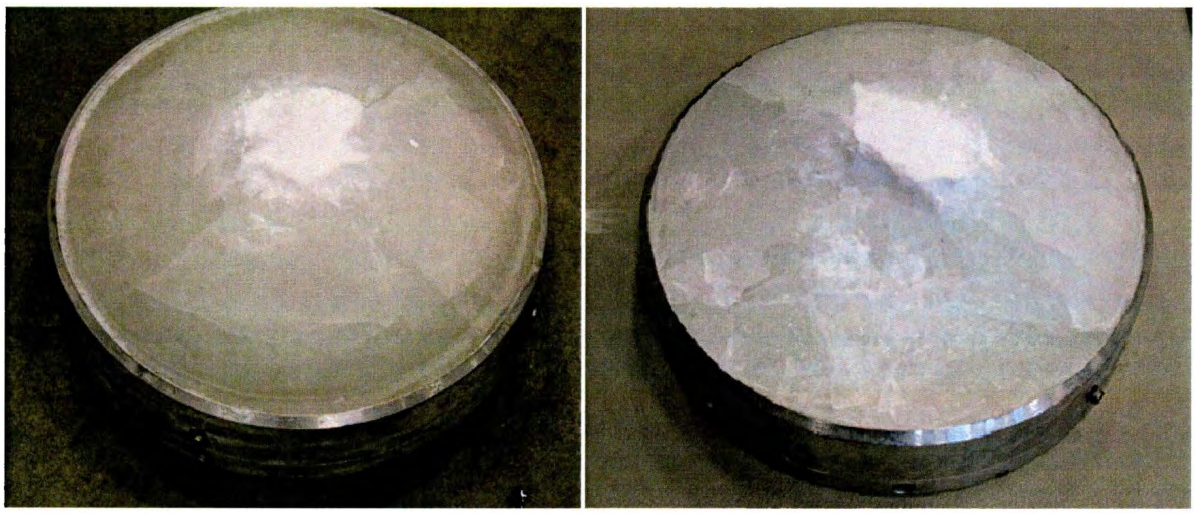

**Figure 6-3: Laboratory (left) and iceberg ice specimen (right) after impact tests**

### 6.3.1 Force Traces

Figure 6-4 below contains the force trace of the 30 degree conical iceberg specimen impacted with the 0.75" thick steel impact plate. Tests 001 and 002 displayed a singular peak, while tests 002 and 004 display two peaks.

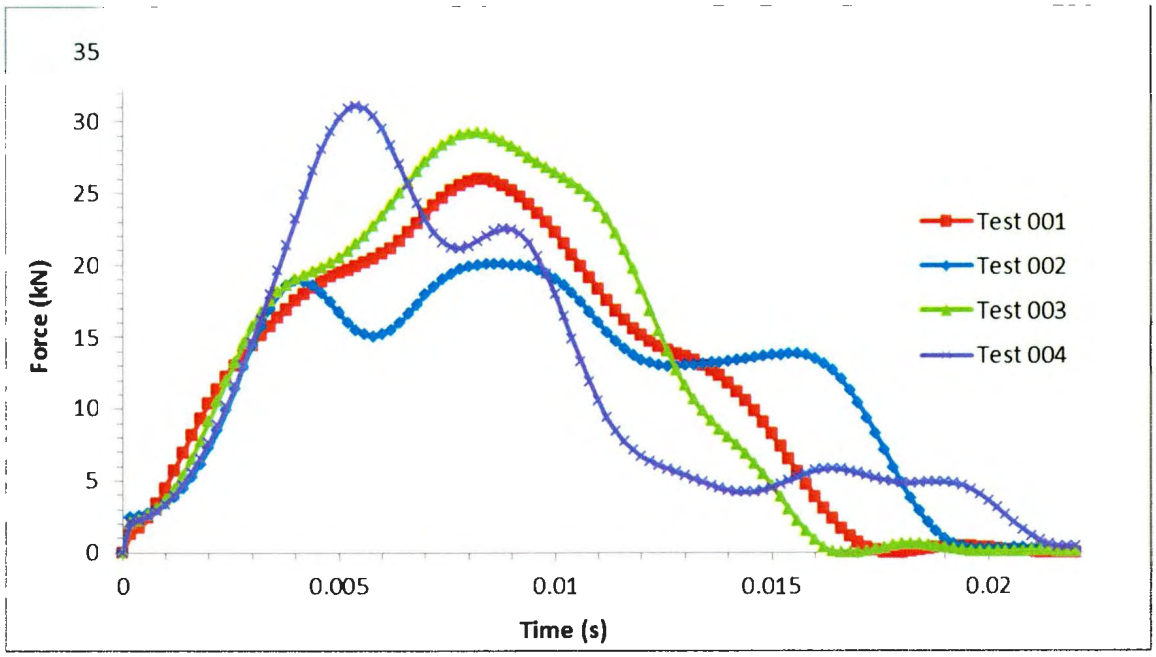


**Figure 6-4: Force trace of iceberg specimens**

Table 6-2 following table contains of peak forces from the iceberg specimens. The peak forces range from 20.0 to 31.1 kN.

**Table 6-2: Peak force values of iceberg specimens**

| Run | Cone Angle (degrees | Plate Thickness (inches) | Peak Force (kN) |
|---|---|---|---|
| 001 | 30 | 0.75 | 25.9 |
| 002 | 30 | 0.75 | 20.0 |
| 003 | 30 | 0.75 | 29.2 |
| 004 | 30 | 0.75 | 31.1 |

Figure 6-5 below contains the peak forces from the laboratory and iceberg specimens. Lower peak forces were observed in the iceberg specimens.

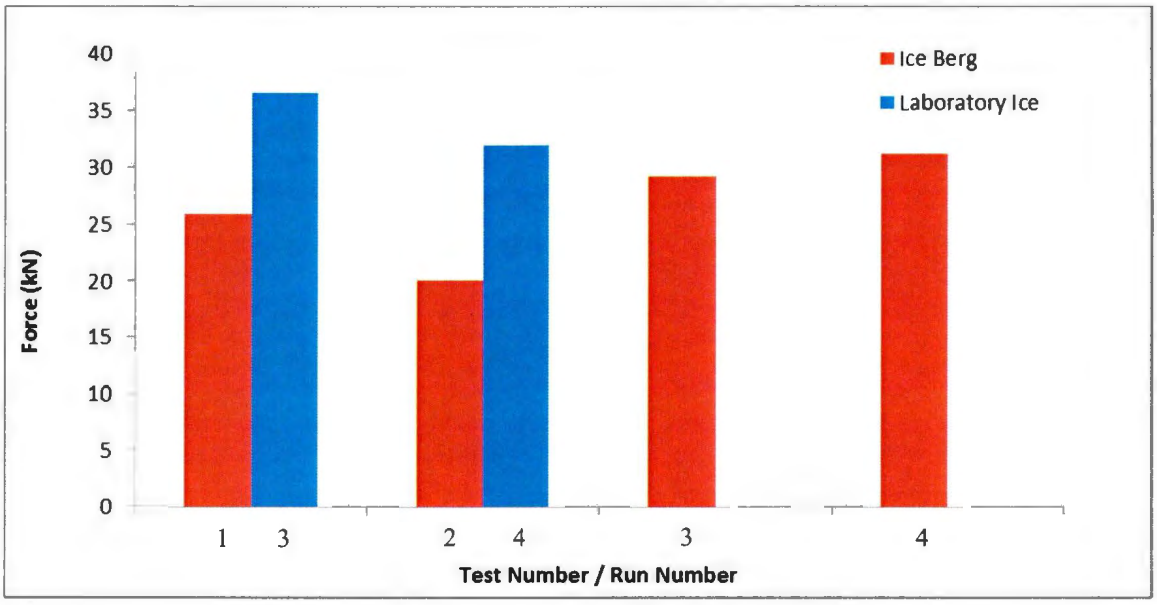


**Figure 6-5: Peak forces of laboratory ice specimens and iceberg specimens**

### 6.3.2 Pressure Area Curves

Table 6-3 and Figure 6-6 presents the pressure area curves and corresponding parameters generated from the 4 iceberg specimens implemented in the pendulum impact apparatus. The data was analyzed consistently with the previous pressure area plots produced from the laboratory ice specimens.

The nominal pressure terms from the iceberg impact tests varied from 1.37 to 3.47 Mpa. Compared with the laboratory specimens the nominal pressures from Runs 3 and 4 were 28.19 and 23.64 Mpa. The larger nominal pressures observed in laboratory ice specimens maybe due to the smaller grain size of the laboratory ice samples.

**Table 6-3: Iceberg pressure area curve parameter values**

| Test # | Nominal Pressure C (Mpa) | Exponent Term (t) | Correlation Coefficient ($R^2$) |
|---|---|---|---|
| 001 | 1.77 | -0.569 | 0.92 |
| 002 | 3.91 | -0.507 | 0.92 |
| 003 | 1.37 | -0.580 | 0.89 |
| 004 | 3.47 | -0.511 | 0.99 |

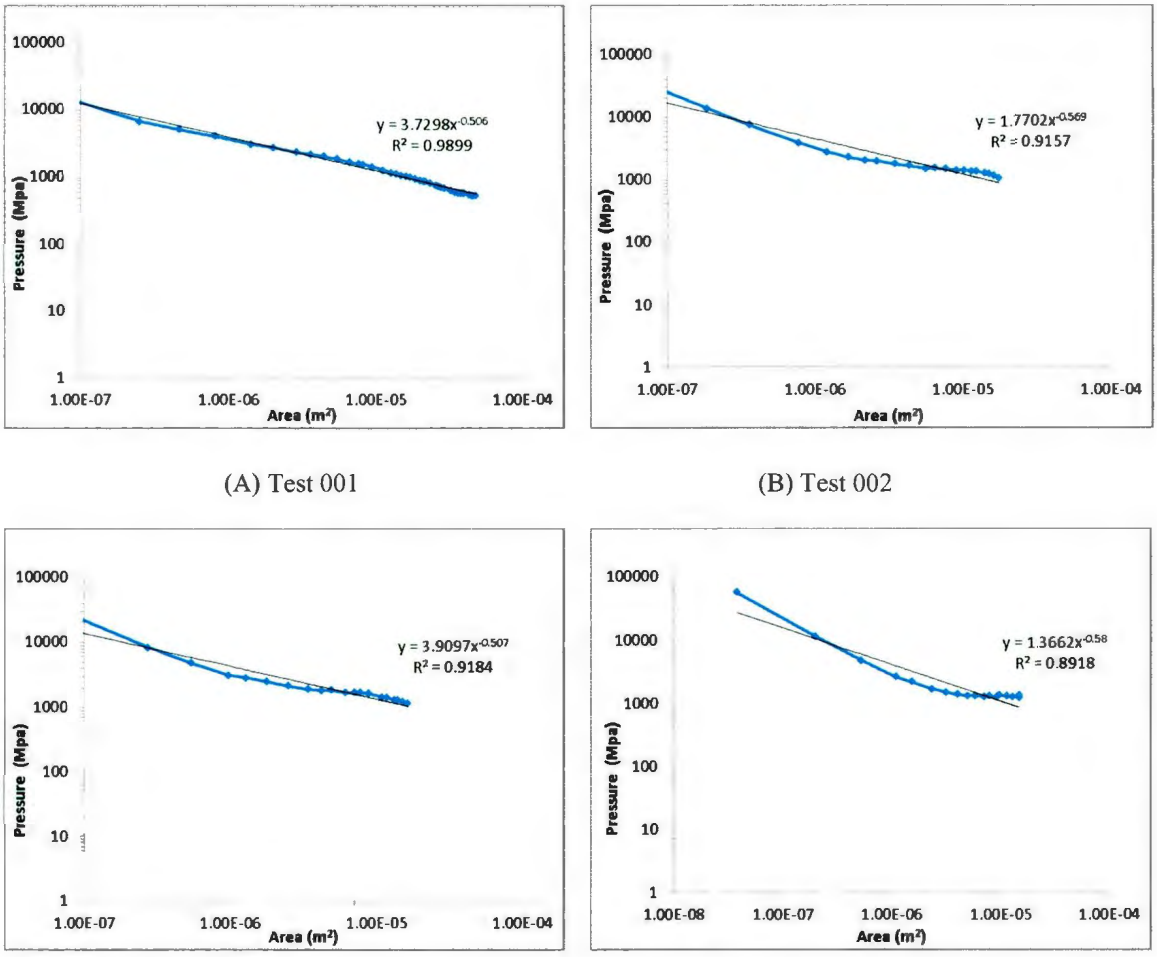


(A) Test 001

(B) Test 002

(C) Test 003

(D) Test 004

**Figure 6-6: Pressure area curves of iceberg specimens**

Figure 6-7 below presents the nominal pressure of the laboratory ice and iceberg specimens. The laboratory ice exhibited significantly higher pressures than the iceberg specimens.

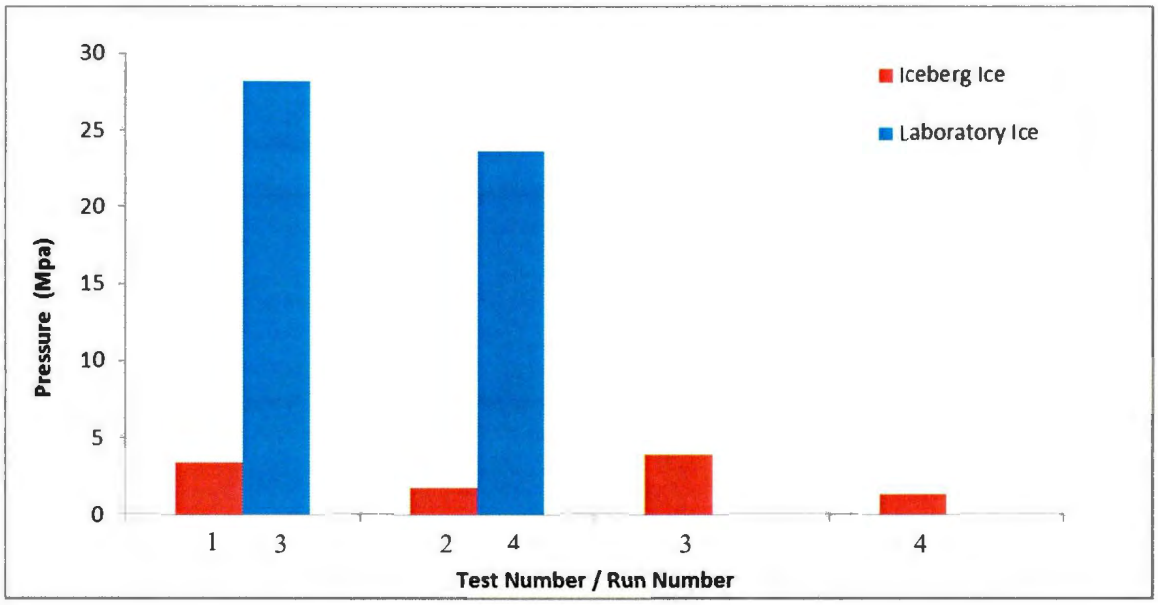


**Figure 6-7: Nominal pressure of laboratory ice vs. iceberg specimen**

Significantly more spalling occurred in the iceberg samples compared with the laboratory ice samples. Larger ice fragments were also observed from the iceberg samples. This phenomenon was evident in the high speed videos. Figure 6-8 compares the difference in the weight of the ice sample before and after the impact for both types of ice specimens. No pre-existing cracks in the iceberg ice where examined by visual inspection before the impact tests. However, non-visible pre-existing flaws and cracks in the iceberg specimens may have also contributed to the lower strength of the iceberg ice. High pressure zones were observed in the center of both iceberg and laboratory ice specimens, indicated by the white zone on each sample.

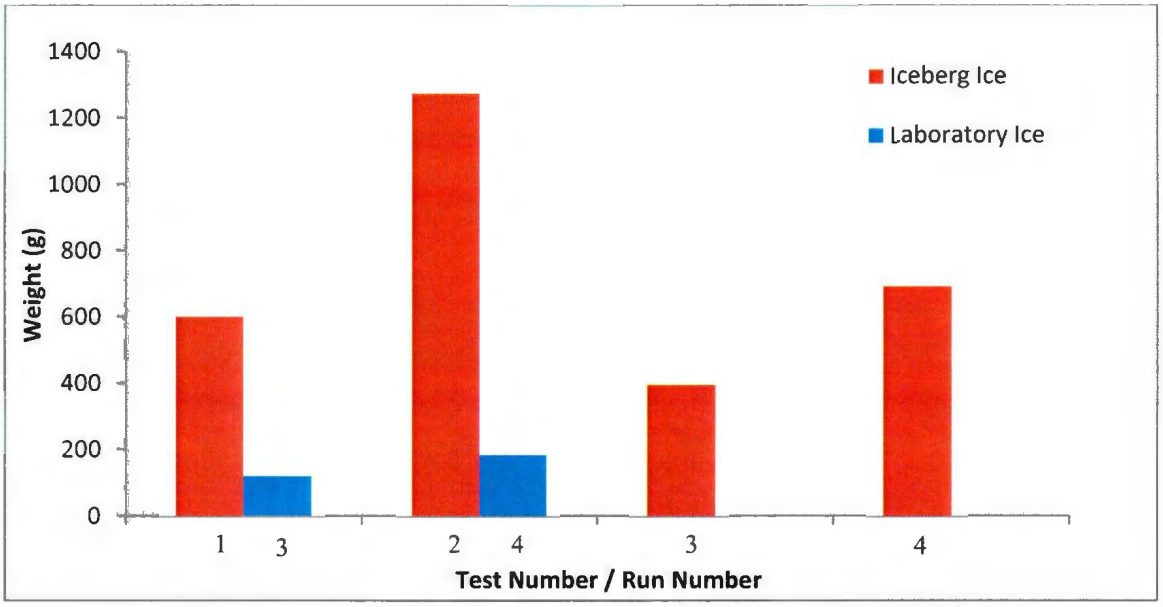


**Figure 6-8: Spall weight of laboratory and iceberg specimens**

### 6.3.3 Energy

Specific energy of the iceberg samples is summarized in Table 6-4 and Figure 6-9 compares the laboratory ice and iceberg specimen specific energy. The iceberg samples exhibited significantly lower specific energy compared with the laboratory ice.

**Table 6-4: Specific energy absorbed of iceberg specimens**

| Run # | Specific Energy Absorbed ($MJ/m^3$) |
|---|---|
| 001 | 0.74 |
| 002 | 0.36 |
| 003 | 1.11 |
| 004 | 0.68 |

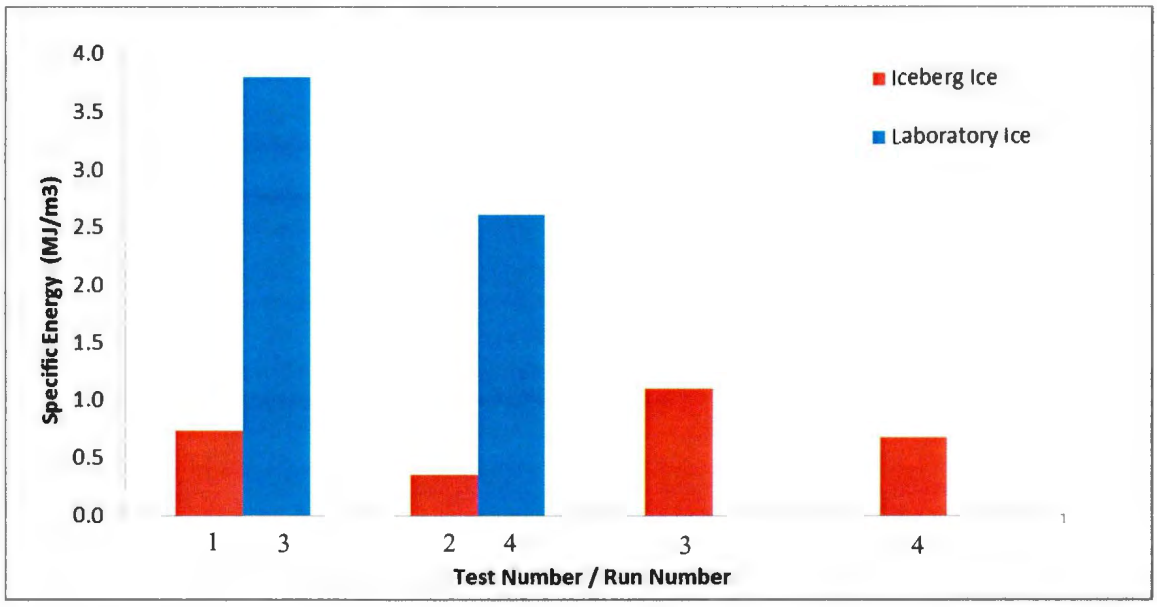


**Figure 6-9: Specific energy of laboratory and iceberg specimens**

# 7 CONCLUSIONS AND RECOMMENDATIONS

## 7.1 Conclusion

In the work covered in this thesis, a new approach was used to measure ice impact loads using a double pendulum apparatus. This apparatus allowed relatively high-energy collisions to be measured with a relatively small apparatus. The results show that the approach and developed impact apparatus allows the impact forces to be measured in a consistent repeatable manner. Also the impact apparatus was shown to produce high quality reliable data that did not raise significant concerns of the influence of the apparatus in the measurements. The measurements were not perfect measurements in regards of measuring the ice-structure loads directly at the contact face. But the ability to measure the motion response of the structural elements, use of a very stiff and responsive load cell in close proximity of the impact zone provides a nearly direct reading of the ice-structure interaction loads. One of the major limitations of the impact apparatus is that the displacements and forces during the experiment cannot be controlled. However, the impact energy can be varied with the pendulum apparatus. In this work the input energy (potential energy) was held constant to focus the study on stiffness. Therefore the impact velocities and total mass of each pendulum were held constant.

The cone shaped ice samples provide a realistic interaction scenario in the sense that the load increases progressively as the contact area of the collision increases. The cone geometry also allowed the ice to spall more naturally compared with a uniform section ice

sample that may cause the ice sample to shatter at impact. There are some uncertainties in determining the apparent contact area as it progressively increases during an impact. However it is more favorable to have a progressive load characteristic which stimulates a more realistic ice-structure interaction scenario.

The results from this thesis, impact experimentation of a conical ice sample with a simplified structure consisting of a simply supported steel plate, have demonstrated that the measured ice load is not an absolute quantity and the apparent load is a function of both the geometry of the ice and the relative compliance of the structure. The results also indicate that the ice cone angle is a form of compliance. In general, a taller ice cone (higher cone angle) is "less stiff" than a shorter the ice cone (lower cone angle).

The data from this study was analyzed using three different methods to quantify the ice loads. Each method was explored to determine the best for presenting the impact results. The three primary methods used are:

- Measured peak force
- Nominal pressure
- Specific energy

In these three methods, both the measured peak force and apparent pressure were shown to be dependent on both the compliance of the structure and geometry of the ice sample. In general, the more "stiff" collision led to higher peak forces and nominal pressures.

However, there is evidence that the ice failure mechanism can limit the effects of reducing stiffness in the collision. The ice strength displayed more dominant load-limit than the structural compliance. This phenomenon of the ice displaying load-limit characteristics was evident in the 40 degree cones where the stiffness of the ice appeared to limit the maximum measured load or pressure.

The nominal pressure data was calculated from the relative displacements and geometry of the ice cone as the collision progressed, this method was based on nominal areas and not the actual contact areas of the collision. This means the data is subjected to more variation and scatter in the pressure-area data. The trends in the nominal pressure data were more pronounced in terms of the "stiffness" of the collision and some cases appeared to be relatively high compared to other reported data, but the results are consistent with the rest of the data in this study. Also, independent of the stiffness in the collision, the trends in apparent pressure showed a decrease in pressure as the collision progressed and contact area increased. This is consistent with most other studies.

Peak force measurements ranged approximately 20 kN to 50 kN while the nominal apparent pressures (referenced at $1m^2$) ranged from approximately 0.1 Mpa (0.25" plate & 40 degree cone) to 90 Mpa (0.75" plate & 20 degree cone). This data shows that the peak force measurements had a relatively narrow range compared to the nominal pressure measurements. Also the peak forces were less scattered and not as pronounced when compared with the nominal pressure results.

The specific energy results were less clear and apparent ice collision energy was higher than the available kinetic energy for the stiffer tests. Specific energy has been shown to be problematic in previous studies and for impact tests it is difficult to quantify elastic, plastic, ice crushing energy and rebound energy in a short period of time. Therefore, in this study, specific energy appears to be less useful for understanding the underlying ice mechanisms due to its complexity.

The following sections discuss the conclusions of the results in more detail.

### 7.1.1 Laboratory Ice Specimens

The measured ice forces from the pendulum impact tests demonstrated that forces of 50 kN can be generated from the impact of two 100 kg objects with closing velocities of approximately 2.15 m/s. The peak forces were shown to vary based on both the compliance of the steel plate and the conical angle of the ice specimen. Based on the statistical analysis, it was concluded that both of these factors were significant. The interaction effect between the two factors was also present. The 20 degree ice specimen produced higher loads than the 40 degree specimen.

The average pressures from the pendulum impact were calculated from the ice displacements and load cell force data from the pendulum impact tests. The nominal pressure value at $1 m^2$ from the process area curve was chosen for analysis. This gave reasonable values for comparison. The statistical analysis of the nominal pressure showed

different variations in trends than the peak force analysis. Both cone angle of the ice specimen, plate compliance and the interaction affect were present in the response surface model. However, the compliance of the plate was observed with a high positive interaction effect with the 20 degree ice specimen and no effect on the nominal pressures from the 40 degree ice specimen. This indicates that the ice "limits" the impact loads in cases where the ice is relatively weak or less "stiff".

Crushing energies have been calculated from the ice specimen geometry and ice crushing displacements from the pendulum impact experiments. In the analysis, the crushing energy exceeded the initial potential energy for the 0.75" plates. The ice crushing energy may have been over estimated when the plate returned to its original position and crushed more ice due to elastic energy stored in the plate. Based on the statistical results, it is concluded that the ice geometry did not have significance in the amount of energy transferred to crush the ice. Compliance of the impact plate was shown to be significant. Results from this report show that higher stiffness had a positive linear effect on the crushing energy. This suggests that more energy is dissipated in crushing the ice for impacts with the stiffer impact plates and more energy was dissipated in deflecting the more compliant plate. Allowing compliance in a structure may be an effective method of mitigating the impact energy.

Energy in the plate was a combination of both plastic and elastic energy. The plate energy at maximum displacement was analyzed with statistical analysis, both the ice specimen

conical angle and compliance of the impact plate were found to be significant. The interaction between the two factors was found to be insignificant. The elastic strain energy in the plate was observed to have significant influence on all the experimental runs.

Specific energy absorbed based on the crushing energy and mass loss due to impact was calculated. The angle of the ice specimen appeared to have a correlation with specific energy. However, the plate compliance was found to significant in determining the specific energy within a confidence interval of 5 percent. As compliance decreased, this was correlated with higher specific energy values.

### 7.1.2 Iceberg Specimens

Four iceberg specimens collected off North West Coast of Newfoundland were shaped at 30 degrees were impacted with a 0.75" impact plate to compare the ice structure interaction with the laboratory ice specimens. Significantly lower peak forces and nominal pressures were observed in the ice berg specimens. Specific energy was also observed to be higher in the ice berg specimens compared with the laboratory ice specimens. The laboratory ice was frozen with a more consistently and smaller grain size than the ice berg specimens. The iceberg specimens spalled into larger fragments, which was evident from the high speed video and photographs. It can be concluded from this that natural ice is generally weaker than the laboratory ice grown for this study.

## 7.2 Recommendations for Future Work

This study explored dynamic ice-structure interactions under simplified conditions and examined a number of methods of presenting the results from the experiments. The data was analyzed statistically with Design of Experiments Methodology and showed distinct trends. However, there are areas that could benefit from future work.

The process pressure-area curves are based on nominal areas. However, the actual area of contact depends on ice spalling and deformation during the impact event. This is difficult to quantify and the next stage would be to determine the actual area during the ice impact and calculate the actual contact pressures. The discrepancies in the calculation of specific energy could not be resolved in this study. Some of the possible causes are:

- Difficulties identifying energy consumption mechanisms
- Difficulties quantifying energy absorbed by the ice
- Slight errors in force or displacement measurements

Additional work of developing methods of measuring the energy balance in impact scenarios is required before the usefulness of the utility of this method can be assessed.

The ice impact experiments in this thesis are preliminary and the interaction scenario was simplified. The trends in the data were clear but there was considerable scatter present. Scatter is a common characteristic of ice strength tests and in general is present in impact

tests. Further experimentation with more complex structural geometry and with other ice shapes would serve to validate the results observed in this study.

The apparent ice strength was observed to be dependent of both the compliance of the structural impact face and the effective "stiffness" of the ice geometry. This provides a preliminary indication that ice loads maybe predicted more accurately by considering the "stiffness" of both contact zones of a the ice-structure interaction. This may have implications for the strength design of structures and the geometry of interacting elements. The study of the implications of these results may guide future experiments or the development of numerical models of ice-structure interactions.

# References

Bai, Y. Y. (1993). Elastic-plastic Behaviour of Offshore Steel Structures Under Impact Loads. *International Journal of Impact Engineering, 13*(1), 99-115.

Baş, D., & Boyacı, İ. H. (2007). Modeling and optimization I: Usability of response surface methodology. *Journal of Food Engineering, 78*(3), 836-845. doi:10.1016/j.jfoodeng.2005.11.024

Brooks, P.N. (1975). The Influence of Static Mechanical Properties on the Resistance of Fresh-water Ice to Ballistic Penetration, Report 4032/75, Defense Research Establishment, Valcartier, Quebec. 29p.

Bruneau, S.E, A.K Dillenburg, S. Ritter, (2011) Ice Specimen Fabrication Techniques and Indentation Experiments, A STePS$^2$ Pilot Laboratory investigation of Ice-Structure Interaction, Internal Report, Memorial University, Sustainable Technology for Polar Ships and Structures (STePS$^2$). St. John's, NL.

Cammaert, A. B., & Muggeridge, D. B. (1988). *Ice interaction with offshore structures*. New York: Van Nostrand Reinhold.

Comfort, G. and Menon, B. (1981). Laboratory Investigation of Ice Impact Pressure. Arctec Canada Ltd., report submitted to Ship Safety Branch, Canadian Coast Guard

Chang, S. S. M. (2000). The principle and applications of piezoelectric crystal sensors. *Materials Science & Engineering.C, Biomimetic and Supramolecular Systems, 12*(1-2), 111-123.

Czitrom, V. (1999). One-factor-at-a-time versus designed experiments. *The American Statistician,* , 126.

Daley, C. (1999). Energy based ice collision forces. *International conference on port & ocean engineering under arctic conditions. proceedings* (pp. 674)

Daley, C. (2004). A study of the process-spatial link in ice pressure-area relationships. Prepared for National Research Council of Canada. PERD/ CHC Report 7-108

El-Tahan, (1984). Strength of Iceberg and Artificial Snow Ice under High Strain Rates and Impact Loads. *Proceedings of the International Offshore Mechanics and Arctic Engineering Symposium, 3*, 158-165.

Gagnon, R. (2004). Analysis of laboratory growler impact tests. *Cold Regions Science and Technology, 39*(1), 1-17.

Gagnon, R. E. (1997). In situ thermal profiles and laboratory impact experiments on iceberg ice. *Journal of Glaciology, 43*(145), 569-582.

Gagnon, R.E. (2008). A New Impact Panel to Study Bergy Bit / Ship Collisions. *Proceedings of 19th IAHR International Symposium on Ice 2008, Vancouver, British Columbia, Canada, Vol. 2,* 783-790.

Gagnon, R., Bugden, A., Ritch, R. (2009). Preliminary testing of a new ice impact panel. *Proceedings of the 20th International Conference on Port and Ocean Engineering under Arctic Conditions, Lulea, Sweden, 9-12 June 2009, POAC09-33: 10 p.*

Gammon, P. H. & Gagnon R.E. (1996). Impact experiments on iceberg ice. *IAHR 96, 13th International Symposium on Ice, Beijing, China.Proceedings, 1*, 62-71.

Gautier, D. D. L. (2009). Assessment of undiscovered oil and gas in the arctic. *Science (New York, N.Y.), 324*(5931), 1175-1179.

Garcia, N.B., Farrell, D. and Mellor, M. (1985). Ice Penetration Tests. Cold Regions Research and Engineering Technology, 11, 223-235.

Gerard, R. (1976). A Simplified Measure of Ice Strength. Third International Symposium on Ice Problems, IAHR, Hanover, NH, U.S.A

Glen, I. F. & Comfort G. (1983). Ice impact pressure and load: Investigation by laboratory experiments and ship trials. *Seventh International Conference on Port and Ocean Engineering Under Arctic Conditions (POAC '83), 5-9 April 1983, Espoo, Finland Proceedings, 1*, 516-533.

Itagaki, K. & Sabourin, R.L (1980). Fracture Behavior of Ice in Charpy Impact Testing. CRREL Report 80-13, 13p

Jordaan, I. J. (1988). Crushing and Clearing of Ice in Fast Spherical Indentation Tests. Paper presented at the *Proceedings of the International Offshore Mechanics and Arctic Engineering Symposium, 4,* 111-116.

Jordaan, I. J. & Mckenna R. F.(1988). Ice Crushing by Impact and Indentation: A Literature Review. National Research Council of Canada, XAQ87-00070(21)/A

Jordaan, I. J. & Garry W. Timco (1988). Dynamics of the Ice-Crushing Process. *Journal of Glaciology, 34(118),*

Kärnä, T. T. (1999). A numerical model for dynamic ice–structure interaction. *Computers & Structures, 72*(4-5), 645-658.

Kawakami, S. (1983). Impact Experiments on Ice. *Journal of Geophysical Research, 88*(b7), 5806-5814.

Kheisin, D. E. (1973). Experimental determination of specific energy of mechanical crushing of ice due to impact. *Probl.Ark.Antark., 41*, 56-61.

Kheisin, D.E. & Likhomanov, V.A (1975). Determination of Specific Breakup Energy and Contact Pressures Produced by the Impact of Solid against Ice. U.S Army Cold regions Research and Engineering laboratory. TL539. English Translation

Kim, E. E. (2012). Mechanisms governing failure of ice beneath a spherically-shaped indenter. *Cold Regions Science and Technology, 78*, 46-63.

Kurdyumov, V.A. & Khesin, D.E. (1976): Hydrodynamic model of the impact of a solid ice. *Pricladnaya Mechanuca*, 12(10), pp103-109.

Masterson, D. M. (1992). The medium scale iceberg impact test program. *IAHR 92.11th International Symposium on Ice, Banff, Alberta, Canada, June 15-19, 1992.Proceedings, 2*, 930-966.

McIntosh, J. A. Young, C.W and Walsh, J. P. (1973). Development of a Sea- Ice Penetrometer. Journal of Petroleum Technology, Vol. 25, 249-256.

Montgomery, D. C. (2009). *Design and analysis of experiments* (7th ed.) John Wiley & Sons.

Montgomery, D. C. (2008). *Design and analysis of experiments [electronic resource]* (7th ed.). Hoboken, NJ: Wiley.

Myers, R. H., & Montgomery, D. C. (2002). *Response surface methodology : Process and product optimization using designed experiments* (2nd ed.). New York: J. Wiley.

Ritch, R. R. (2008). Local ice pressures measured on a strain gauge panel during the CCGS terry fox bergy bit impact study. *Cold Regions Science and Technology, 52*(1), 29-49.

Ross, B (1969). Perforation of the Artic Sea-ice Covered by Projectile Impact. Journal of Hydronautics, Hokkaido University, Sapporo.

Ross, B (1967). *Penetration and Fracture of Sea Ice due to Impact Loading. Physics of Snow and Ice, Proc. Of Intl. Conf. on Low Temperature Science, Hokkaido University, Sapporo.*

Rychnovsky, R. (1987). *Deep Ice Penetrator. Proc. 9th Int. Conf. on Port and Ocean Engineering under Arctic Conditions, Fairbanks, Alaska.*

Sanderson, T. J. O. (1988) *Ice Mechanics: Risk to Offshore Structures.* Graham & Troutman, London UK.

St. John, J.W. (1987). Bering Sea Winter Ice Edge Data Collection Aboard USCGC Polar Sea Volume II: Hull-Ice Impact Loads, Arctec Engineering, Inc., Report No. 1272C

Timco, G. W. G. (1993). Laboratory impact tests on freshwater ice. *Cold Regions Science and Technology, 22*(1), 77-97.

Timco, G.W. & Martin, R. A. (1979) Impact Strength Tests on Ottawa River Ice, NRCA, Division of Mechanical Engineering Report LTR-LT-97, 20p.

Weiss, D. J. (2006). *Analysis of variance and functional measurement [electronic resource]: A practical guide.* Oxford; New York: Oxford University Press.

Yen, Y-C, et al. (1970) *Impact of Spheres on Ice. Proc. A.S.C.E., Eng. Mech. Division, Vol 36, No. EM5, October.*

Young, C.W. (1974). *Penetration of Spheres on Ice. Proc. A.S.C.E., Eng. Mech. Division, Vol. 36, No. EM5 October.*

Yuan, M. M. (2007). An efficient variable selection approach for analyzing designed experiments. *Technometrics, 49*(4), 430-439.

# APPENDIX A:

# UNFILTERED FORCE PLOTS

# Appendix A1:

## Unfiltered Force Trace for 20 Degree Ice Specimens

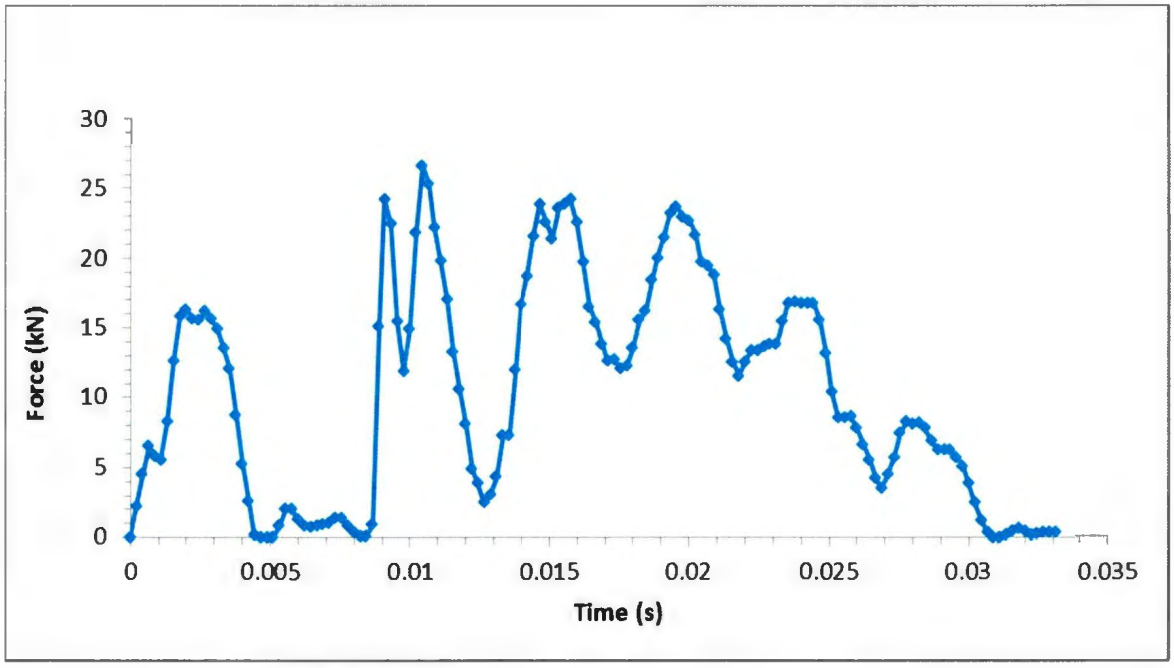


**Run 8: 20 Degree ice specimen impacted with 0.25" plate**

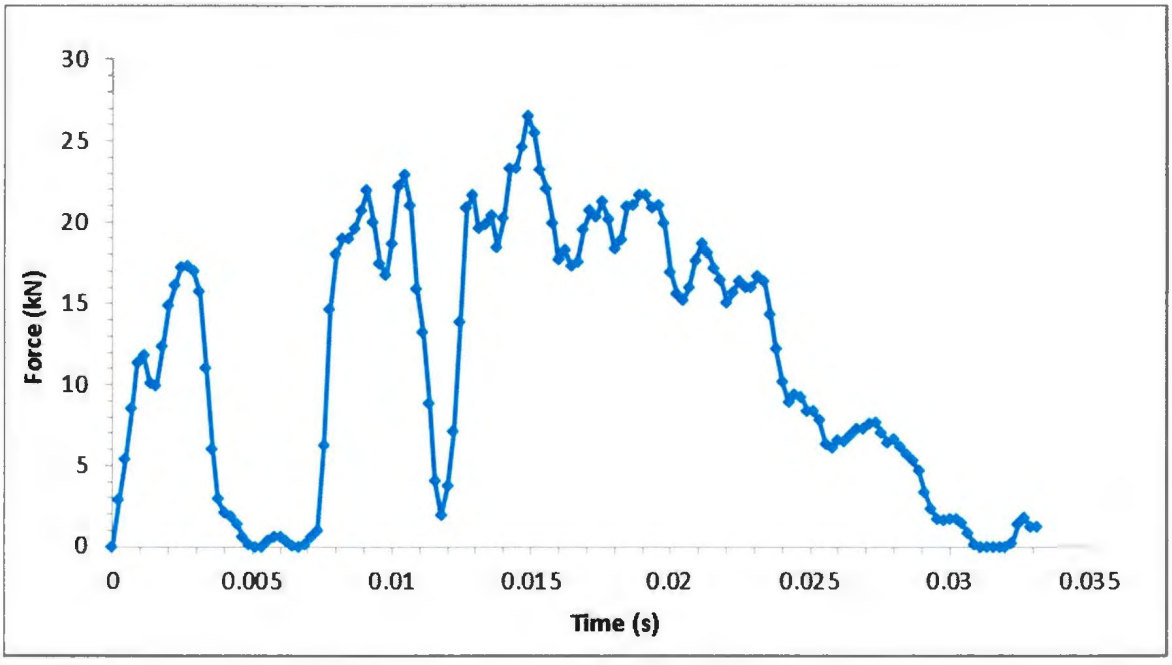


**Run 9: 20 Degree ice specimen impacted with 0.25" plate**

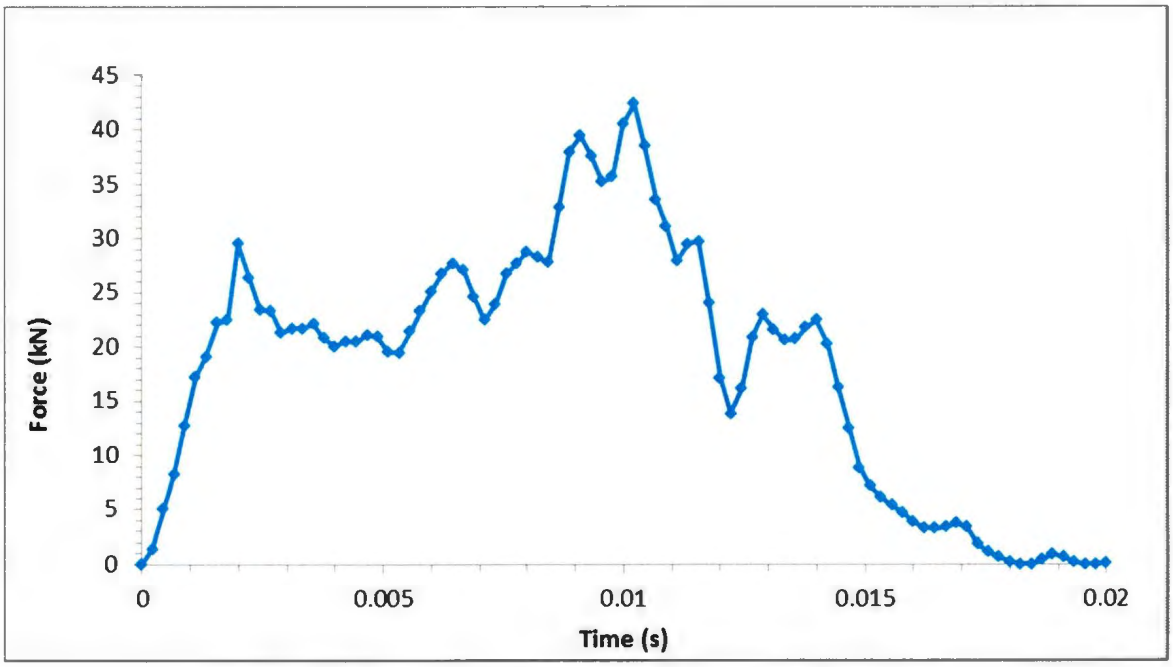


**Run 13: 20 Degree ice specimen impacted with 0.5" plate**

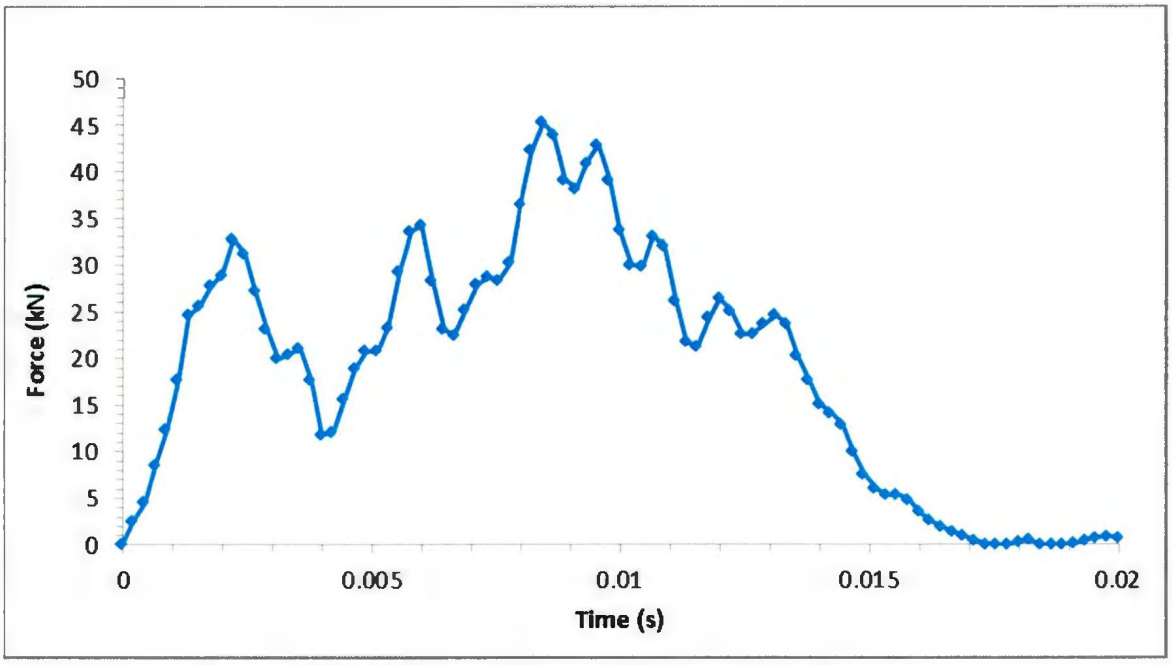


**Run 15: 20 Degree ice specimen impacted with 0.5" plate**

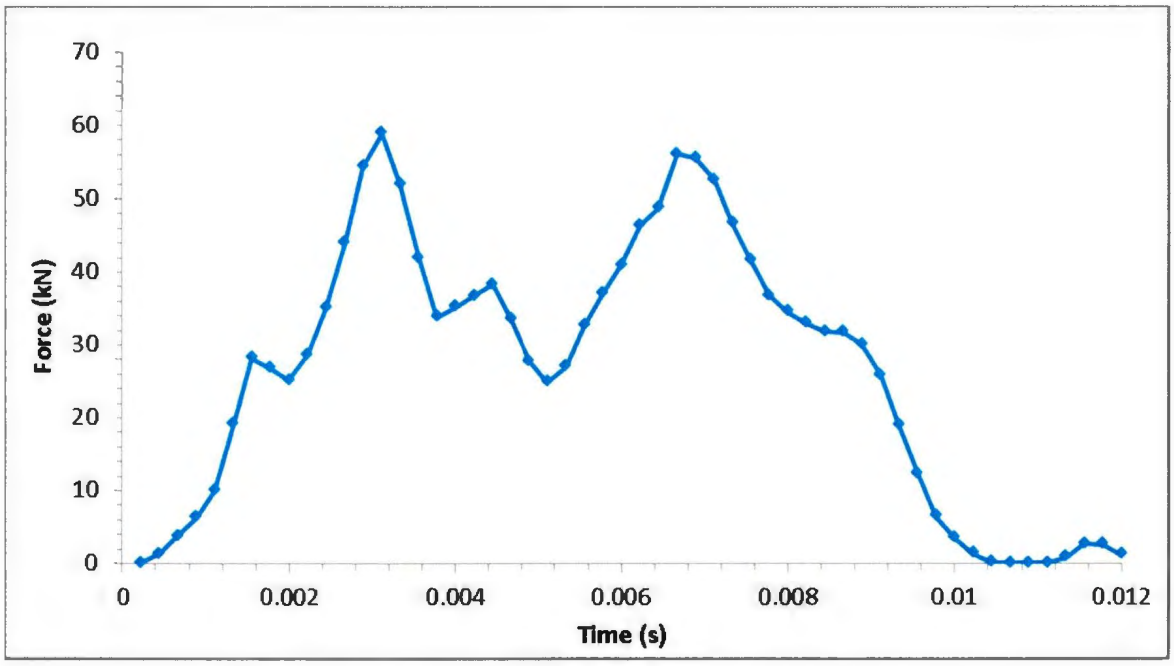


**Run 1: 20 Degree ice specimen impacted with 0.75" plate**

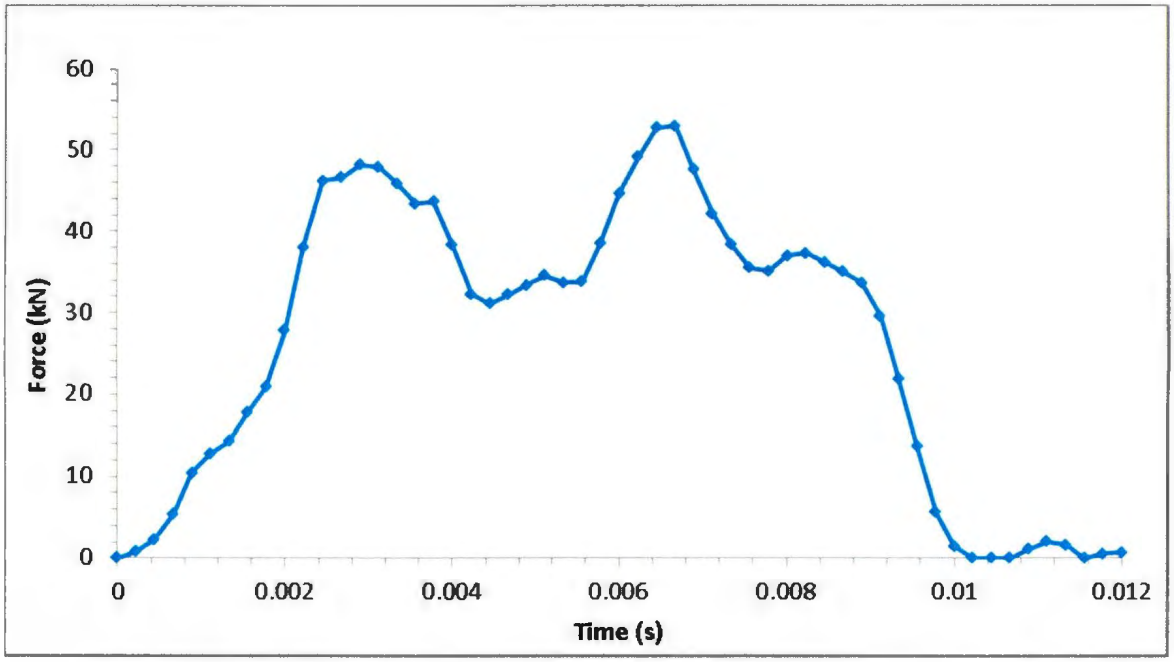


**Run 17: 20 Degree ice specimen impacted with 0.75" plate**

# Appendix A2:

## Unfiltered Force Trace Plots for 30 Degree Ice Specimens

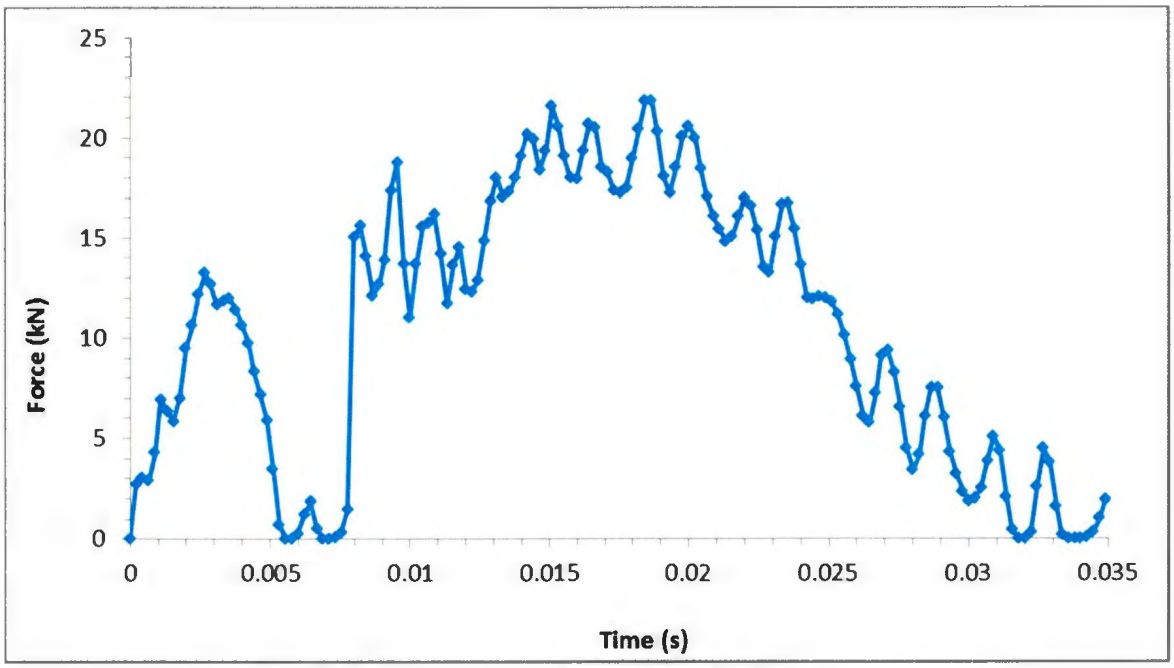


**Run 2: 30 Degree ice specimen impacted with 0.25" plate**

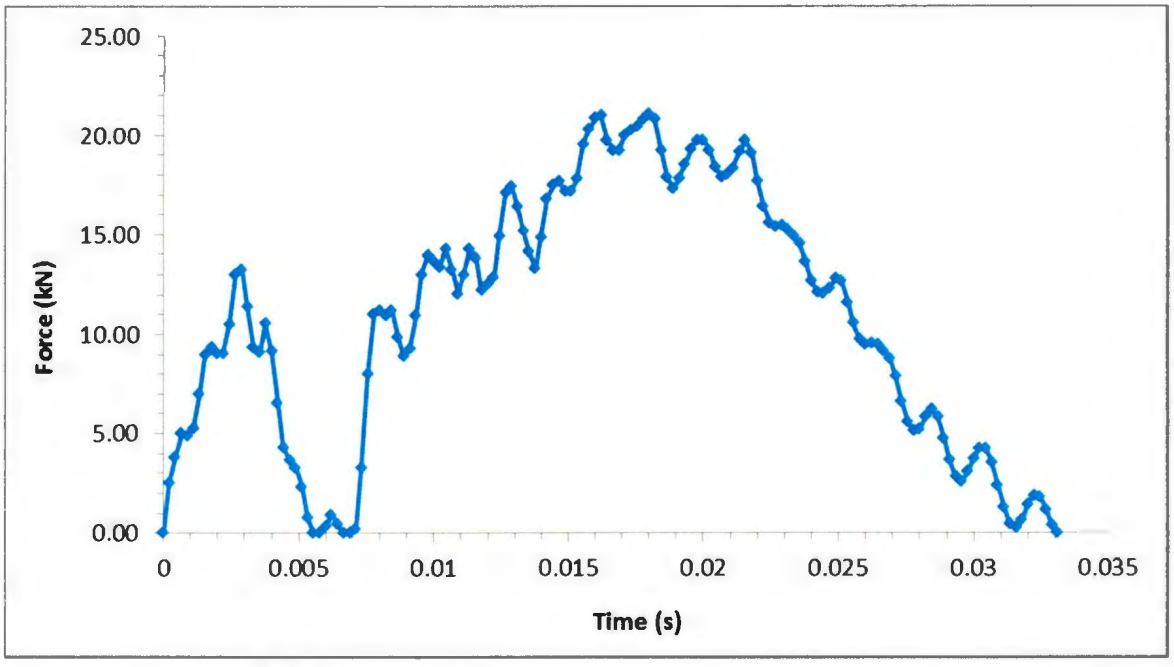


**Run 12: 30 Degree ice specimen impacted with 0.25" plate**

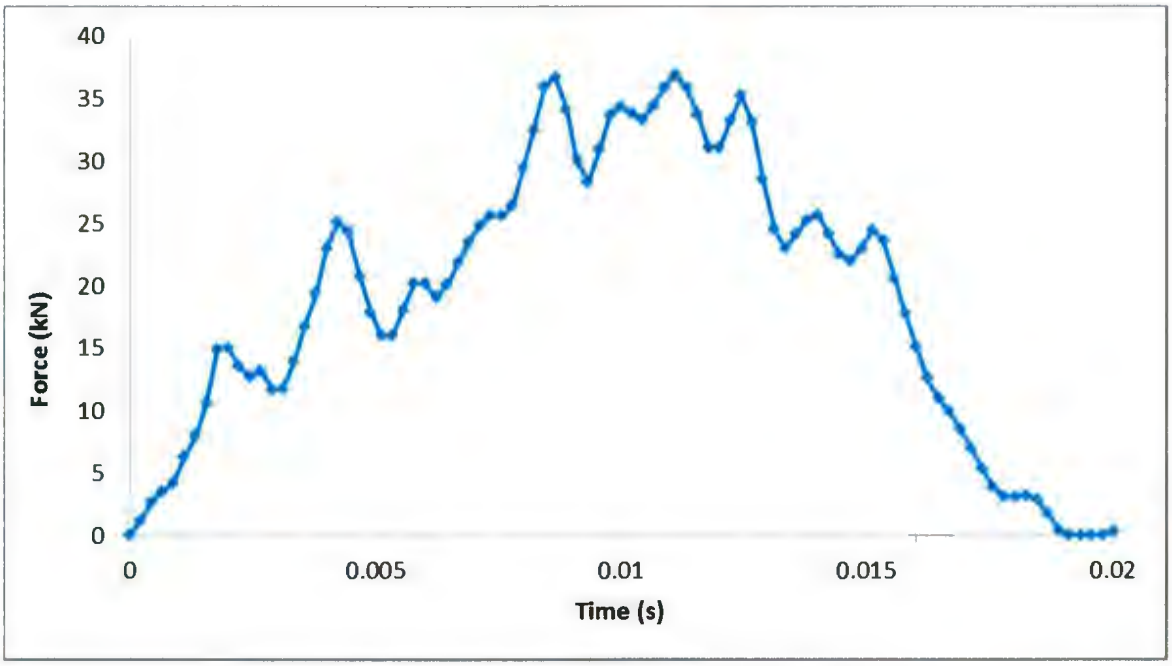


**Run 6: 30 Degree ice specimen impacted with 0.5" plate**

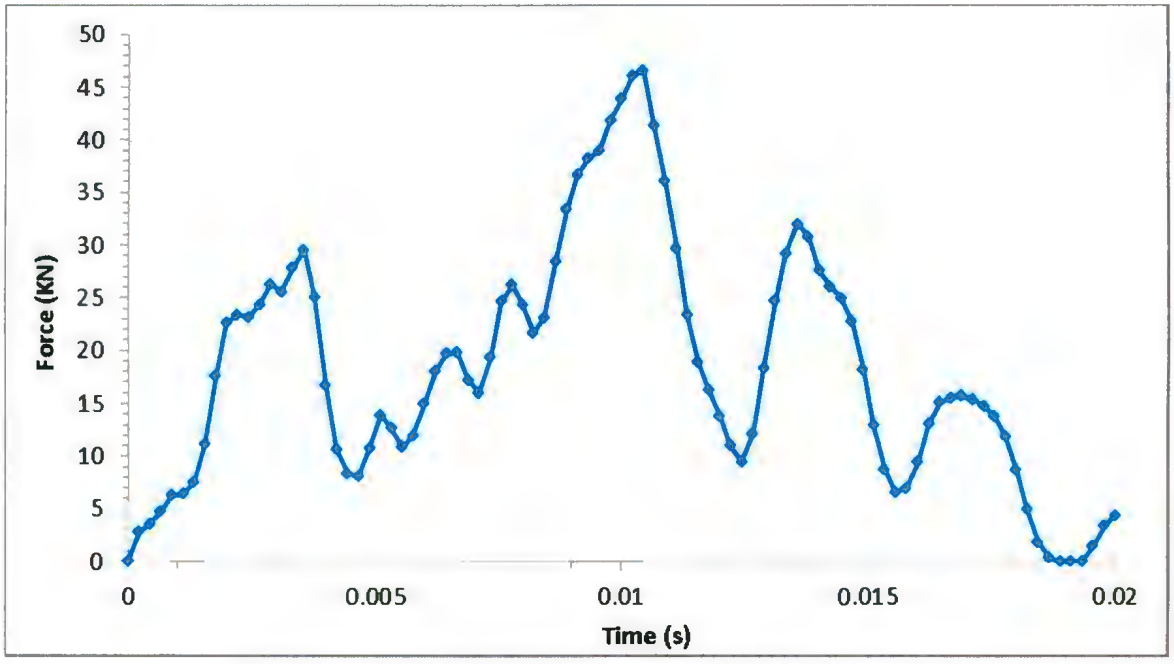


**Run 16: 30 Degree ice specimen impacted with 0.5" plate**

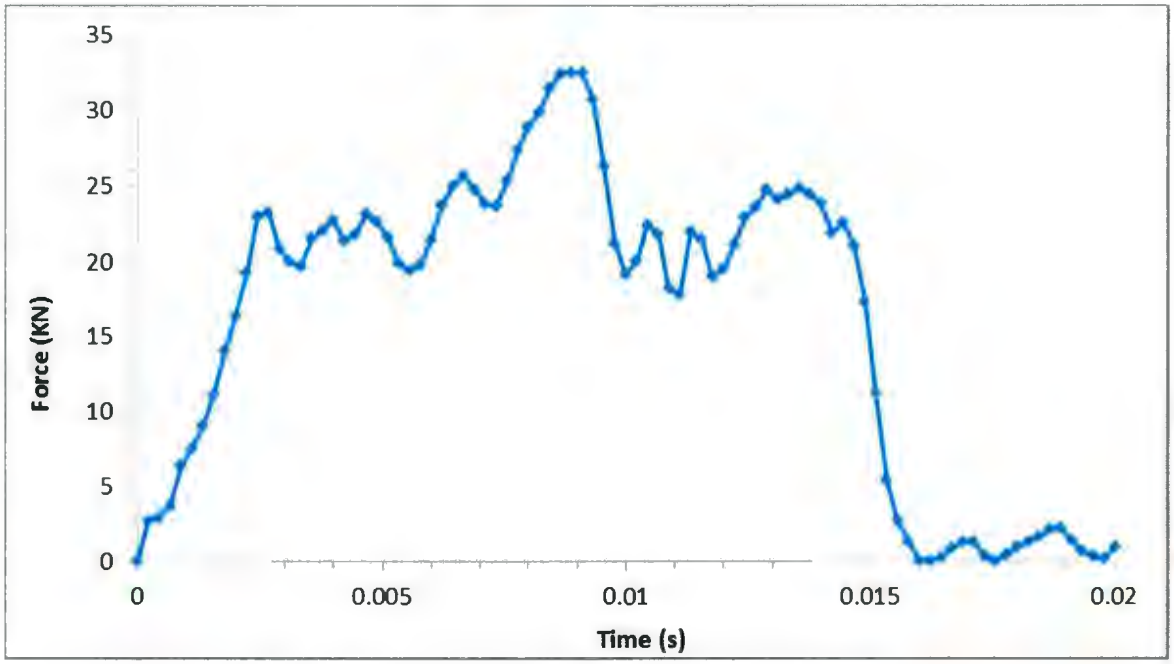


**Run 18: 30 Degree ice specimen impacted with 0.5" plate**

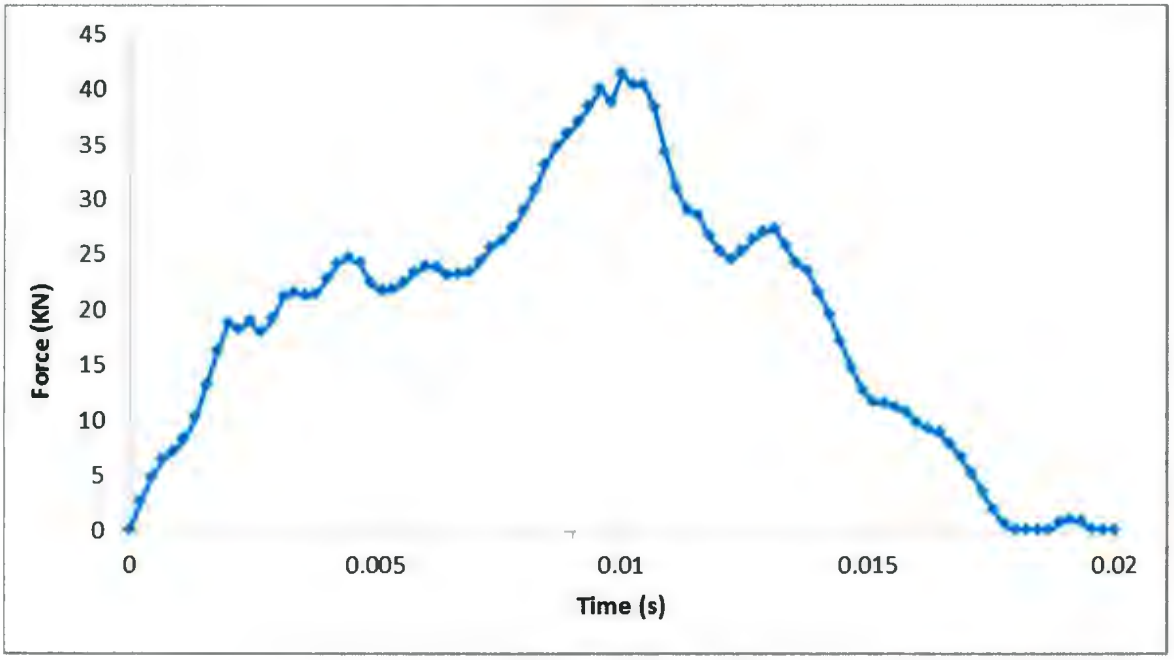


**Run 19: 30 Degree ice specimen impacted with 0.5" plate**

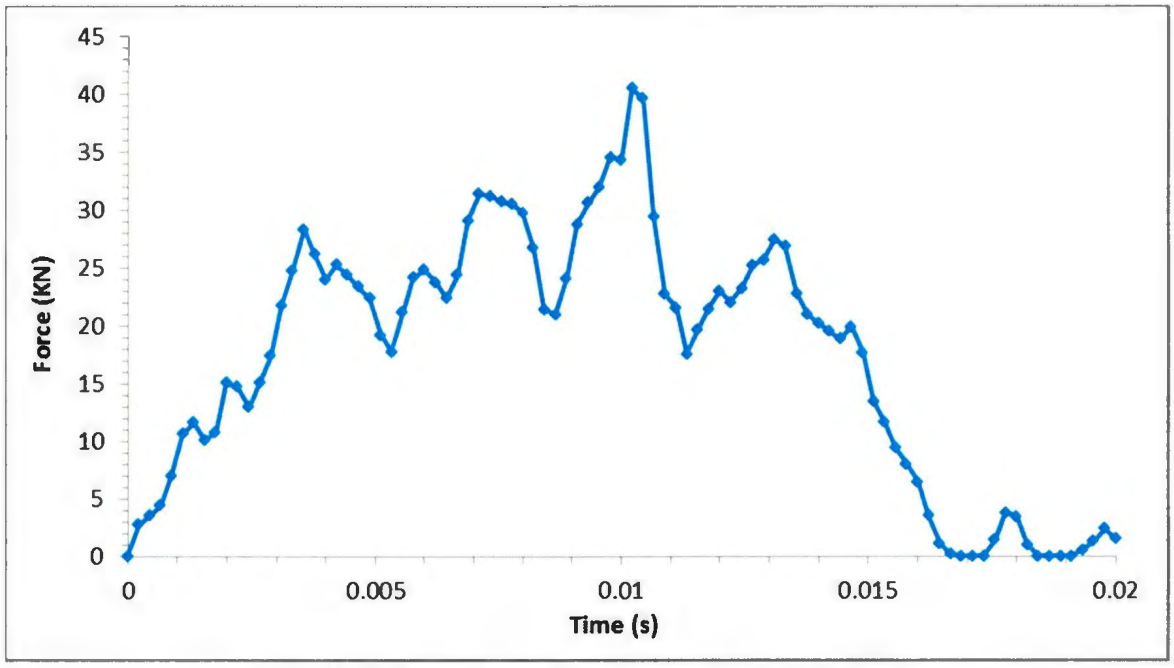


**Run 21: 30 Degree ice specimen impacted with 0.5" plate**

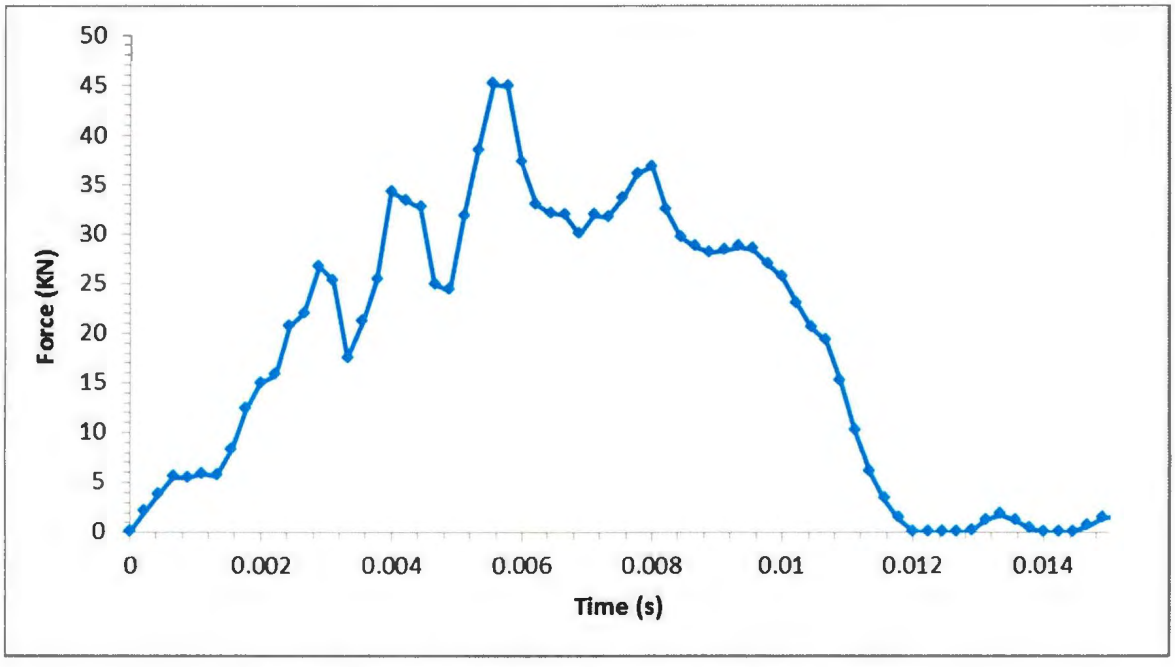


**Run 3: 30 Degree ice specimen impacted with 0.75" plate**

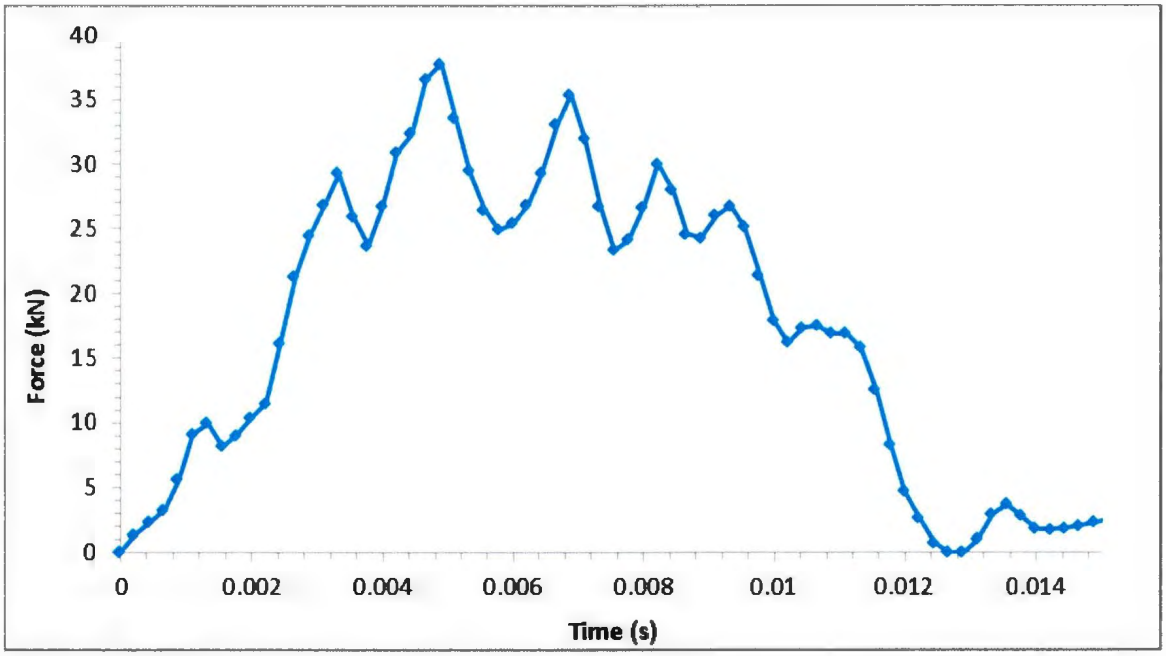


**Run 4: 30 Degree ice specimen impacted with 0.75" plate**

# Appendix A3:

## Unfiltered Force Plots for 40 Degree Ice Specimens

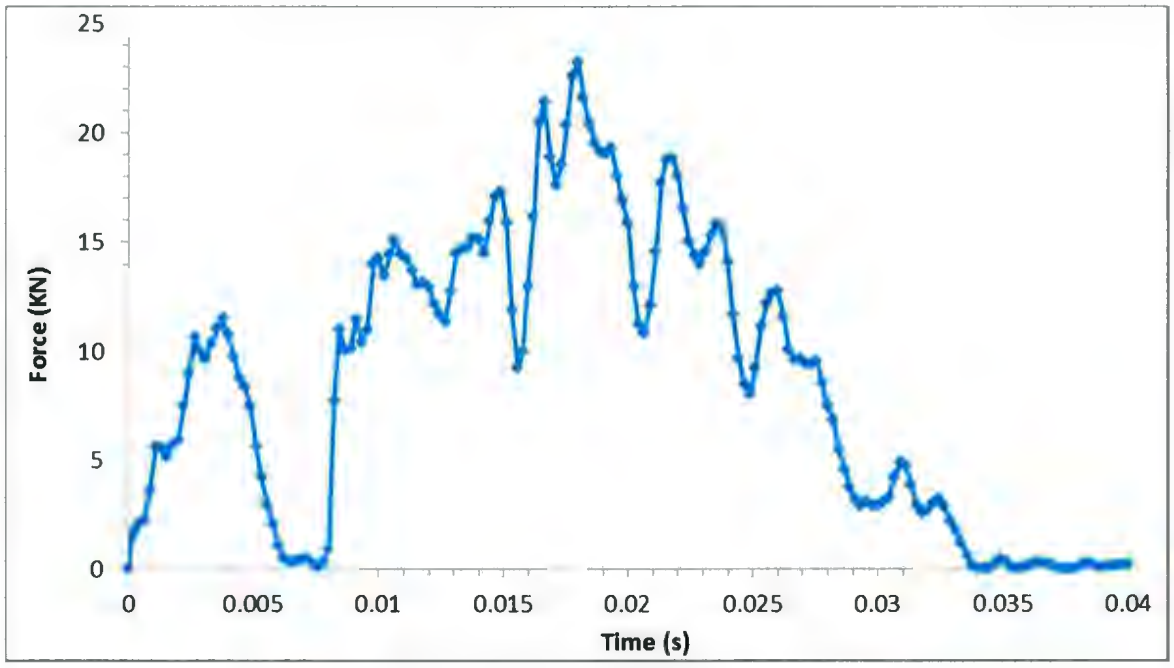


**Run 5: 40 Degree ice specimen impacted with 0.25" plate**

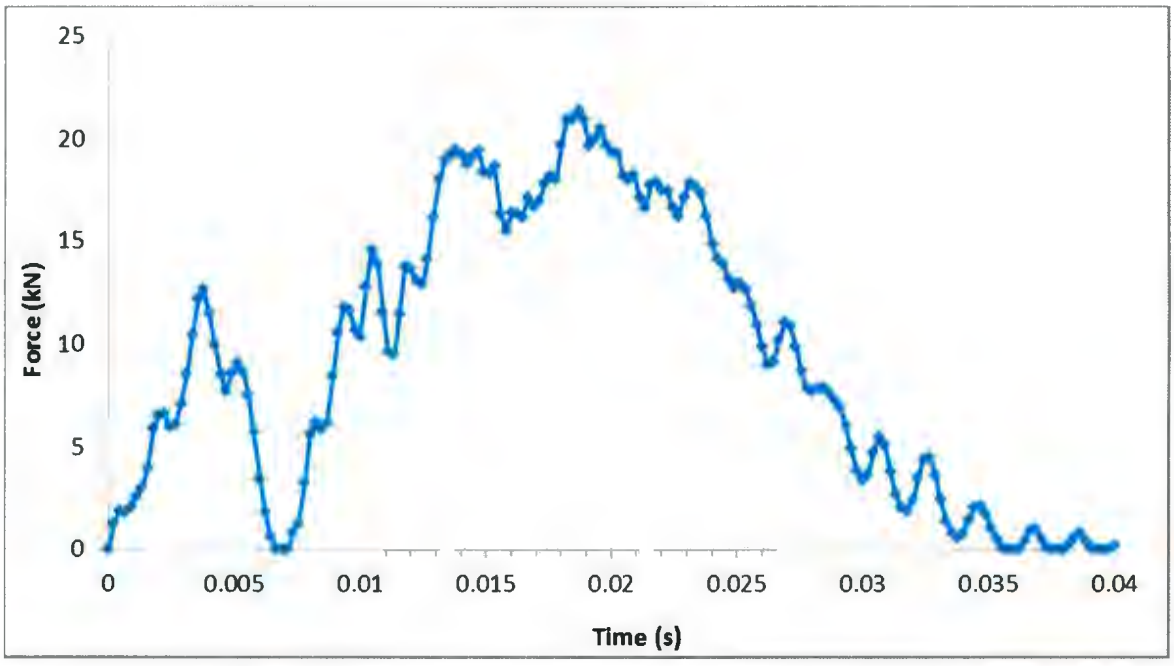


**Run 14: 40 Degree ice specimen impacted with 0.25" plate**

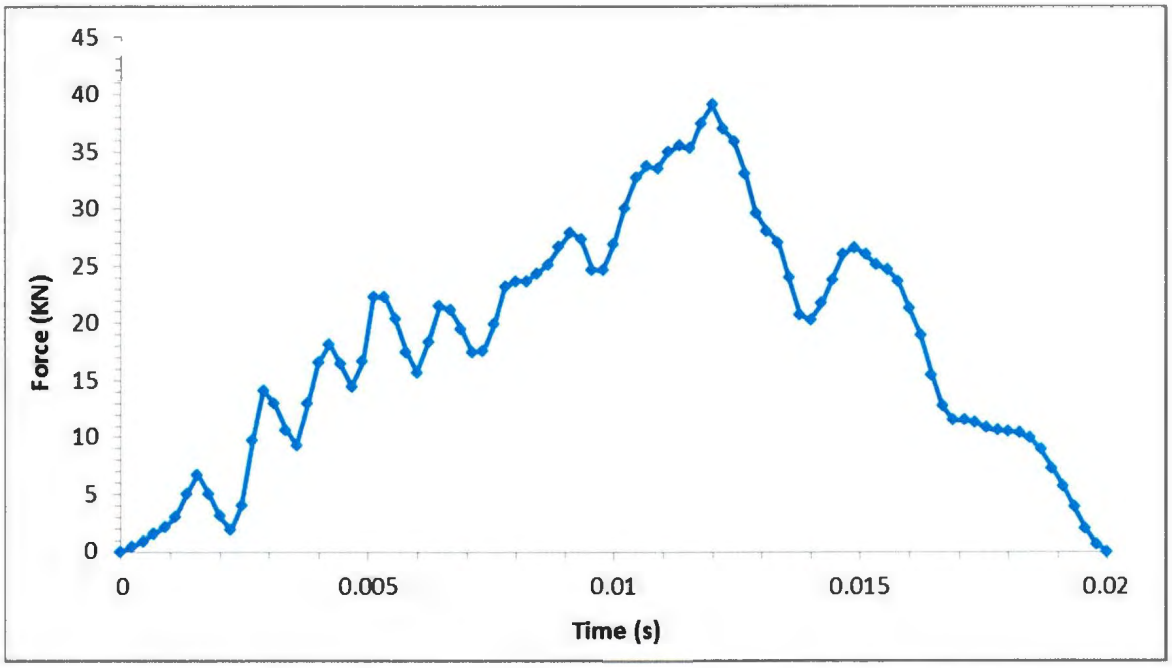


**Run 7: 40 Degree ice specimen impacted with 0.5" plate**

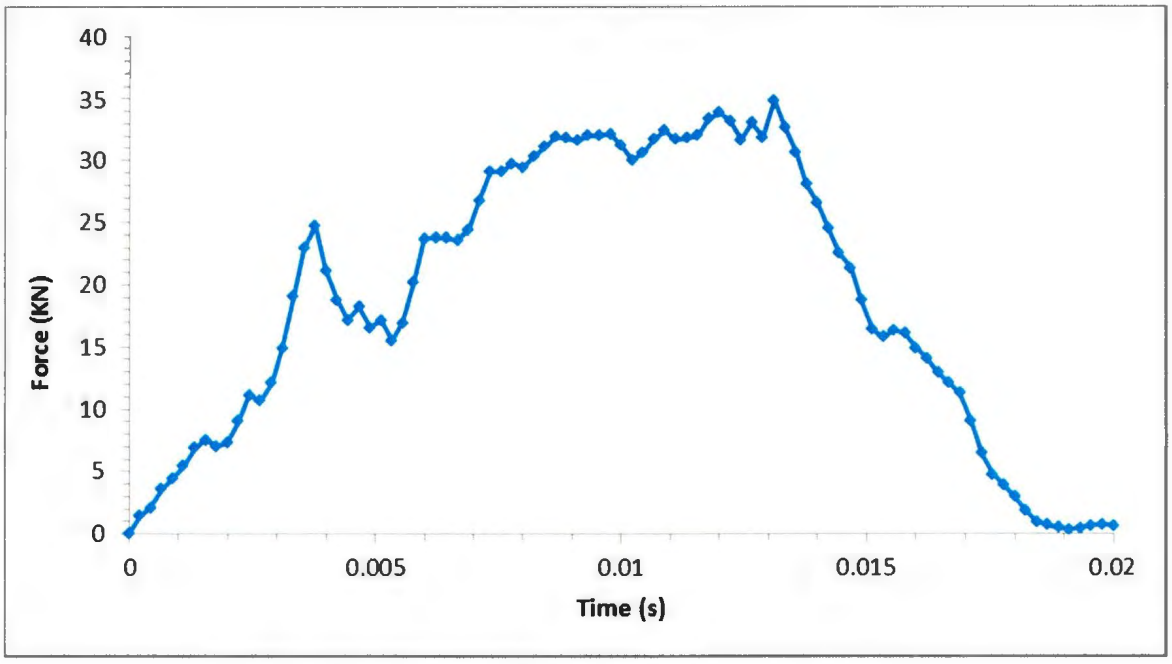


**Run 10: 40 Degree ice specimen impacted with 0.5" plate**

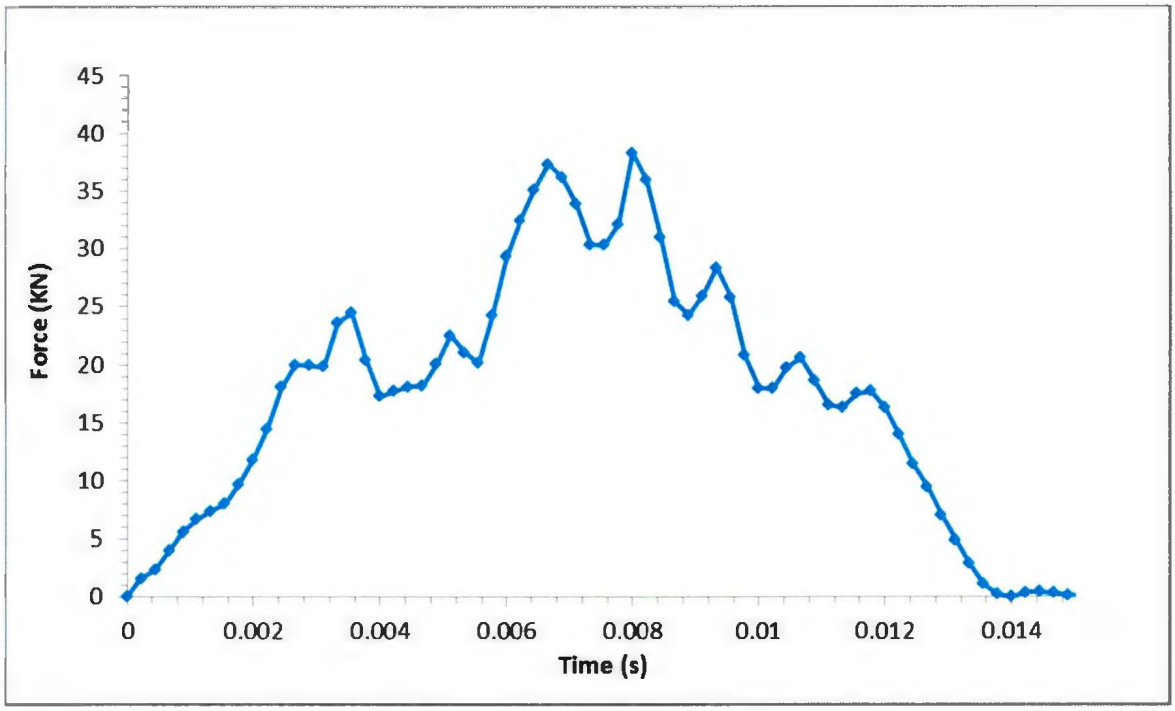


**Run 11: 40 Degree ice specimen impacted with 0.75" plate**

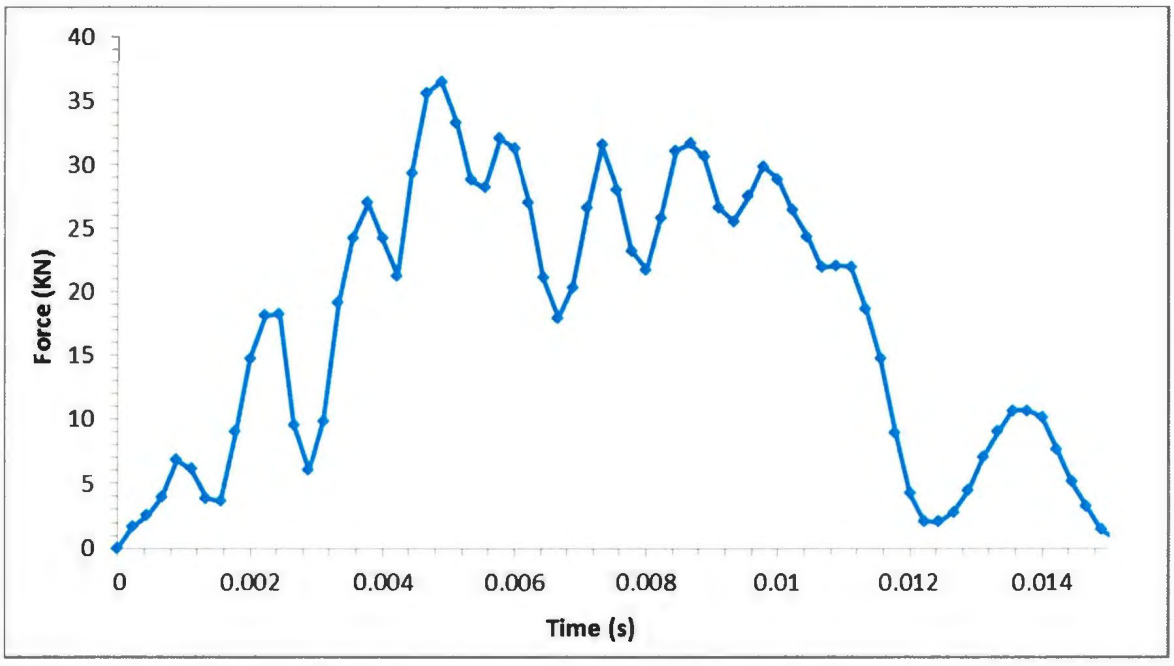


**Run 20: 40 Degree ice specimen impacted with 0.75" plate**

# APPENDIX B:

# RESPONSE SURFACE DIAGNOSTIC PLOTS

# Appendix B1:

## Peak Force Model Diagnostic Plots

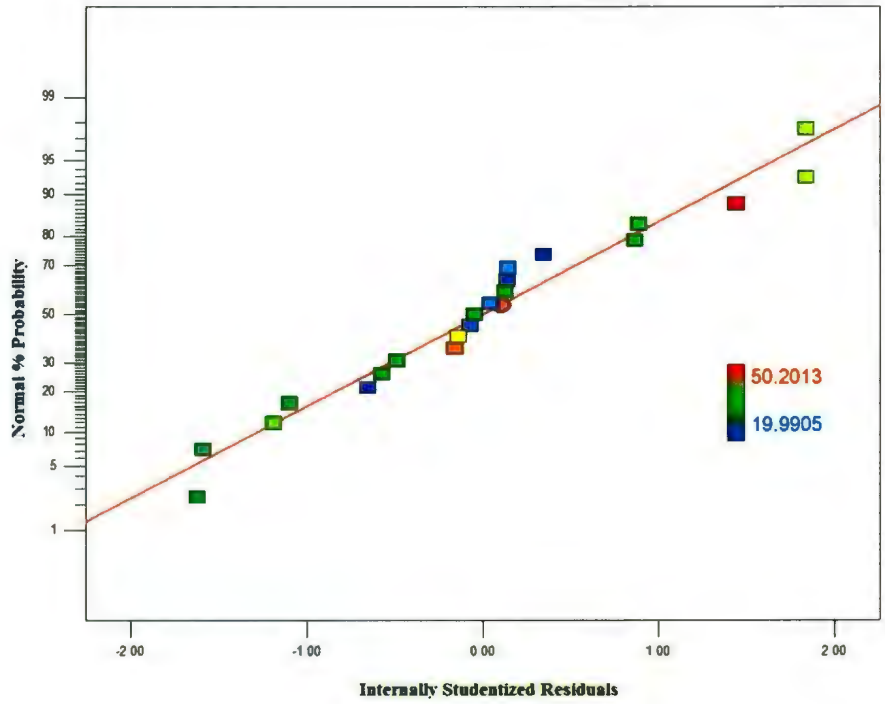


**Normal plot of residuals**

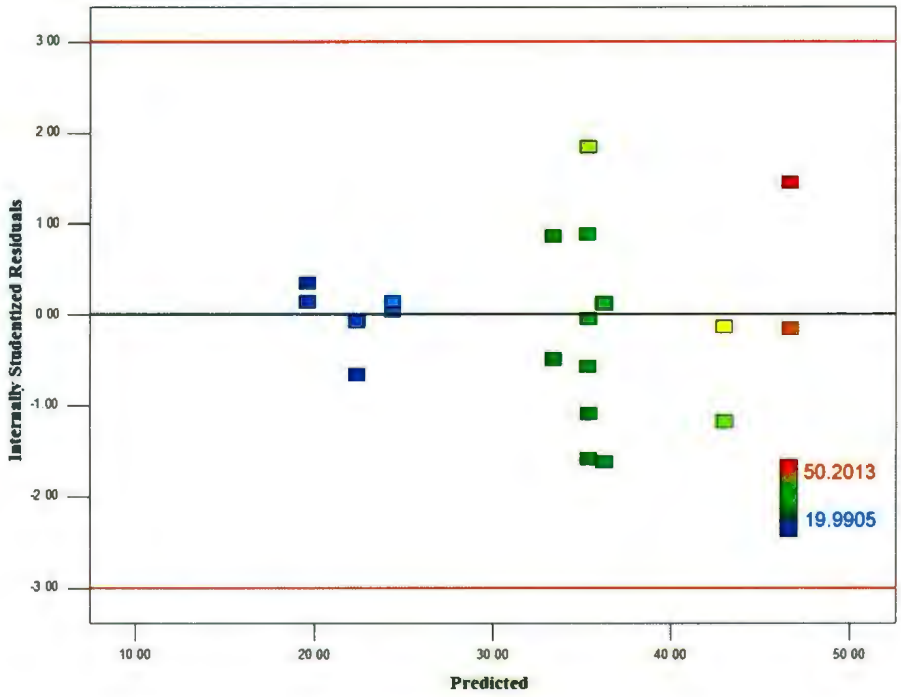


**Residuals vs. predicted**

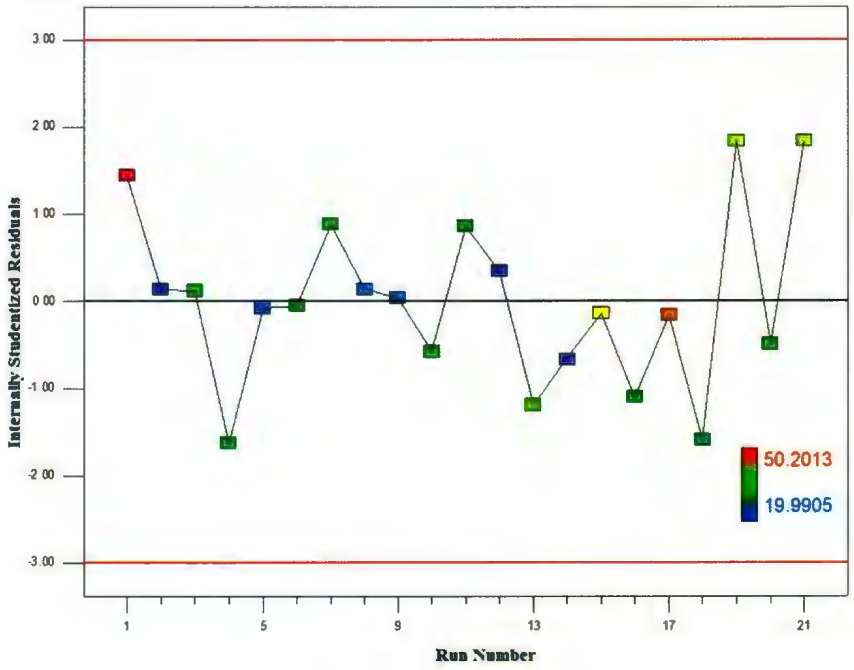


**Model residuals vs. run number**

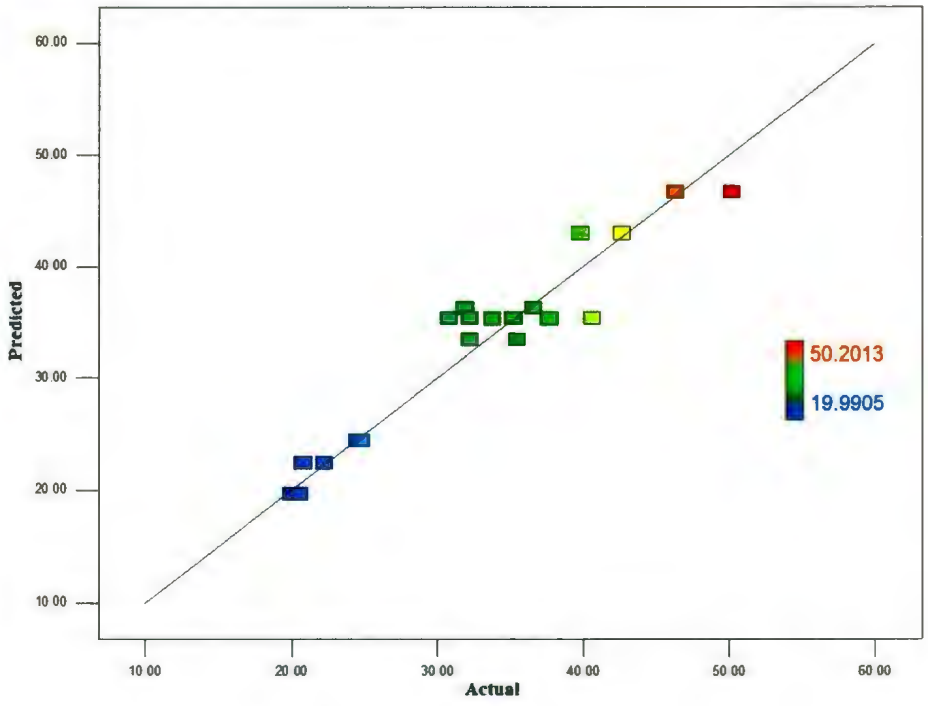


**Model predicted vs. actual**

# Appendix B2:

## Nominal Pressure Model Diagnostic Plots

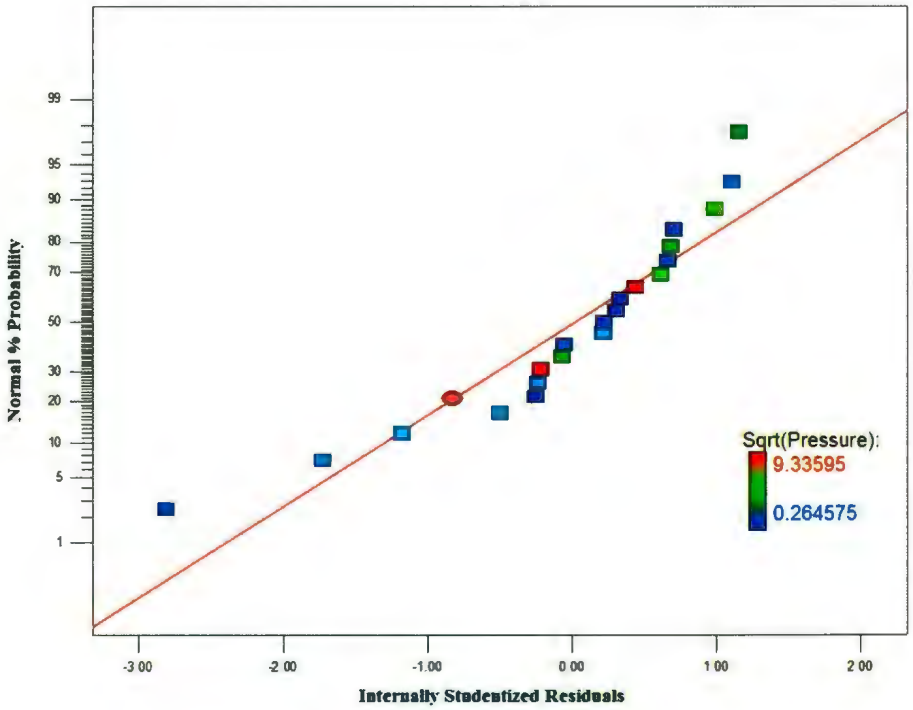


**Normal plot of residuals**

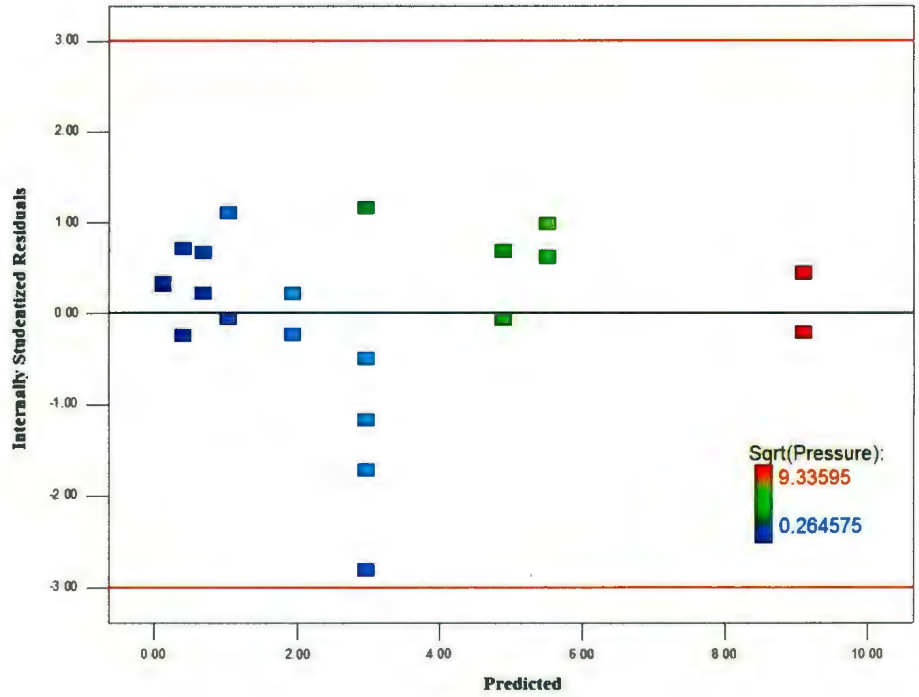


**Residuals vs. predicted**

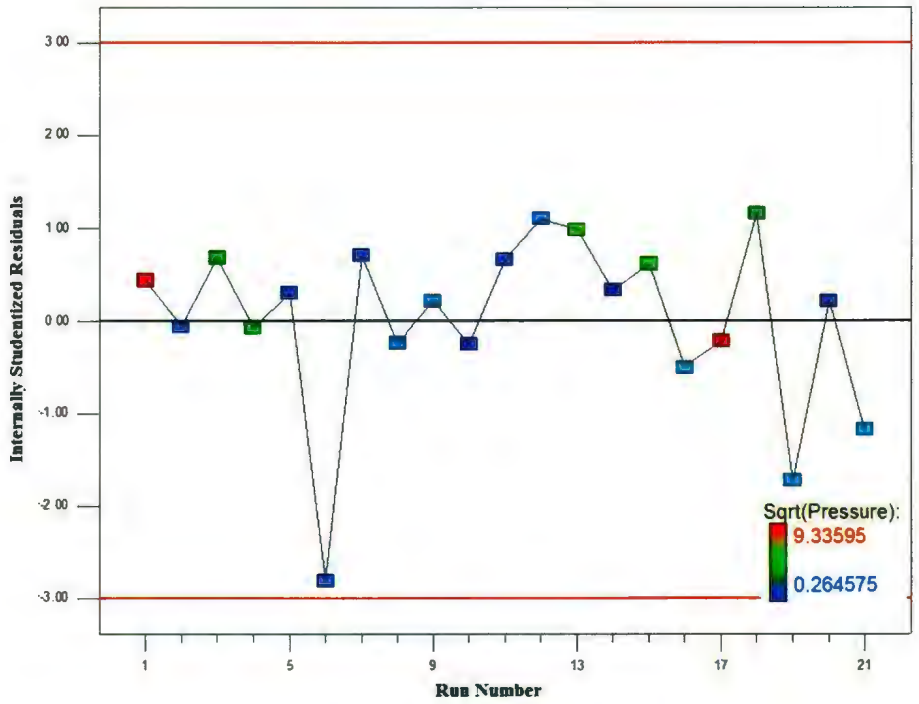


**Residuals vs. run number**

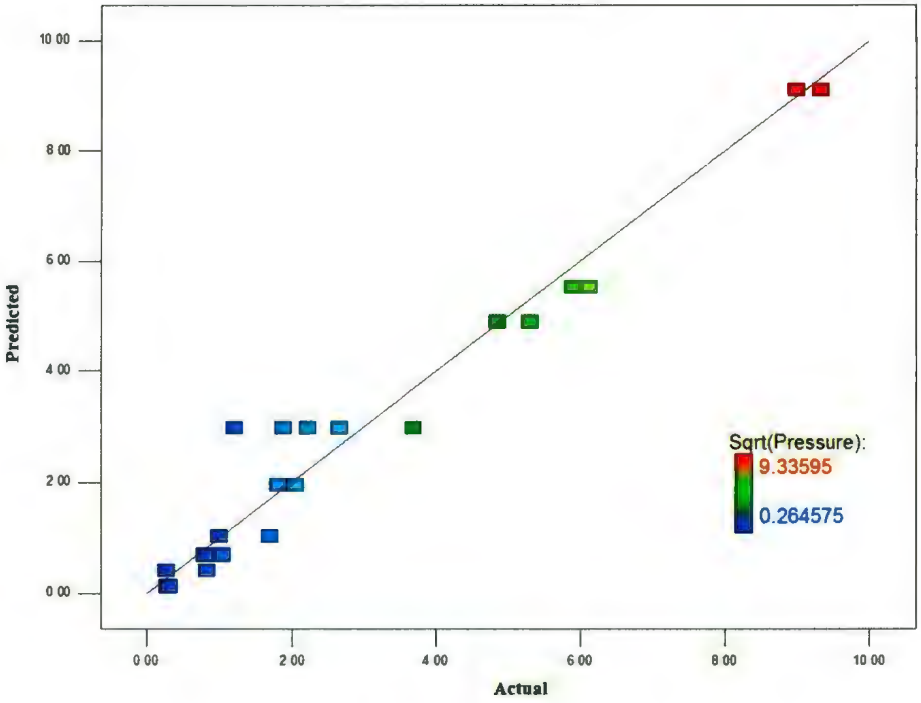


**Predicted vs. actual**

# Appendix B3:

## Cushing Energy Diagnostic Plots

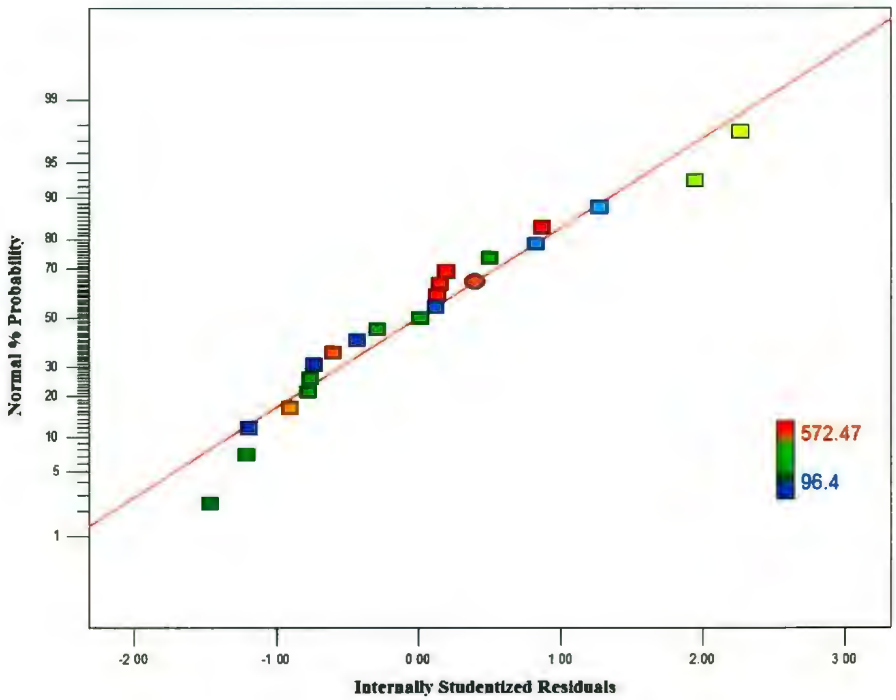


**Normal plot of residuals**

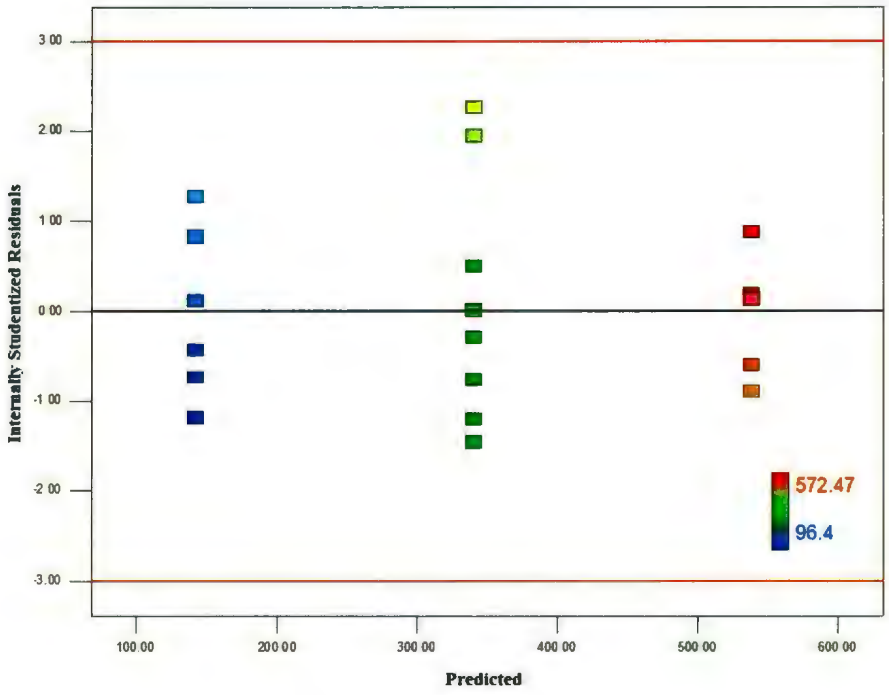


**Residuals vs. predicted**

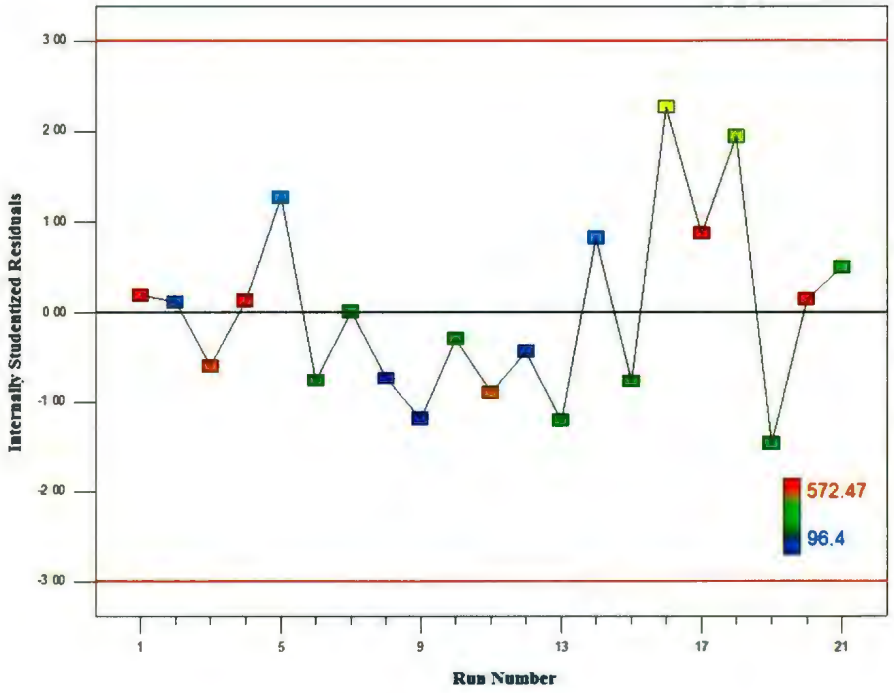


**Residuals vs. run number**

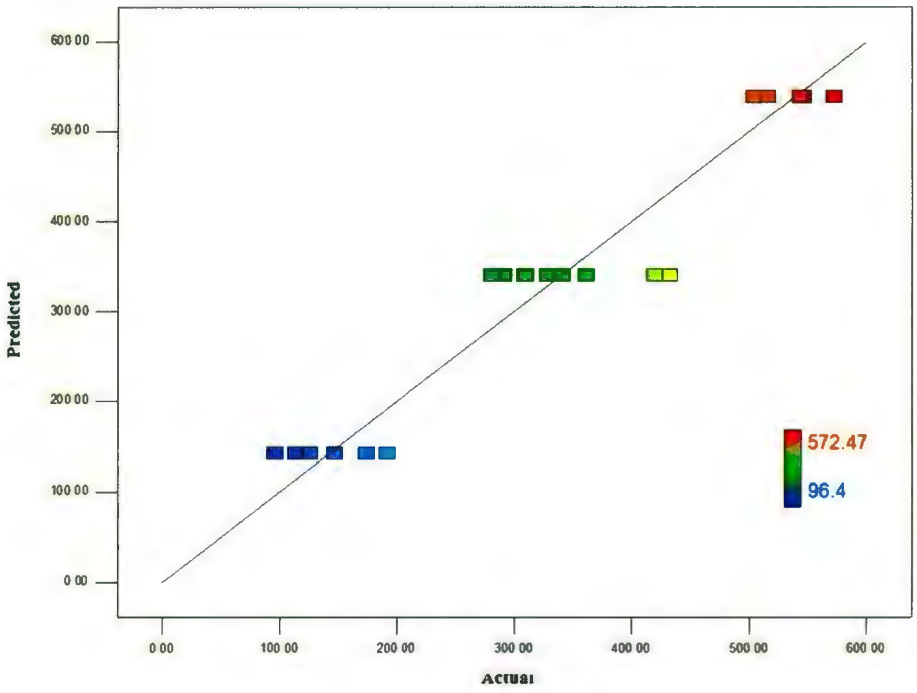


**Predicted vs. actual**

# Appendix B4:

## Plate Energy Diagnostic Plots

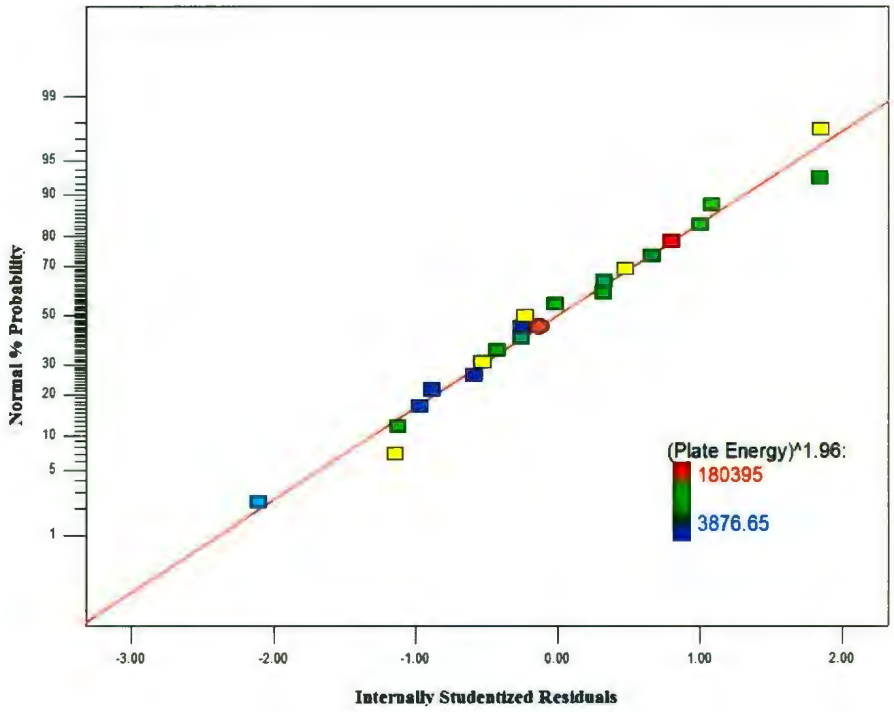


**Normal plot of residuals**

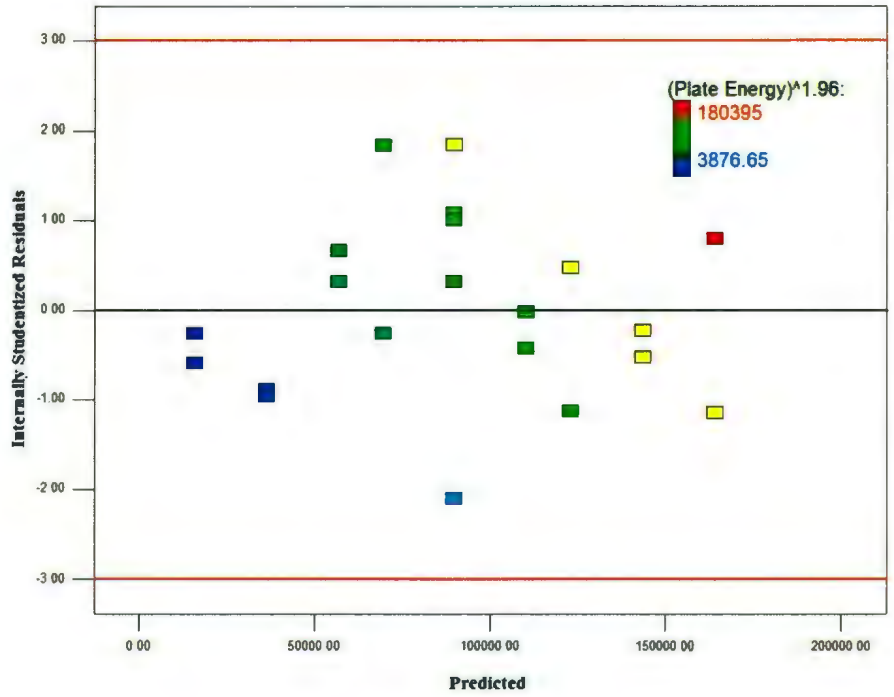


**Residuals vs. predicted**

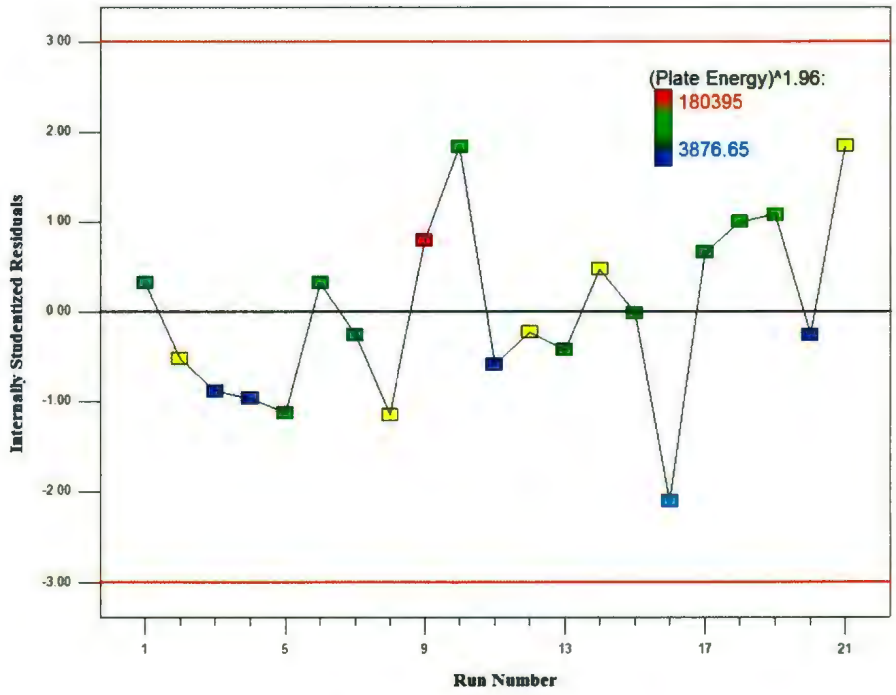


**Residuals vs. run number**

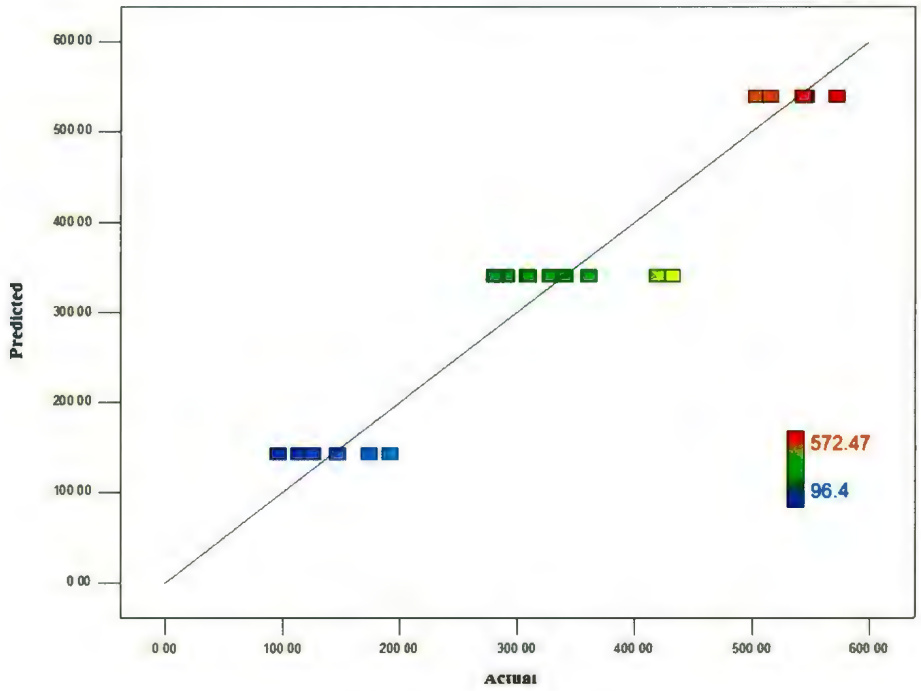


**Model Predicted vs. actual**

# Appendix B5:

## Specific Energy Diagnostic Plots

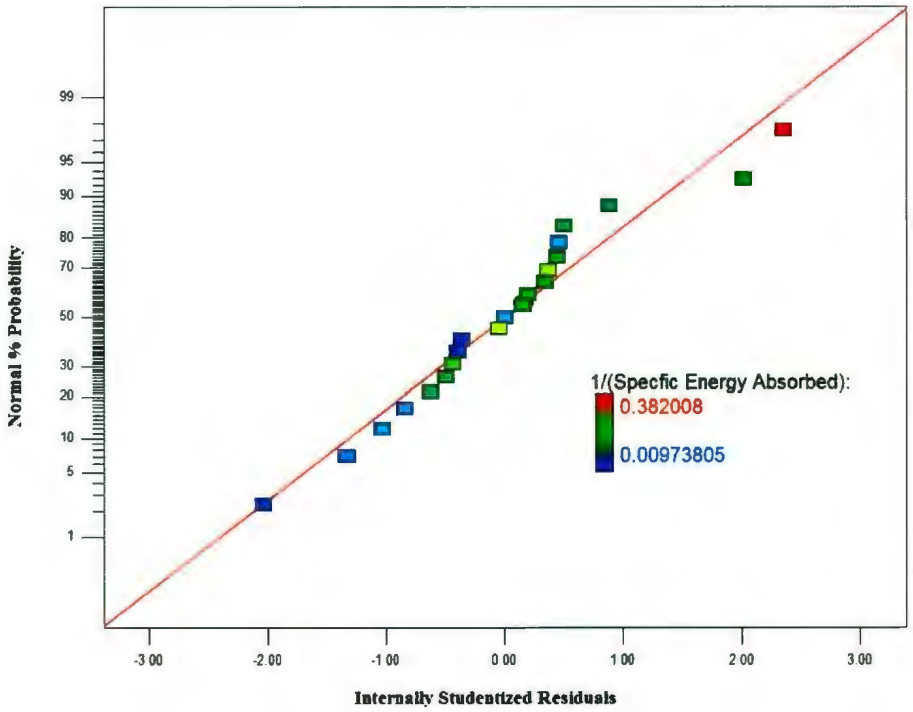


**Normal plot of residuals**

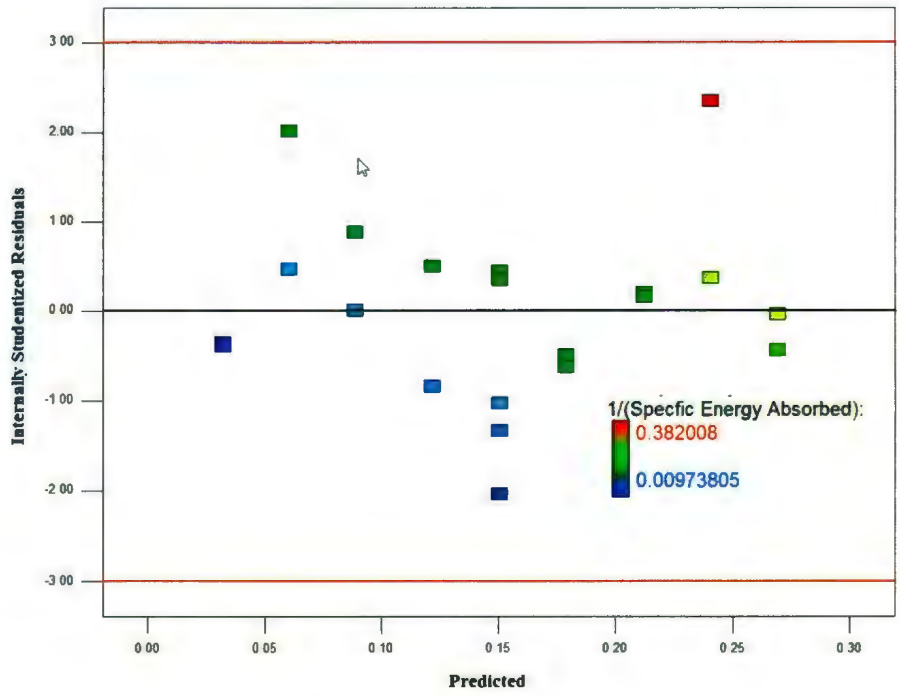


**Residuals vs. predicted**

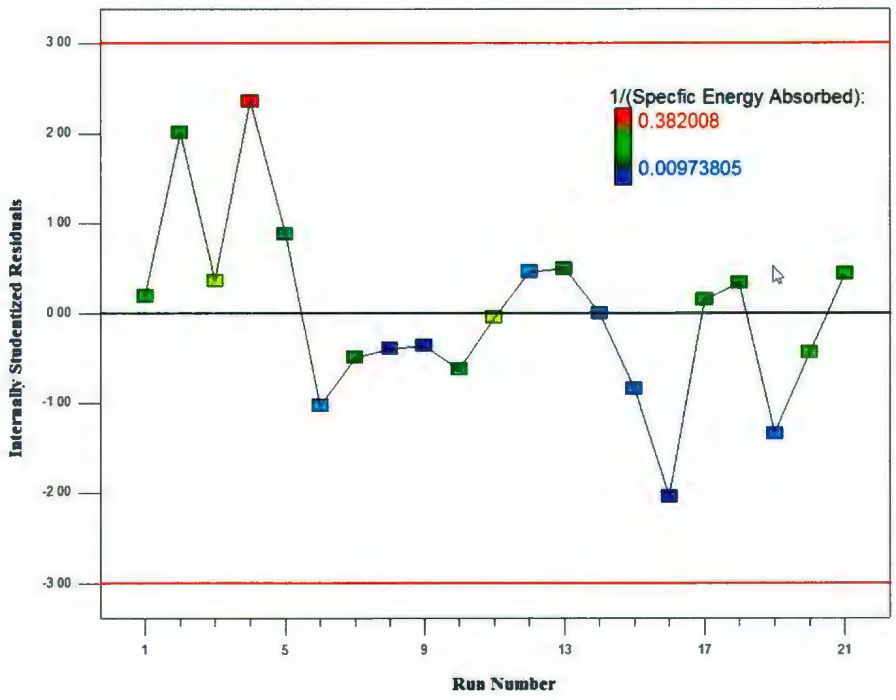


**Residuals vs. run number**

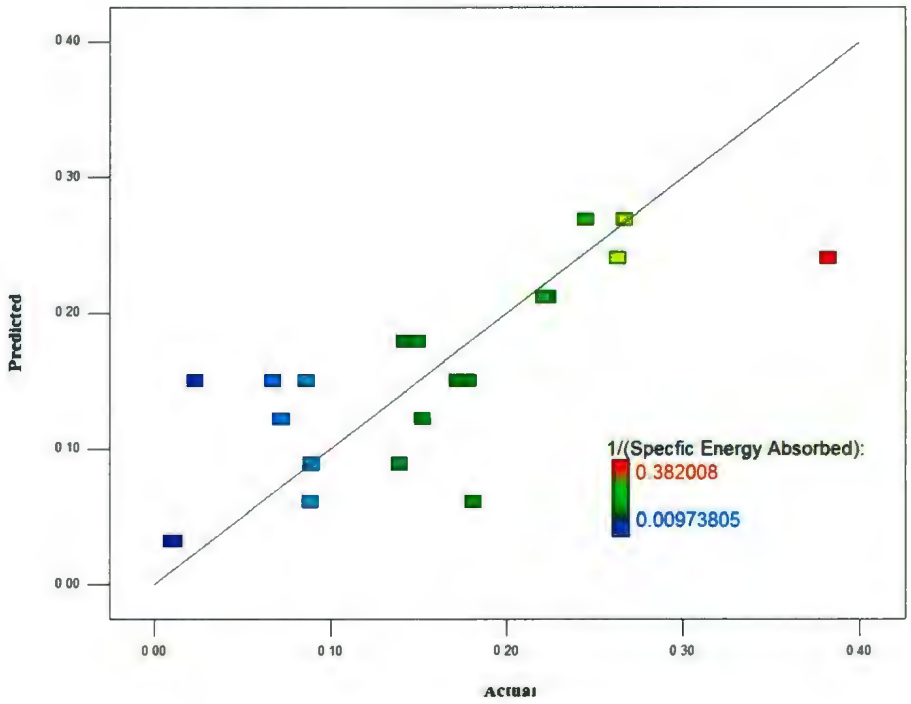


**Model predicted vs. actual**

# APPENDIX C:

# FORCE VS. DISPLACEMENT PLOTS

# Appendix C1:

## 20 Degree Ice Specimen Force vs. Displacement Plots

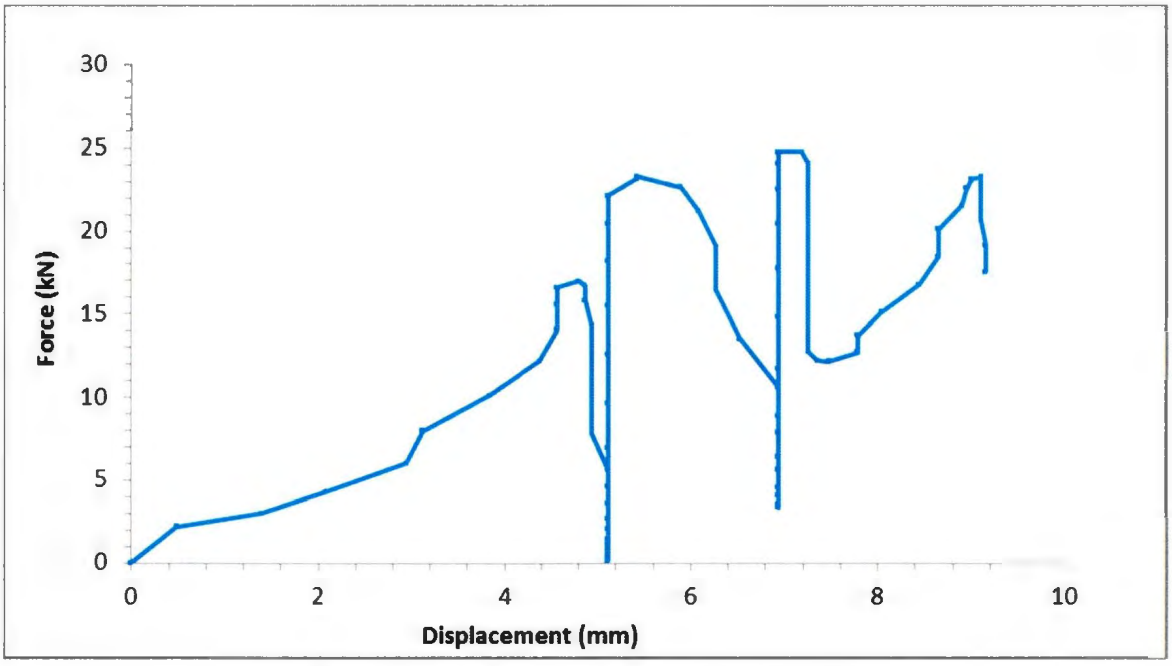


**Run 8: 20 Degree ice specimen impacted with 0.25" plate**

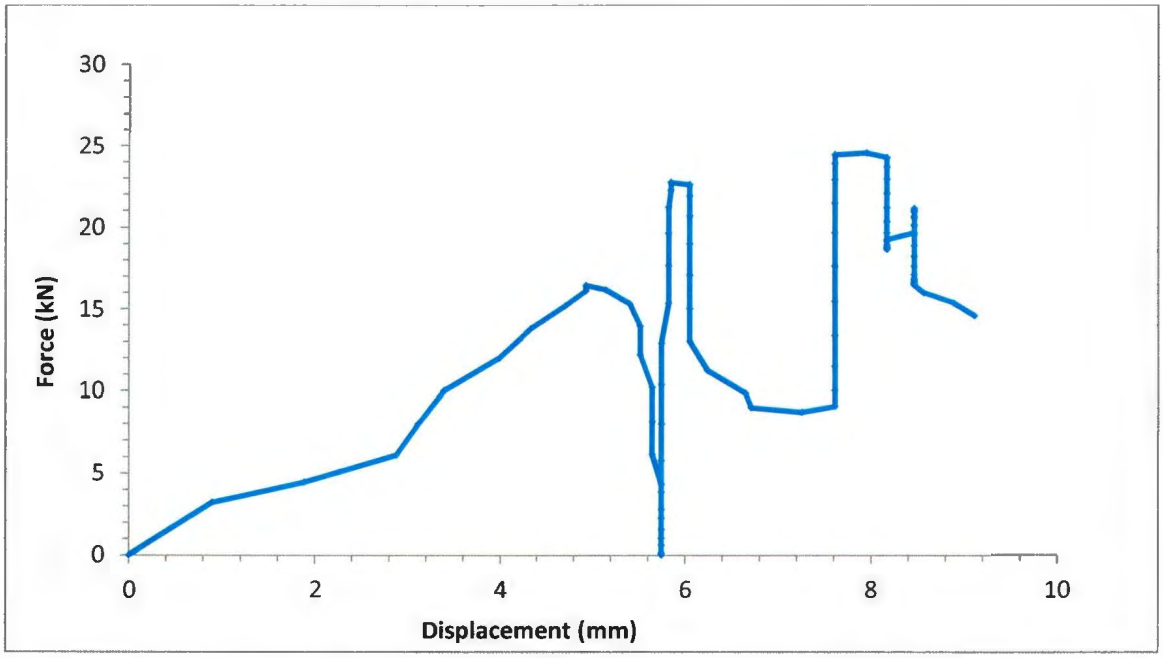


**Run 9: 20 Degree ice specimen impacted with 0.25" plate**

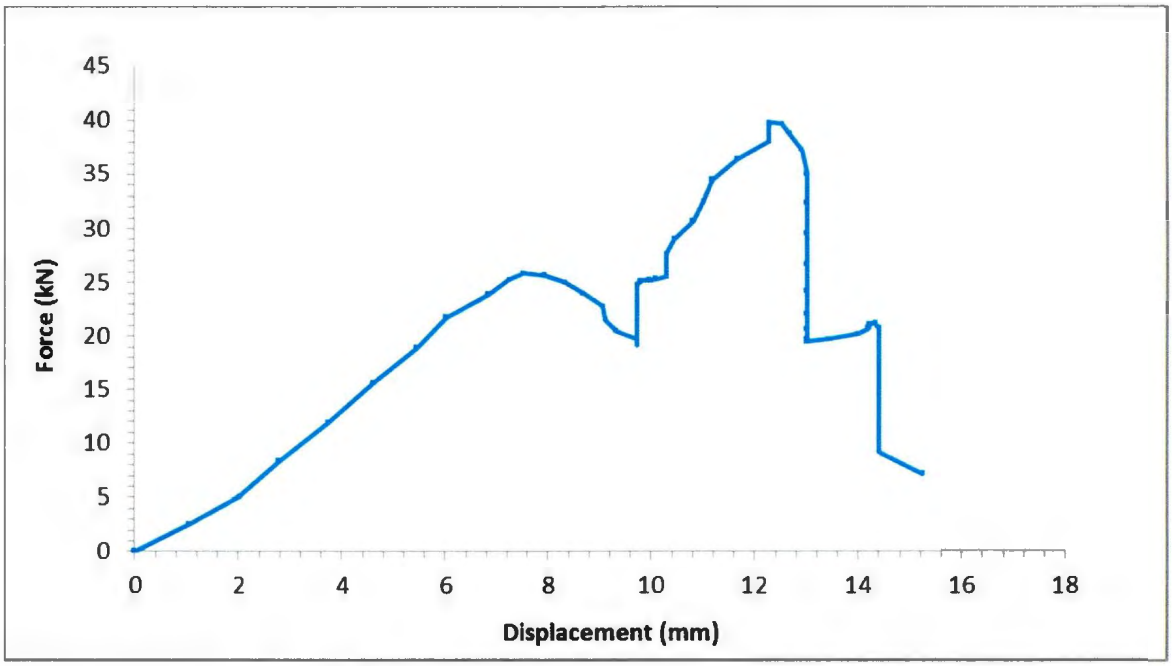


**Run 13: 20 Degree ice specimen impacted with 0.5" plate**

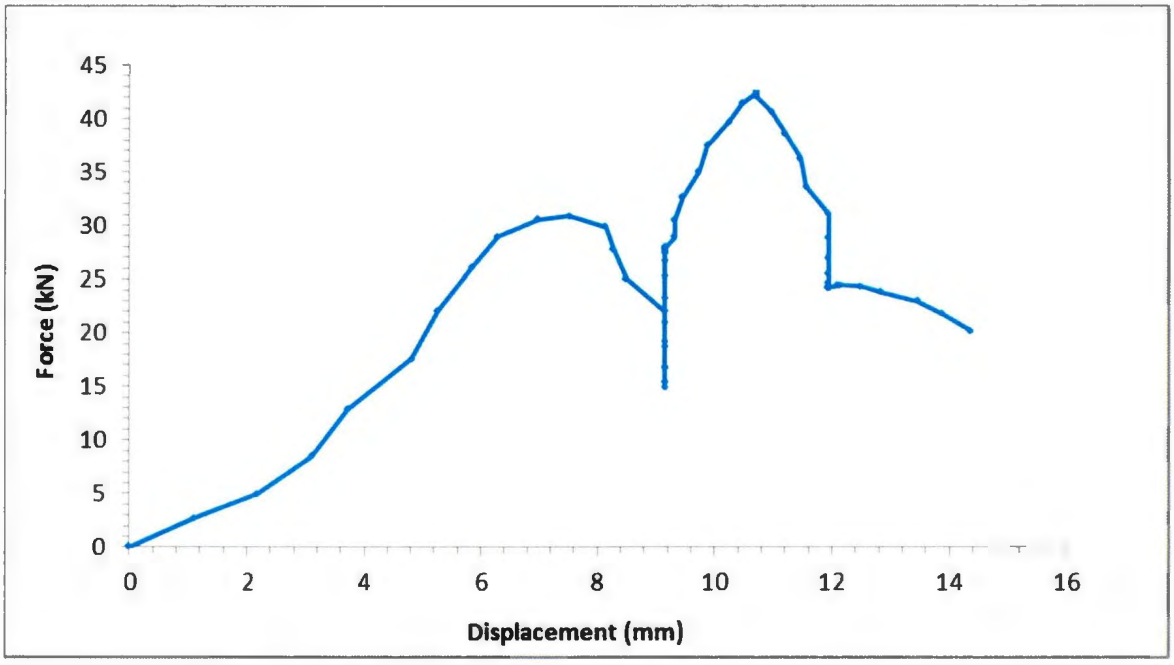


**Run 15: 20 Degree ice specimen impacted with 0.5" plate**

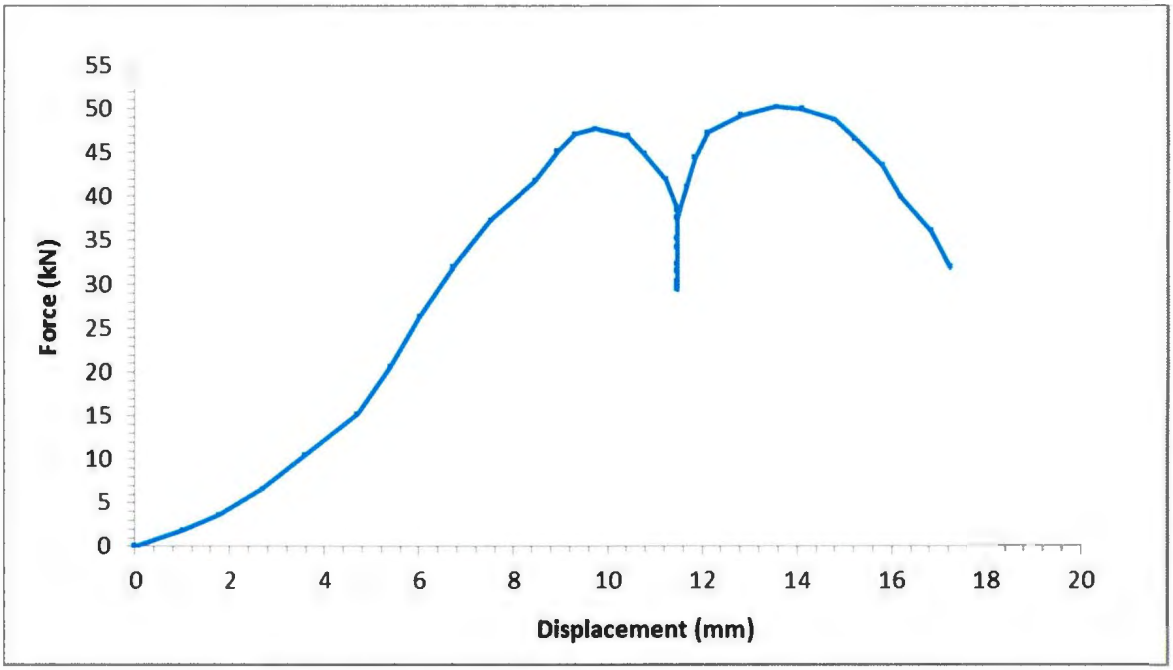


**Run 1: 20 Degree ice specimen impacted with 0.75" plate**

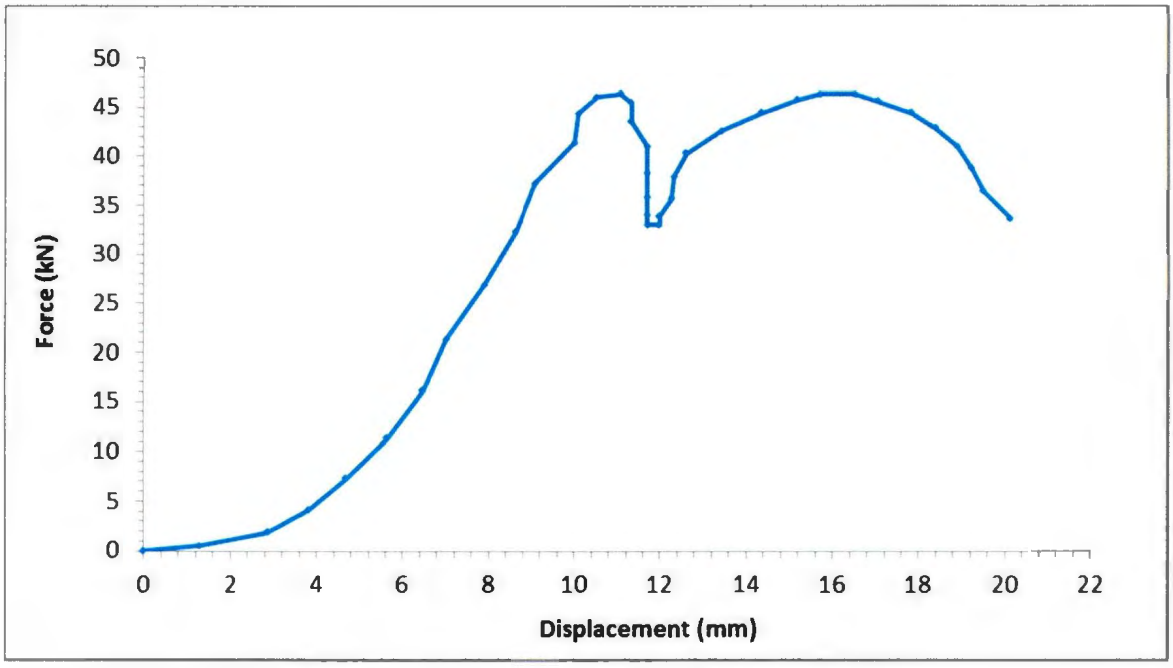


**Run 17: 20 Degree ice specimen impacted with 0.75" plate**

# Appendix C2:

## 30 Degree Ice Specimen Force vs. Displacement Plots

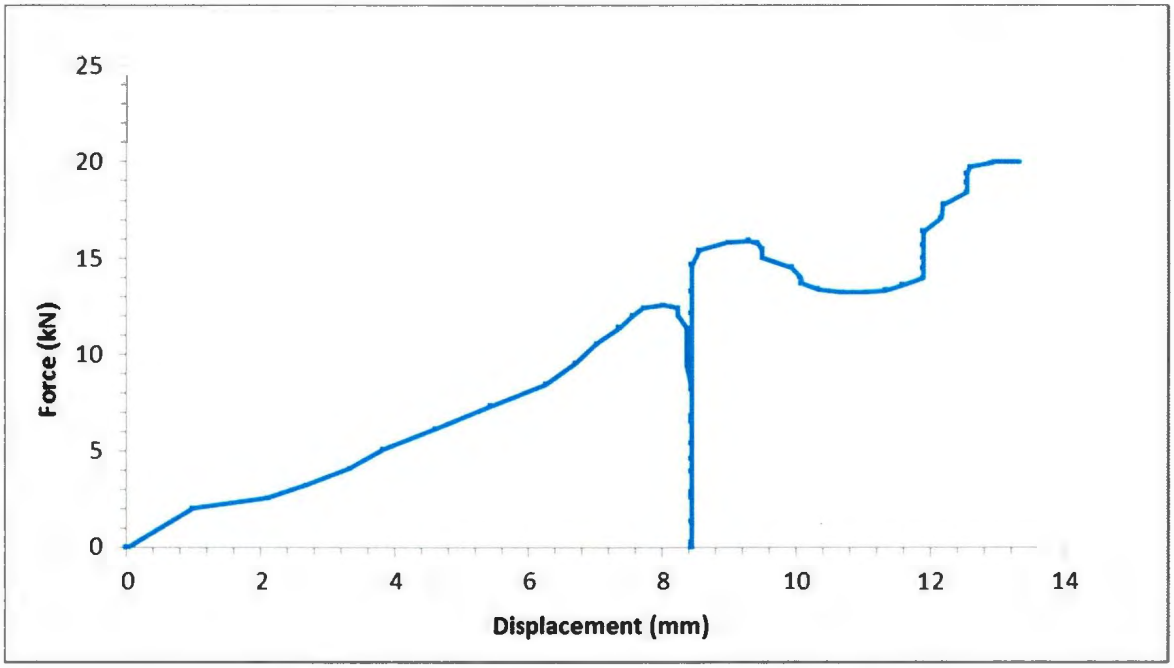


**Run 2: 30 Degree ice specimen impacted with 0.25" plate**

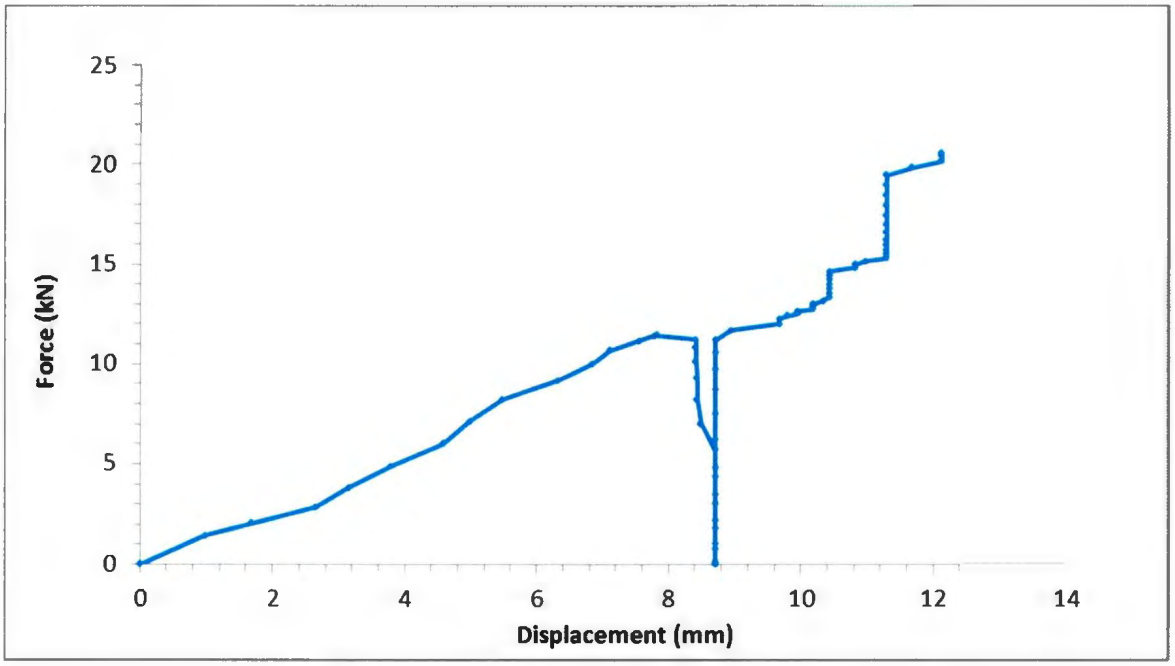


**Run 12: 30 Degree ice specimen impacted with 0.25" plate**

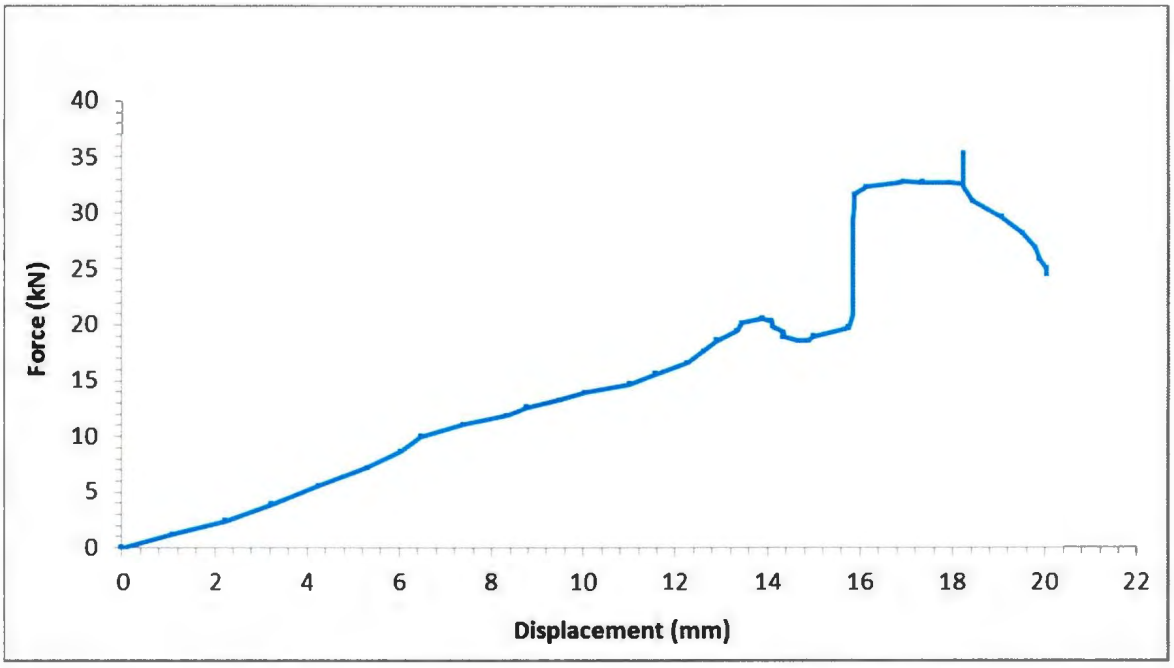


**Run 6: 30 Degree ice specimen impacted with 0.5" plate**

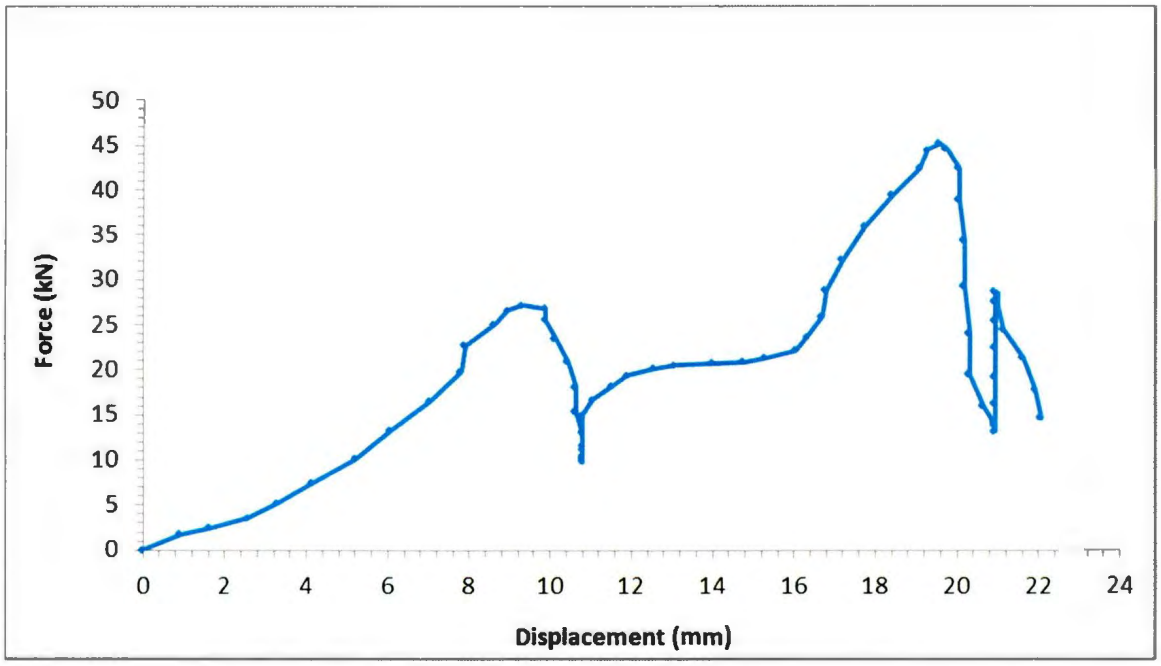


**Run 16: 30 Degree ice specimen impacted with 0.5" plate**

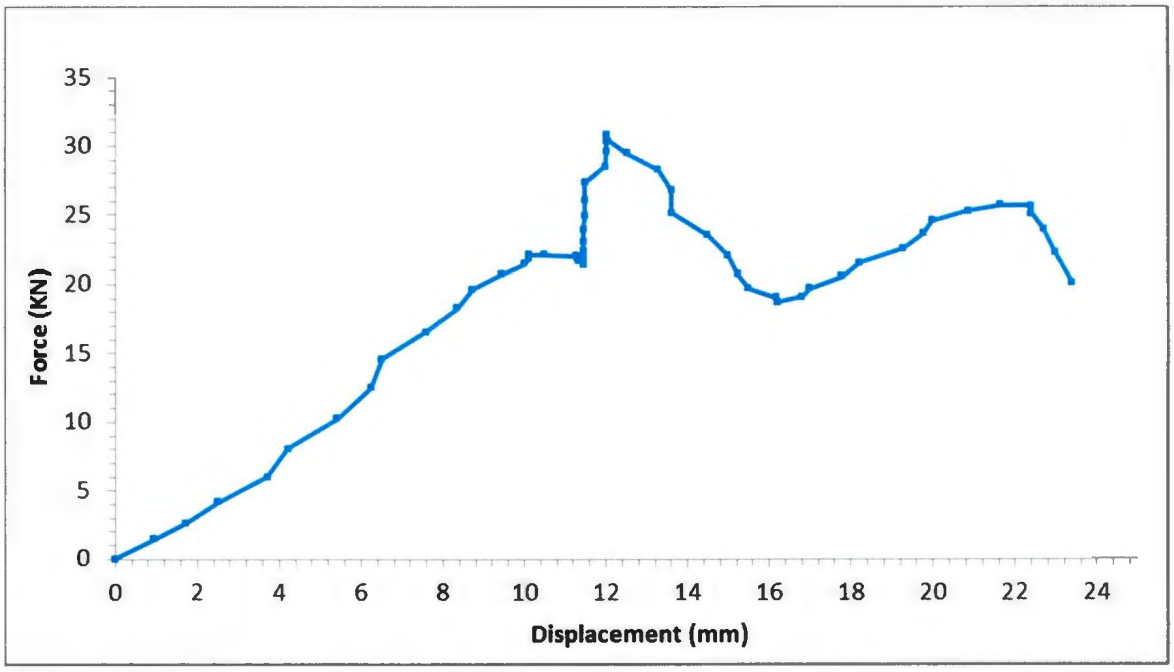


**Run 18: 30 Degree ice specimen impacted with 0.5" plate**

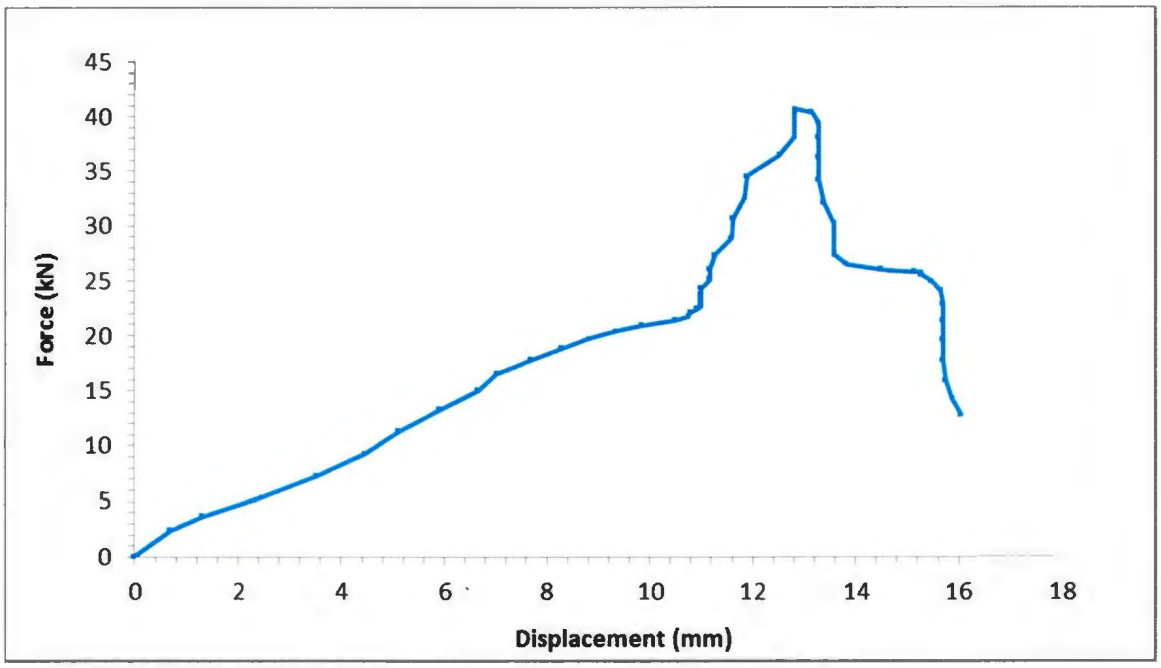


**Run 19: 30 Degree ice specimen impacted with 0.5" plate**

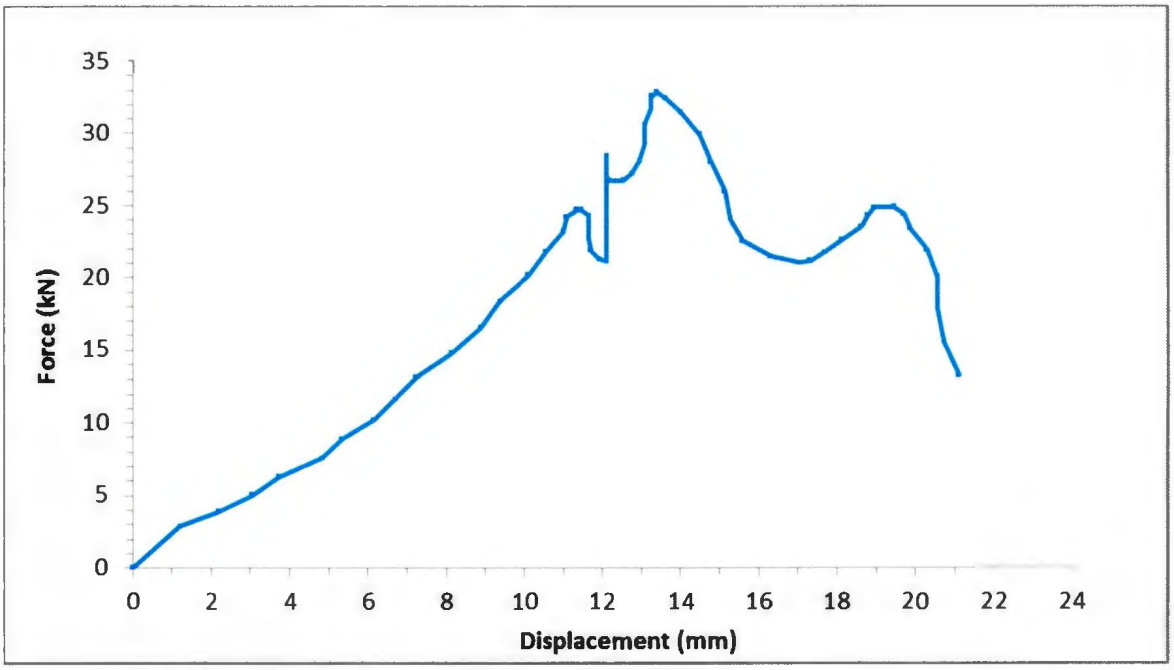


**Run 21: 30 Degree ice specimen impacted with 0.5" plate**


**Run 3: 30 Degree ice specimen impacted with 0.75" plate**

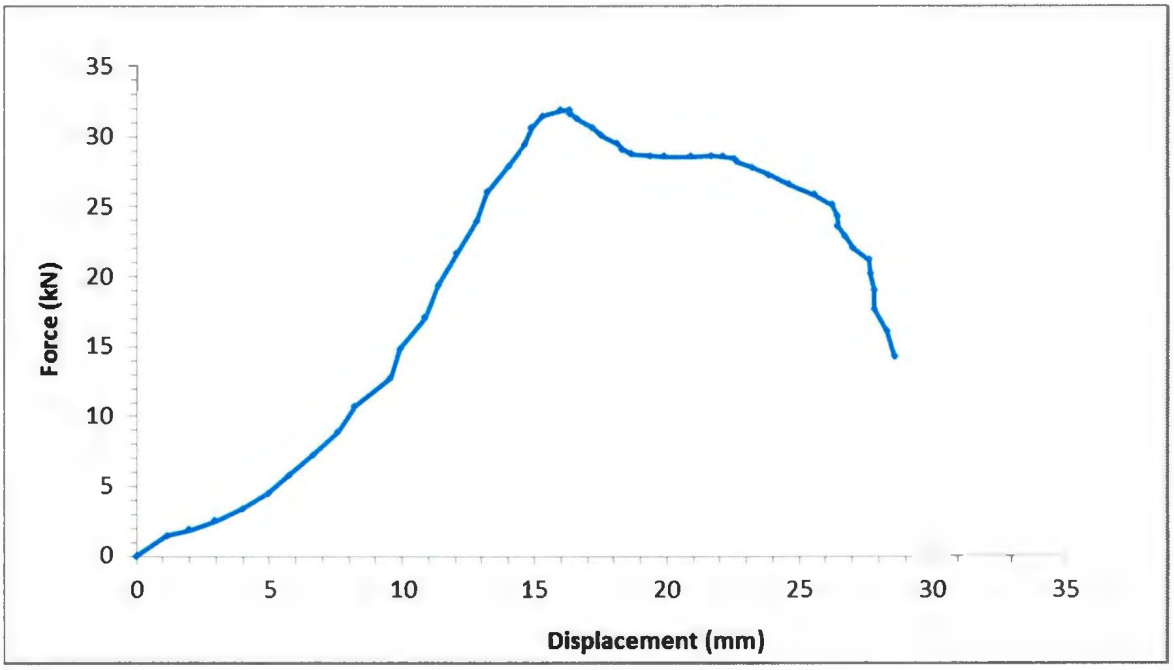


**Run 4: 30 Degree ice specimen impacted with 0.75" plate**

# Appendix C3:

## 40 Degree Ice Specimen Force vs. Displacement Plots

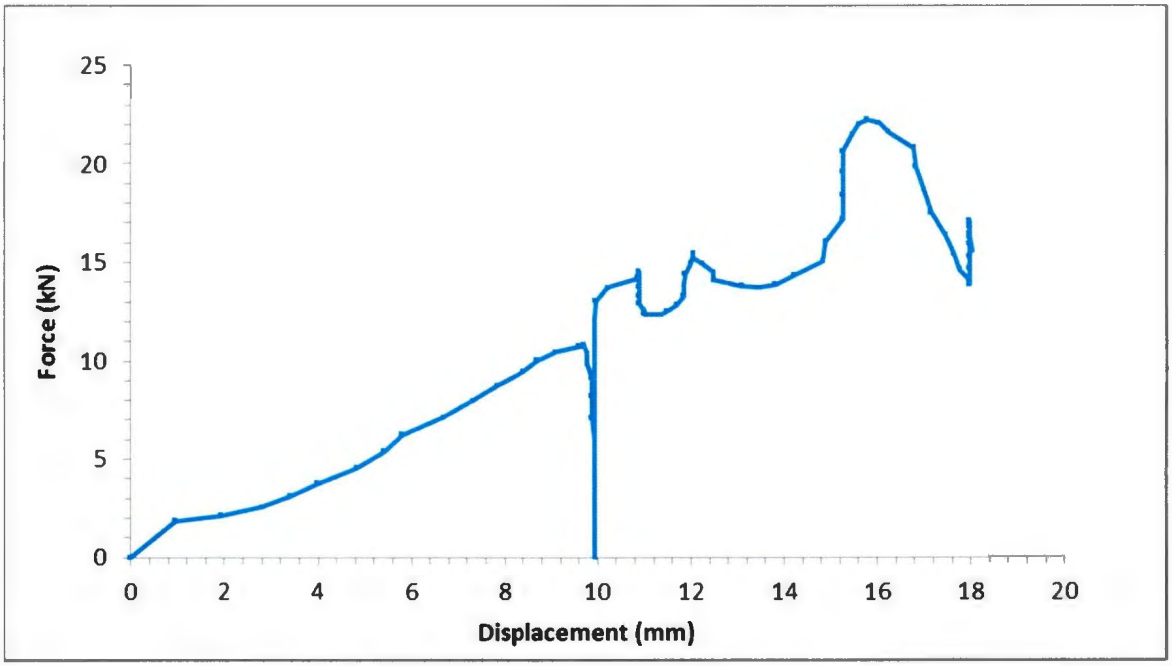


**Run 5: 40 Degree ice specimen impacted with 0.25" plate**

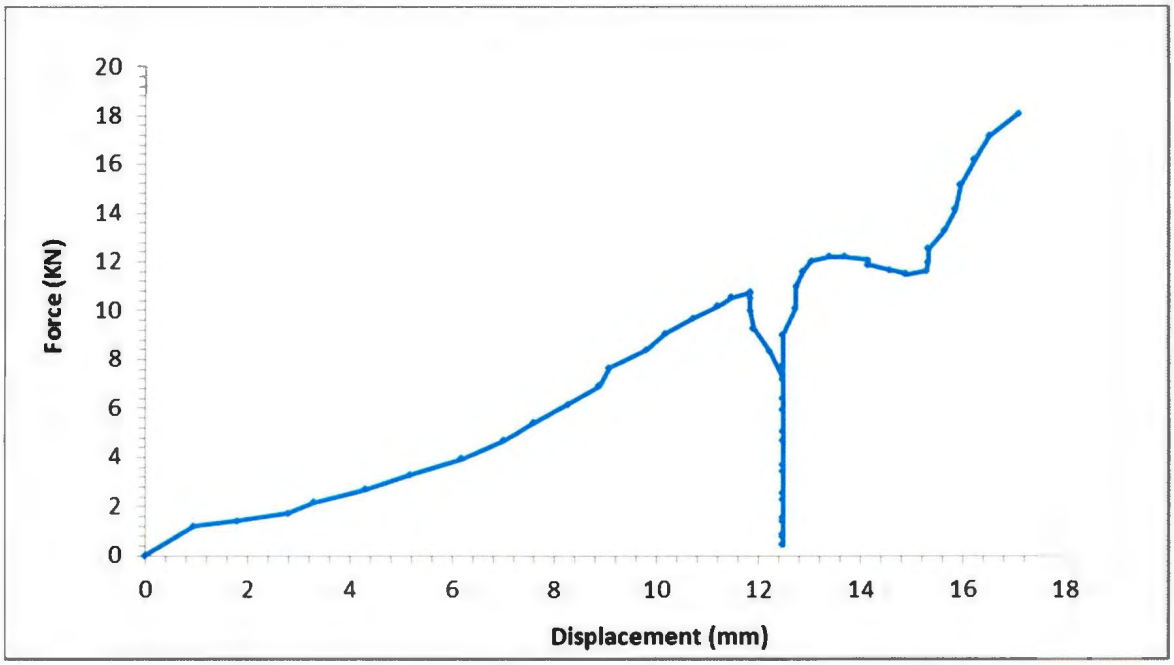


**Run 14: 40 Degree ice specimen impacted with 0.25" plate**

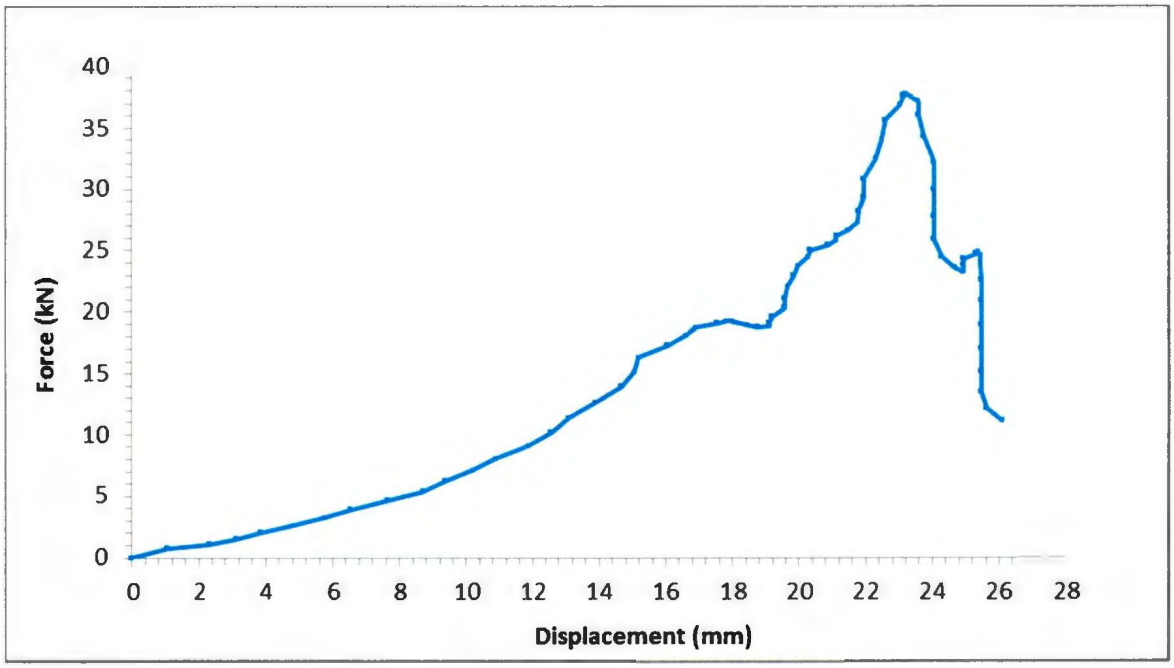


**Run 7: 40 Degree ice specimen impacted with 0.5" plate**

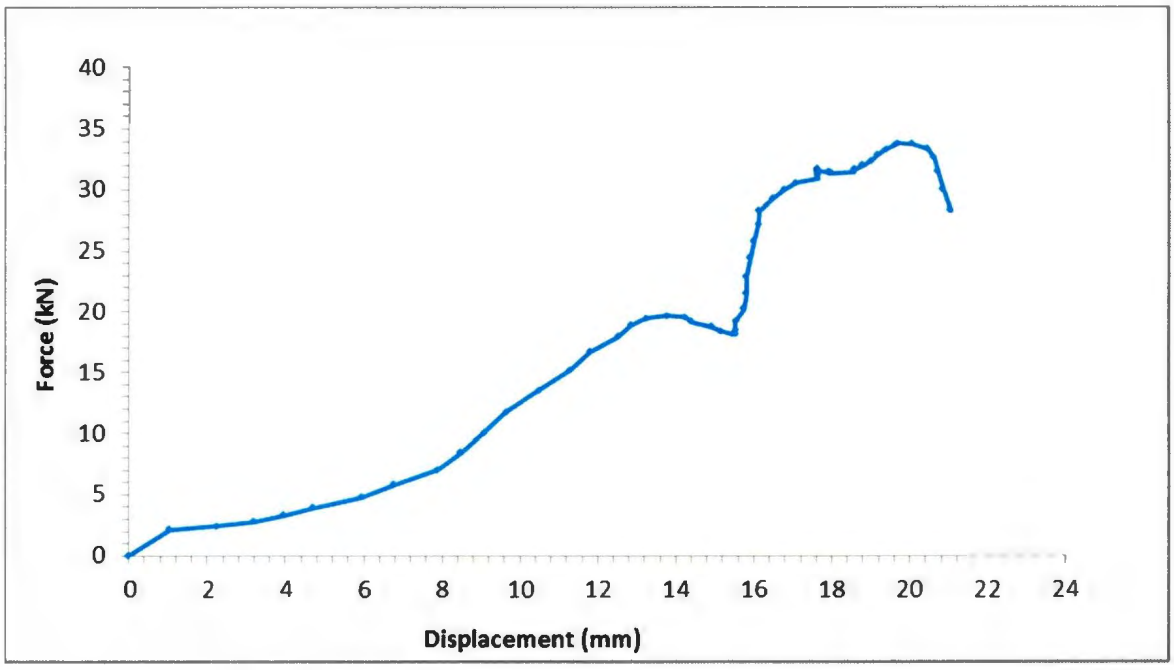


**Run 10: 40 Degree ice specimen impacted with 0.5" plate**

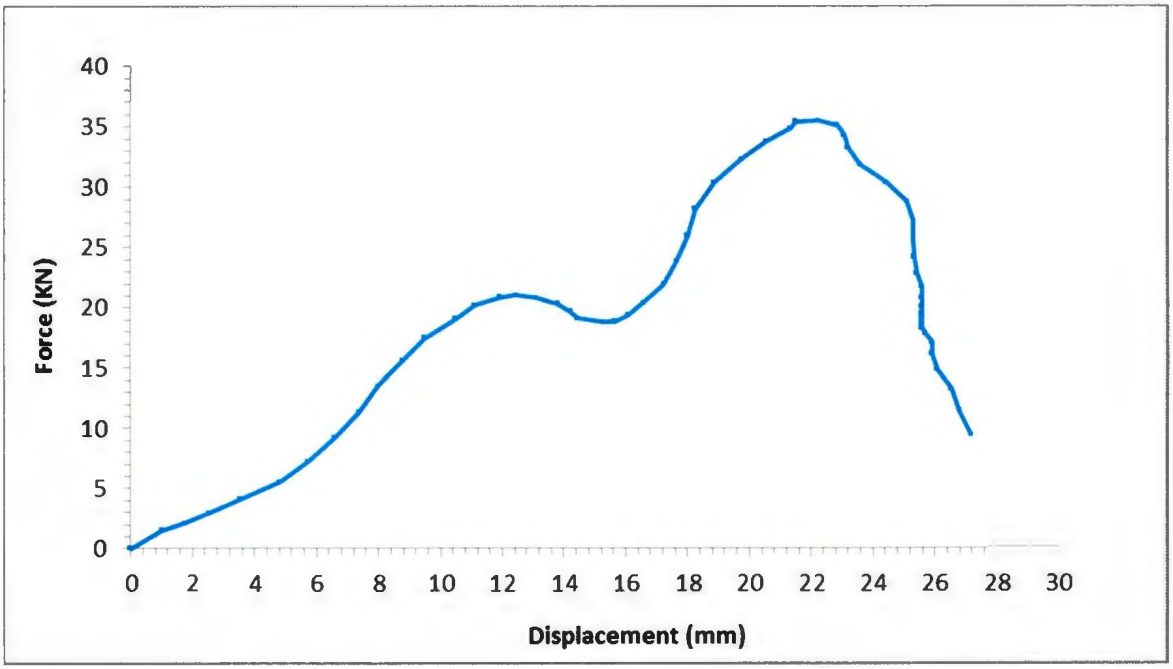


**Run 11: 40 Degree ice specimen impacted with 0.75" plate**

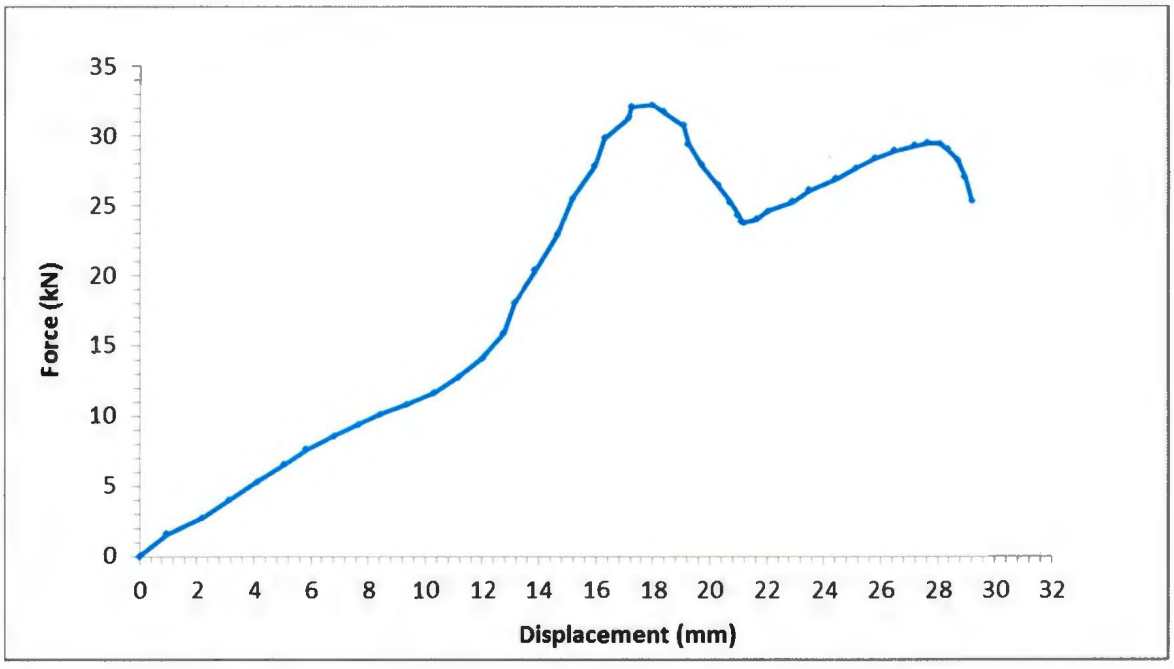


**Run 20: 40 Degree ice specimen impacted with 0.75" plate**

# APPENDIX D:

# ENERGY PLOTS

# Appendix D1:

## Energy Plots for 20 Degree Ice Specimens

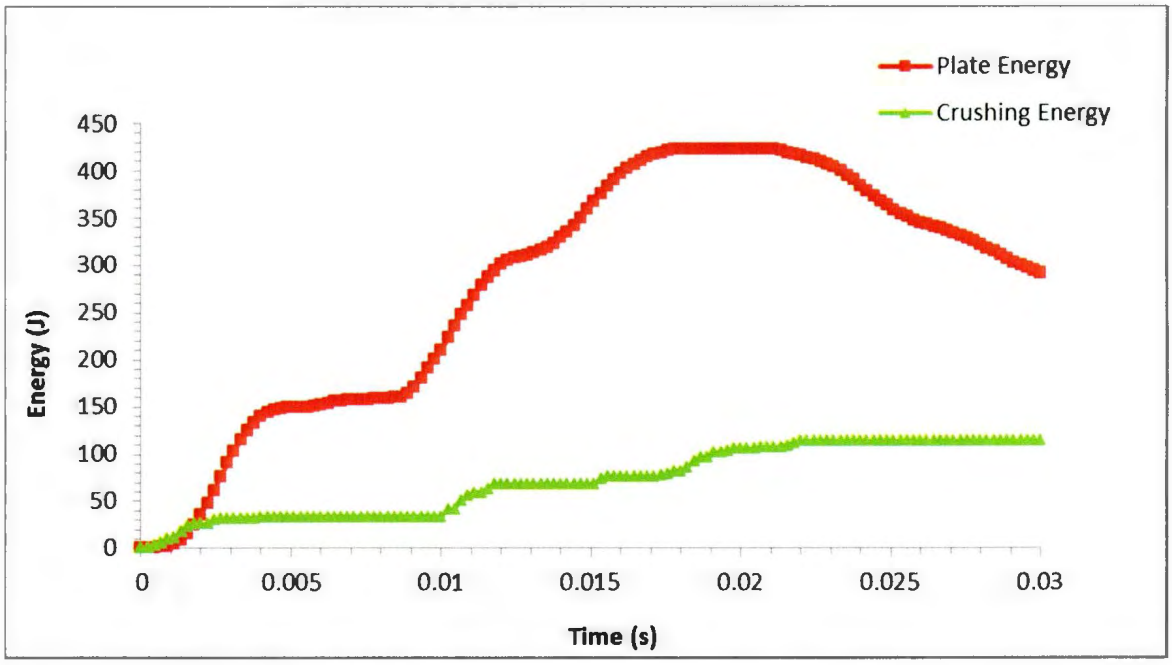


**Run 8: 20 Degree ice specimen impacted with 0.25" plate**

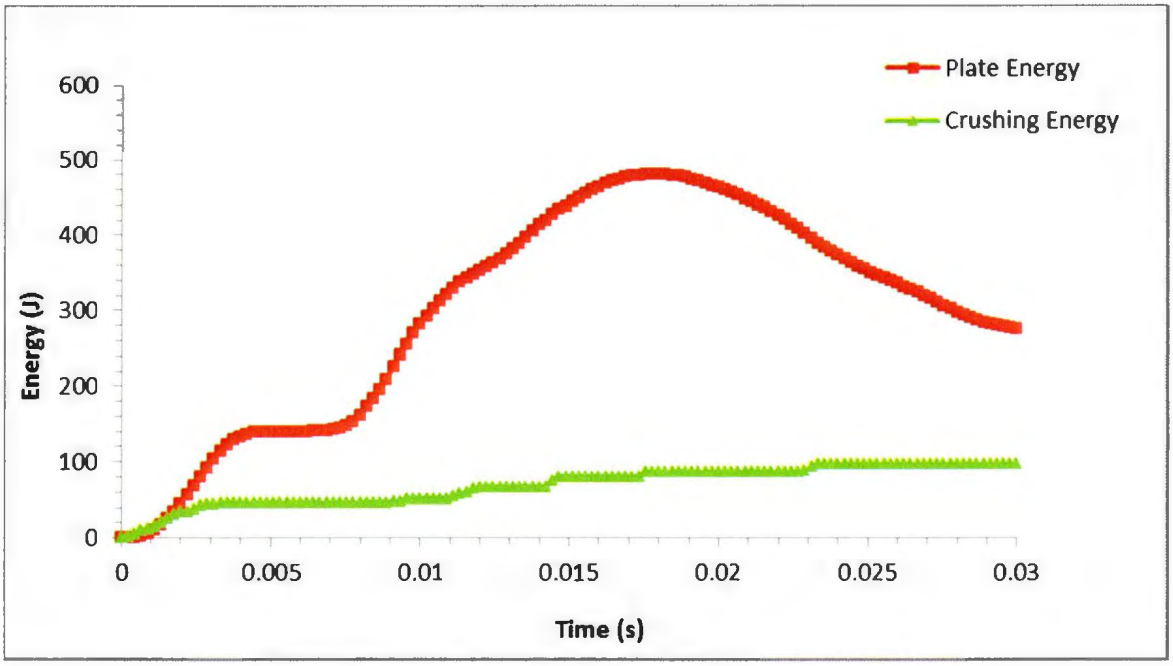


**Run 9: 20 Degree ice specimen impacted with 0.25" plate**

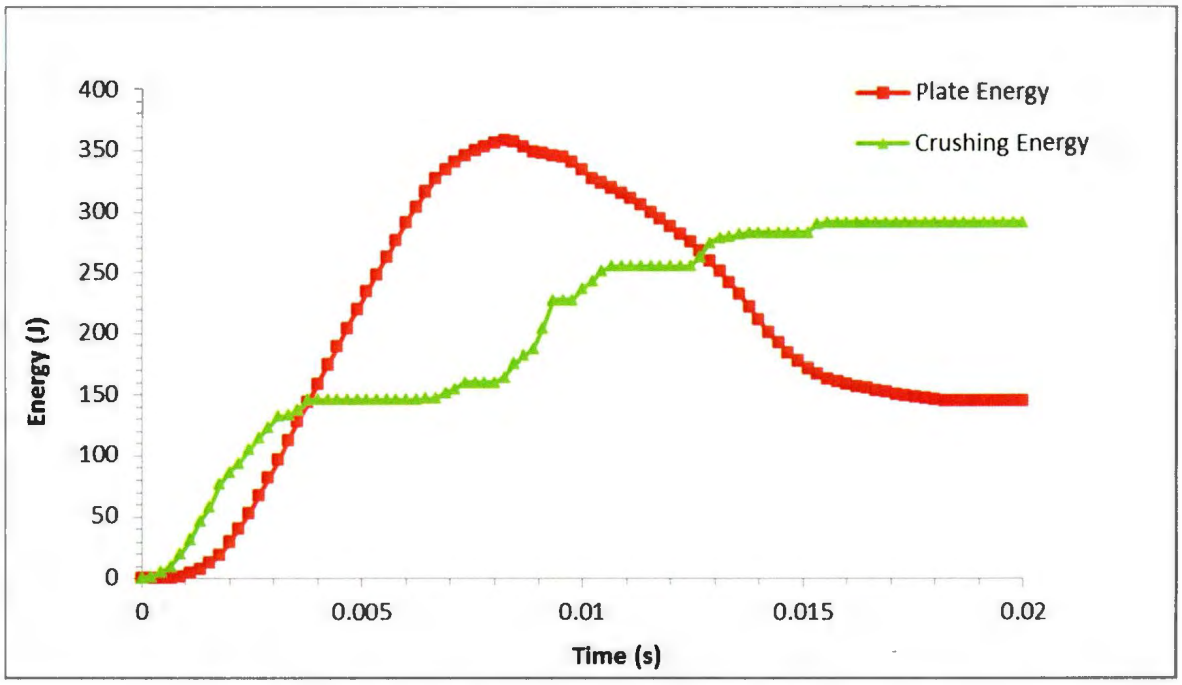


**Run 13: 20 Degree ice specimen impacted with 0.5" plate**

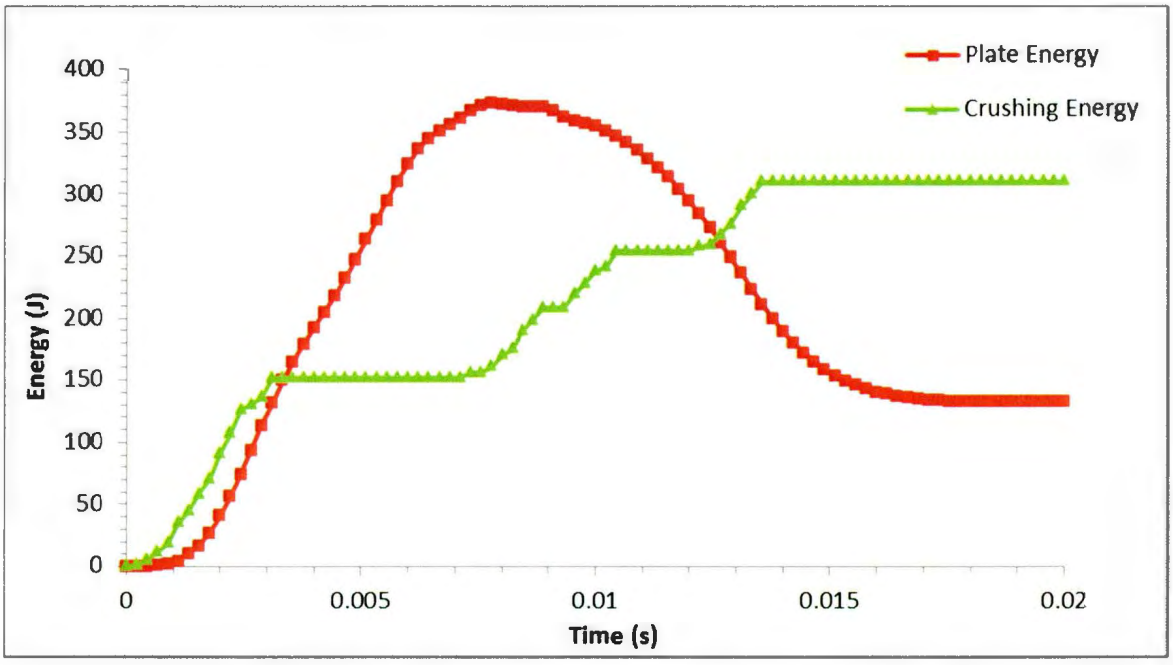


**Run 15: 20 Degree ice specimen impacted with 0.5" plate**

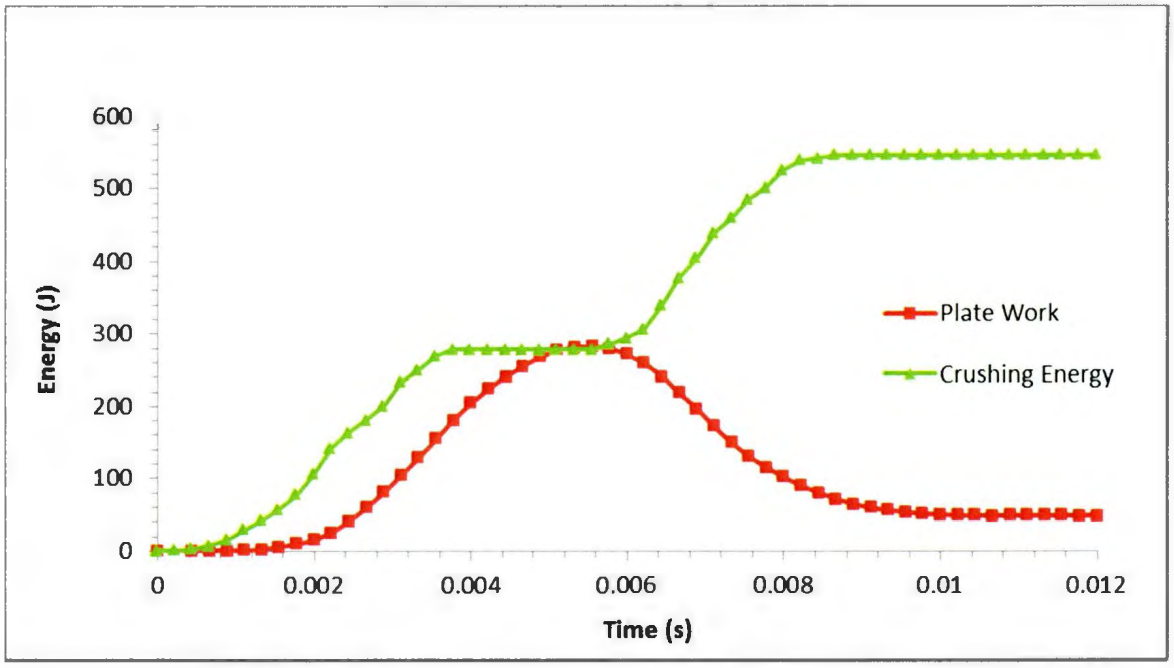


**Run 1: 20 Degree ice specimen impacted with 0.75" plate**

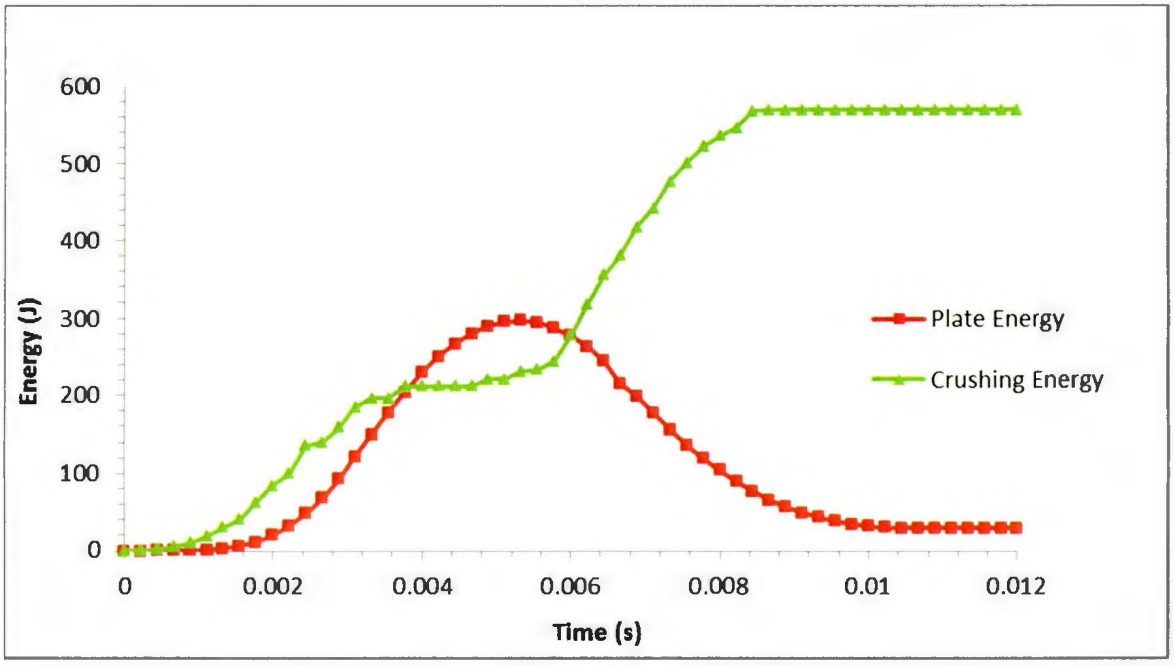


**Run 17: 20 Degree ice specimen impacted with 0.75" plate**

# Appendix D2:

## Energy Plots for 30 Degree Ice Specimens

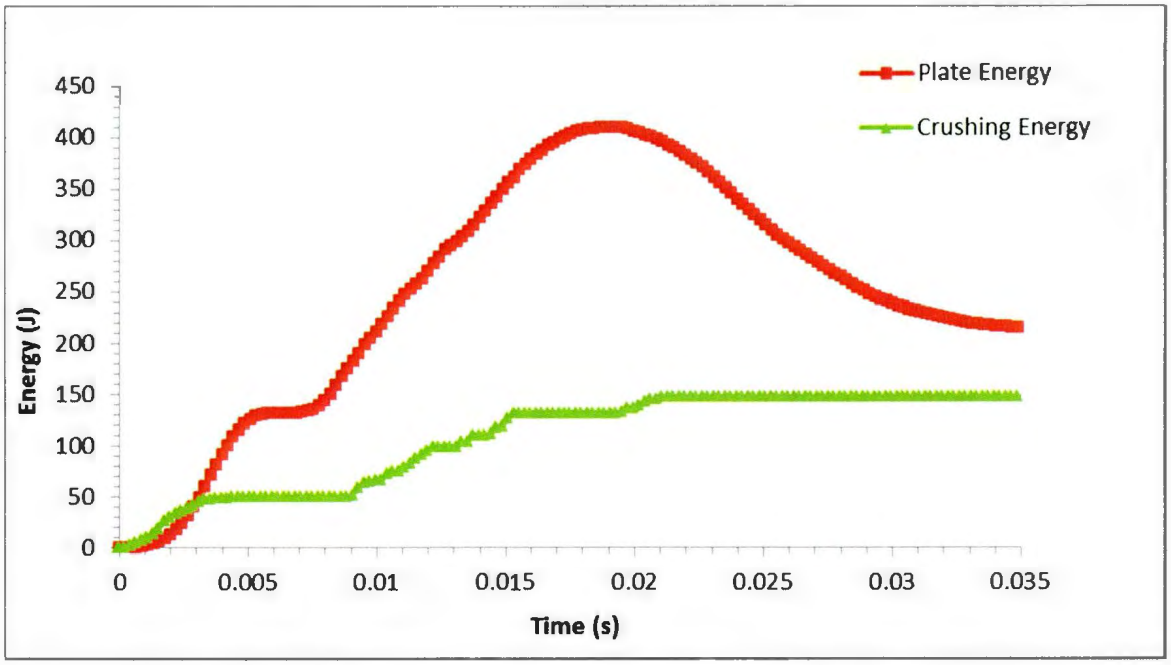


**Run 2: 30 Degree ice specimen impacted with 0.25" plate**

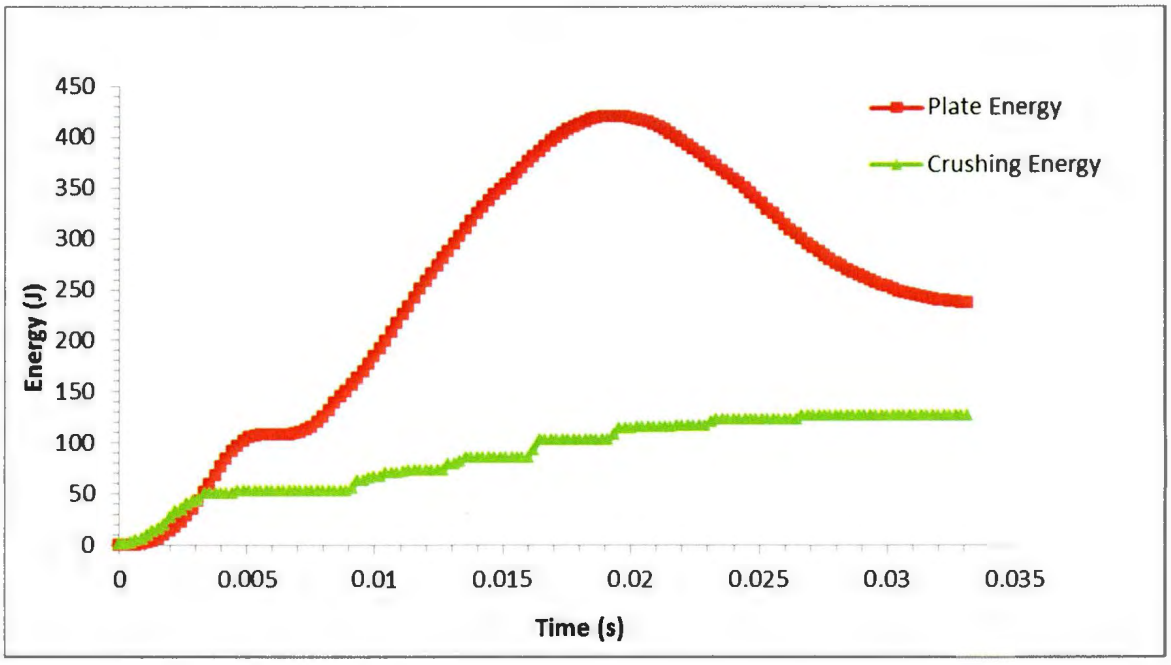


**Run 12: 30 Degree ice specimen impacted with 0.25" plate**

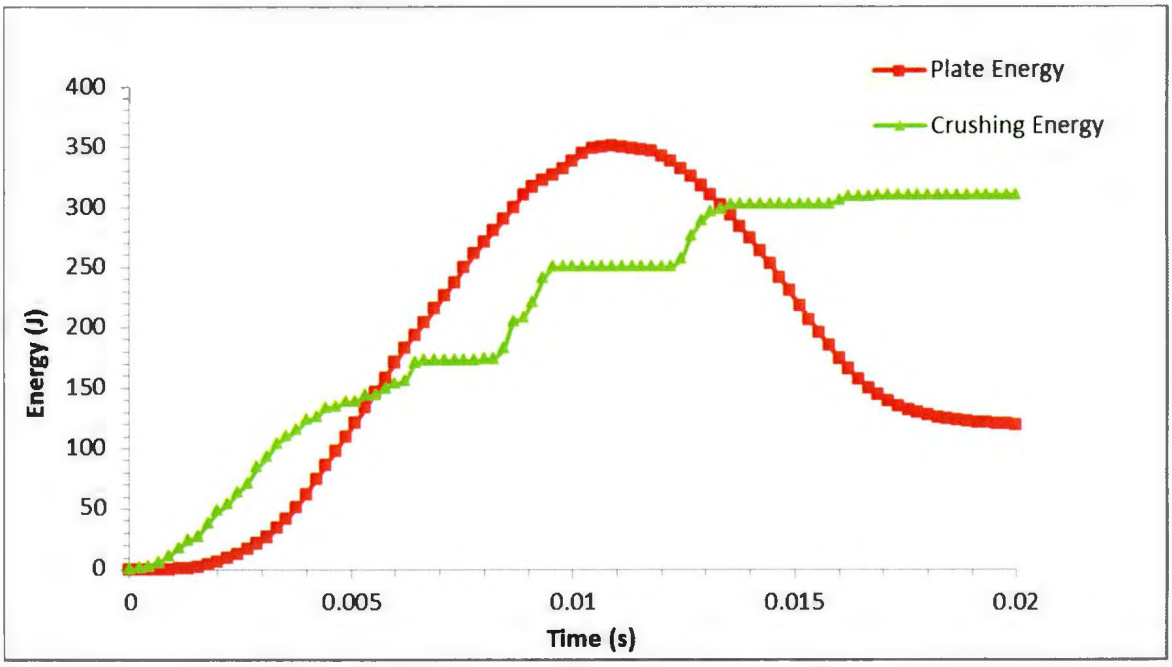


**Run 6: 30 Degree ice specimen impacted with 0.5" plate**

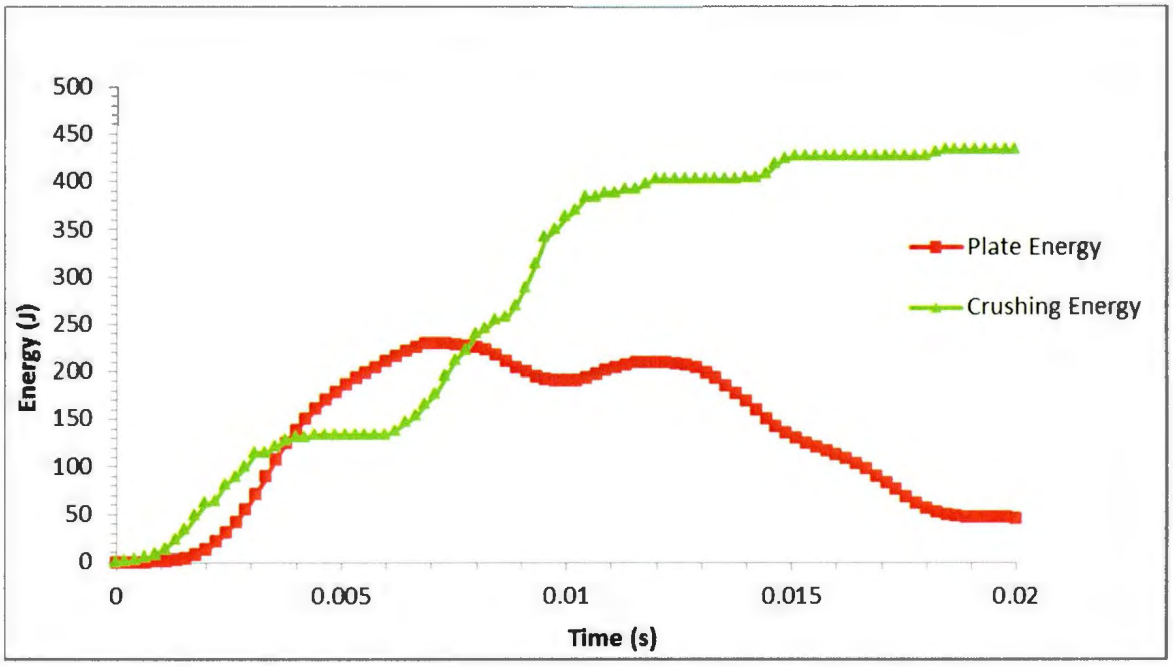


**Run 16: 30 Degree ice specimen impacted with 0.5" plate**

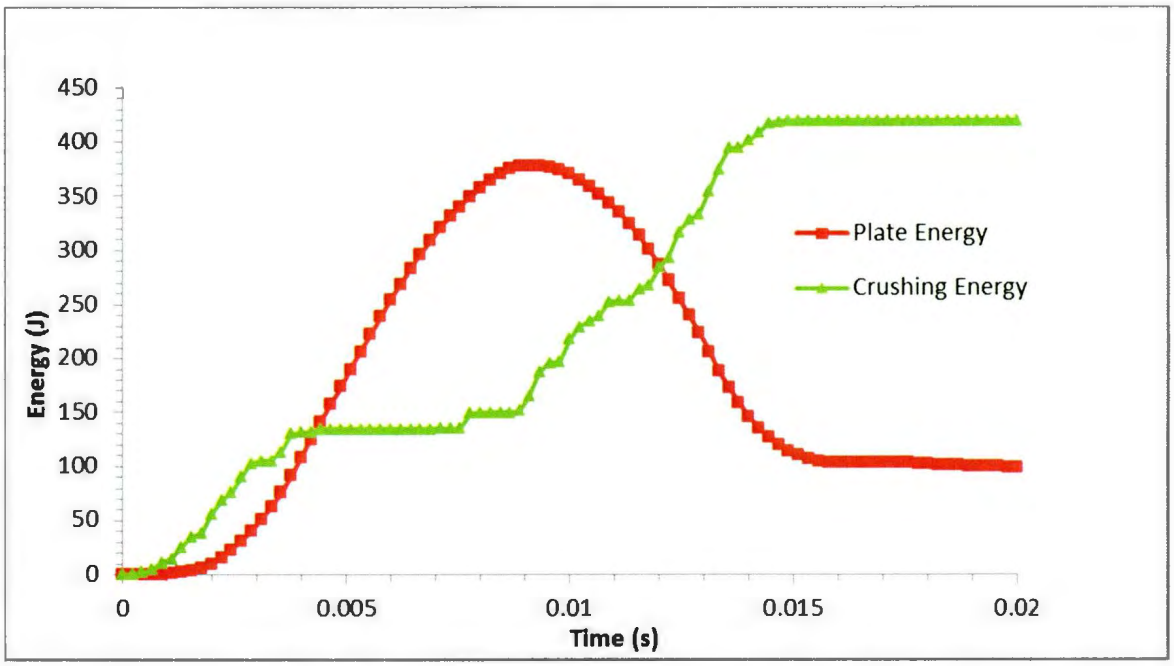


**Run 18: 30 Degree ice specimen impacted with 0.5" plate**

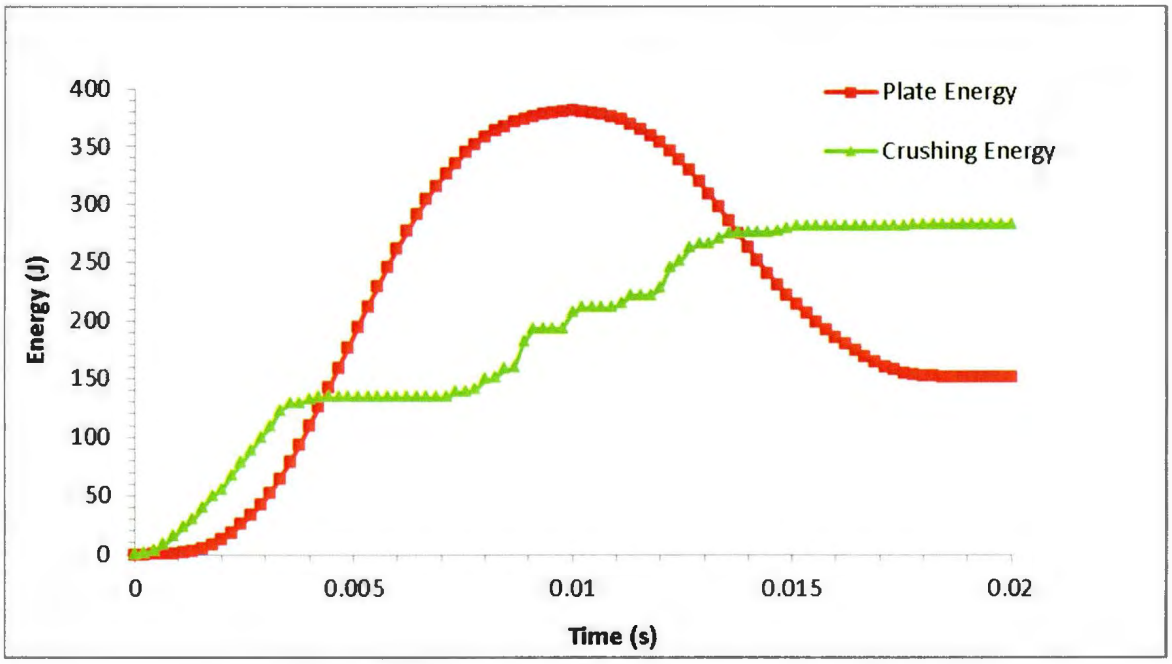


**Run 19: 30 Degree ice specimen impacted with 0.5" plate**

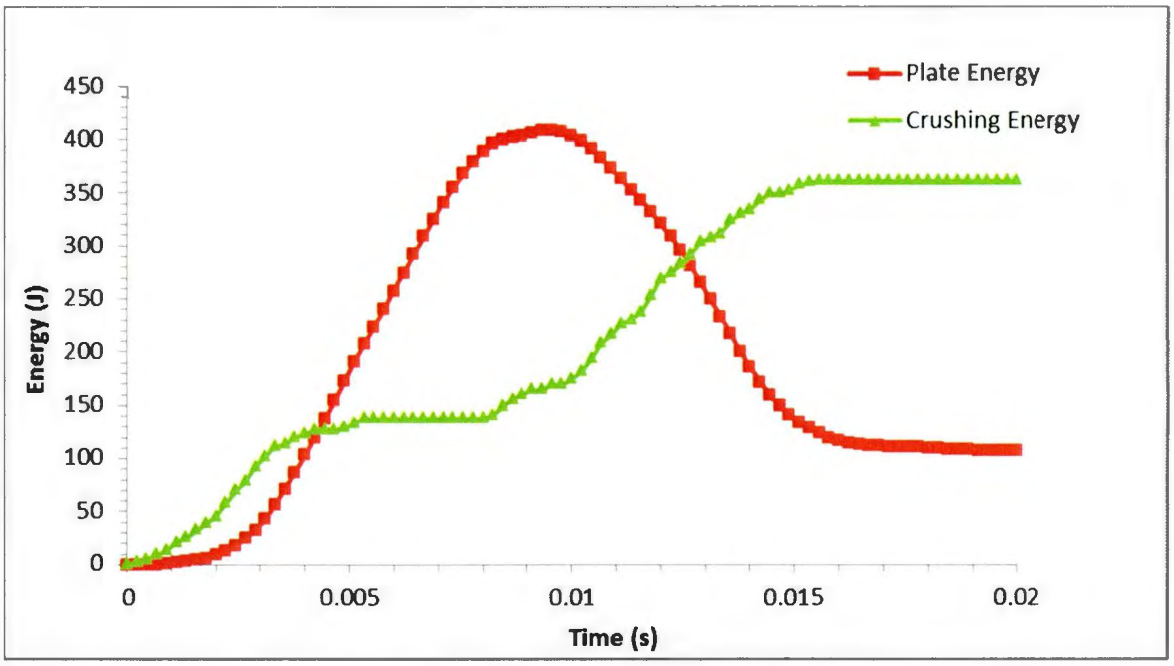


**Run 21: 30 Degree ice specimen impacted with 0.5" plate**

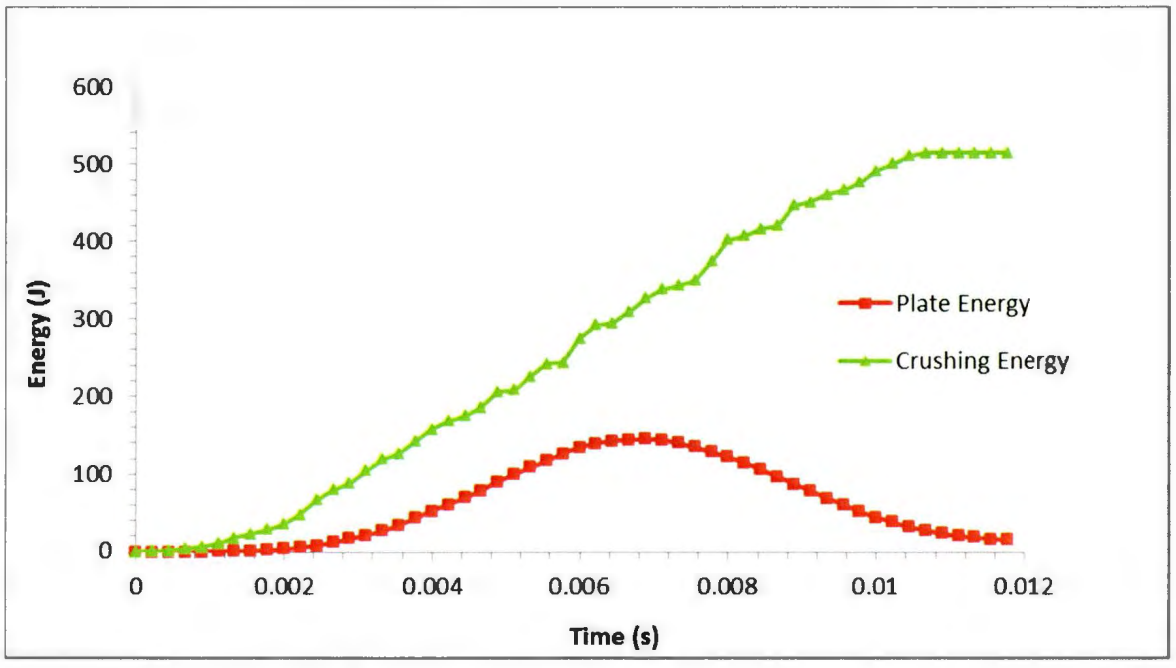


**Run 3: 30 Degree ice specimen impacted with 0.75" plate**

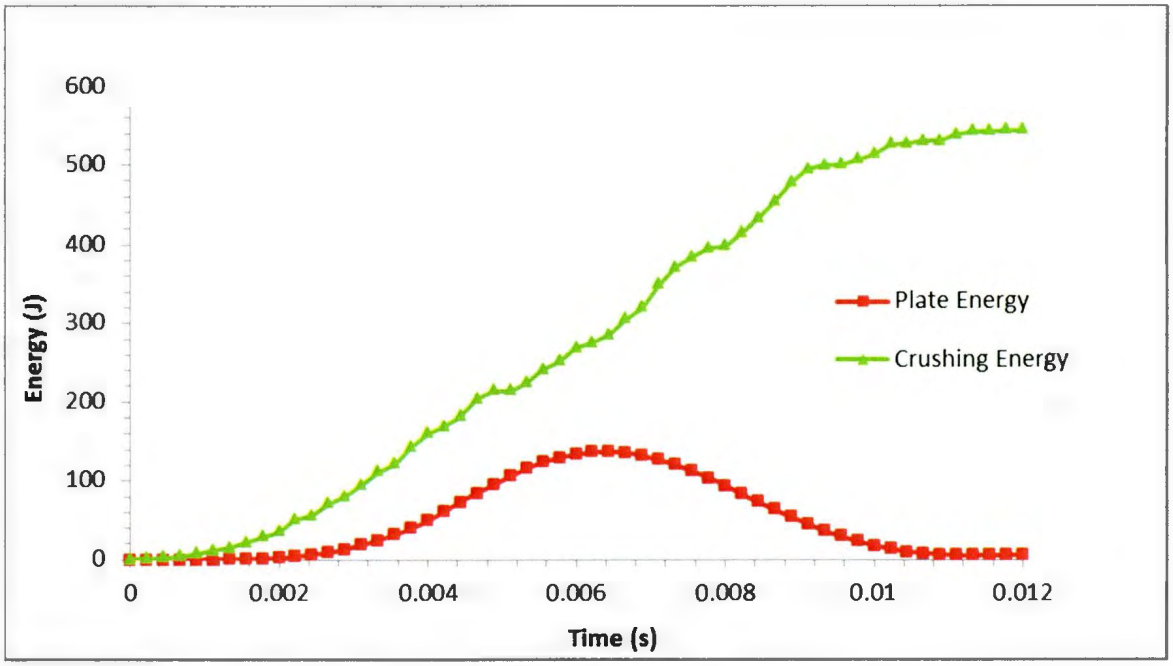


**Run 4: 30 Degree ice specimen impacted with 0.75" plate**

# Appendix D3:

## Energy Plots for 40 Degree Ice Specimens

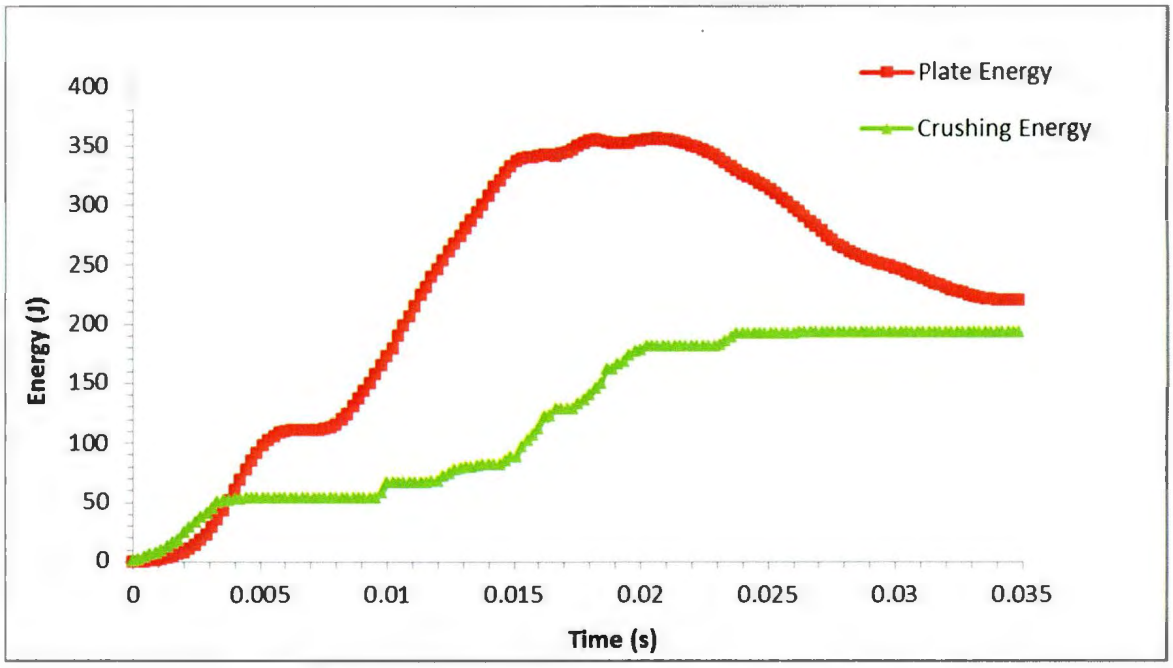


**Run 5: 40 Degree ice specimen impacted with 0.25" plate**

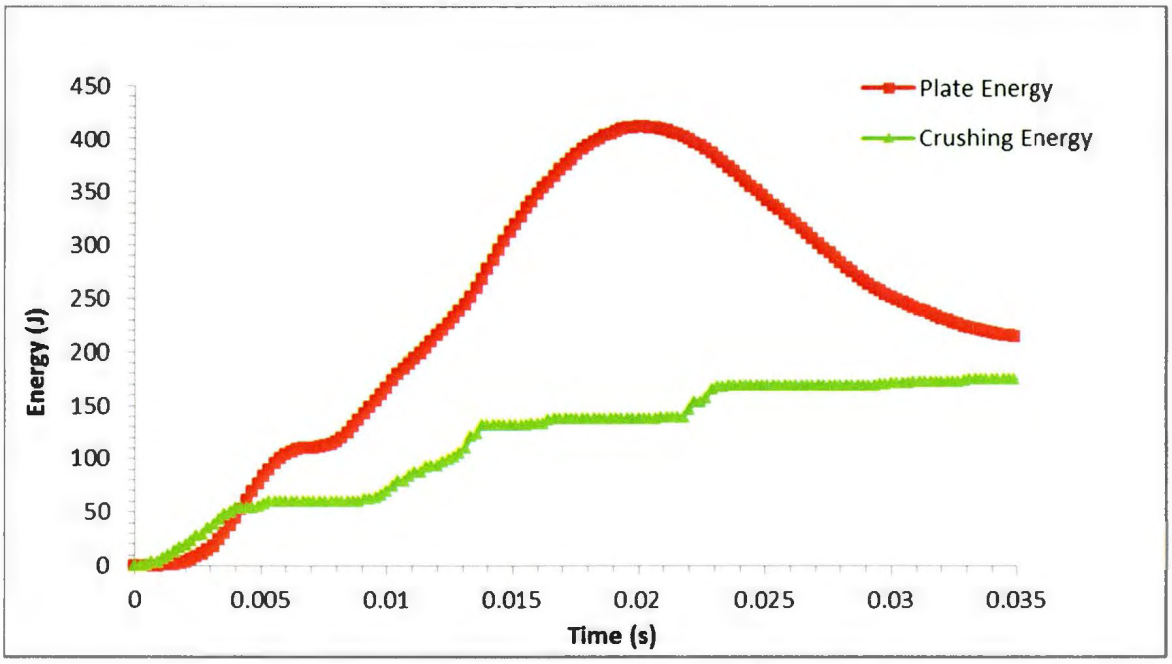


**Run 14: 40 Degree ice specimen impacted with 0.25" plate**

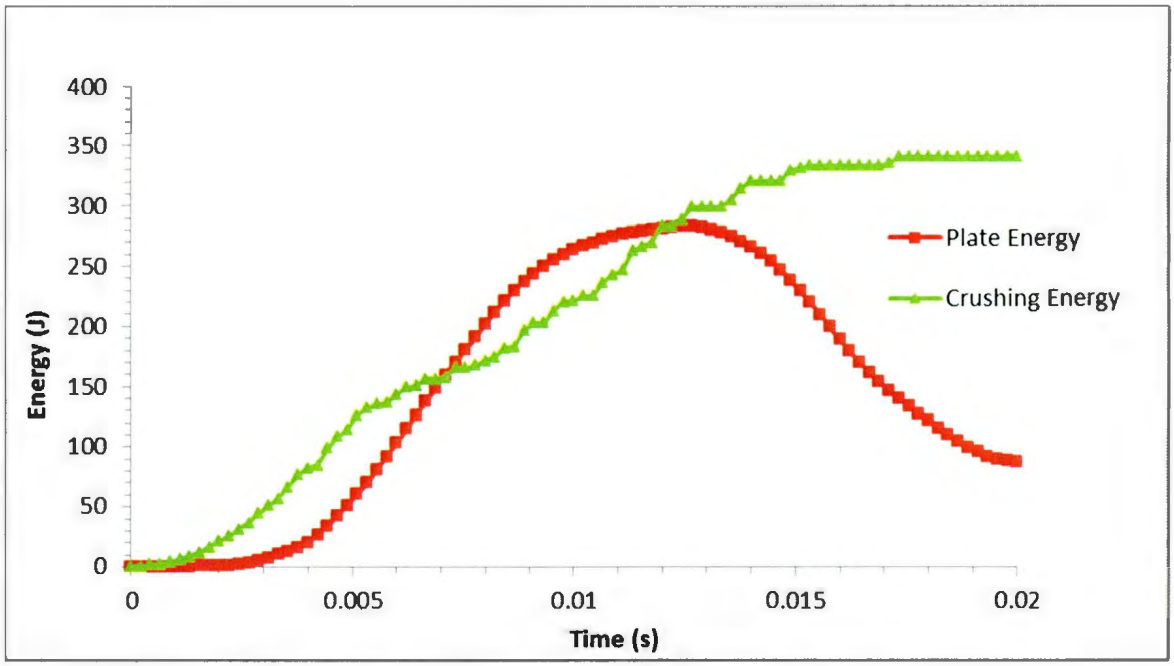


**Run 7: 40 Degree ice specimen impacted with 0.5" plate**

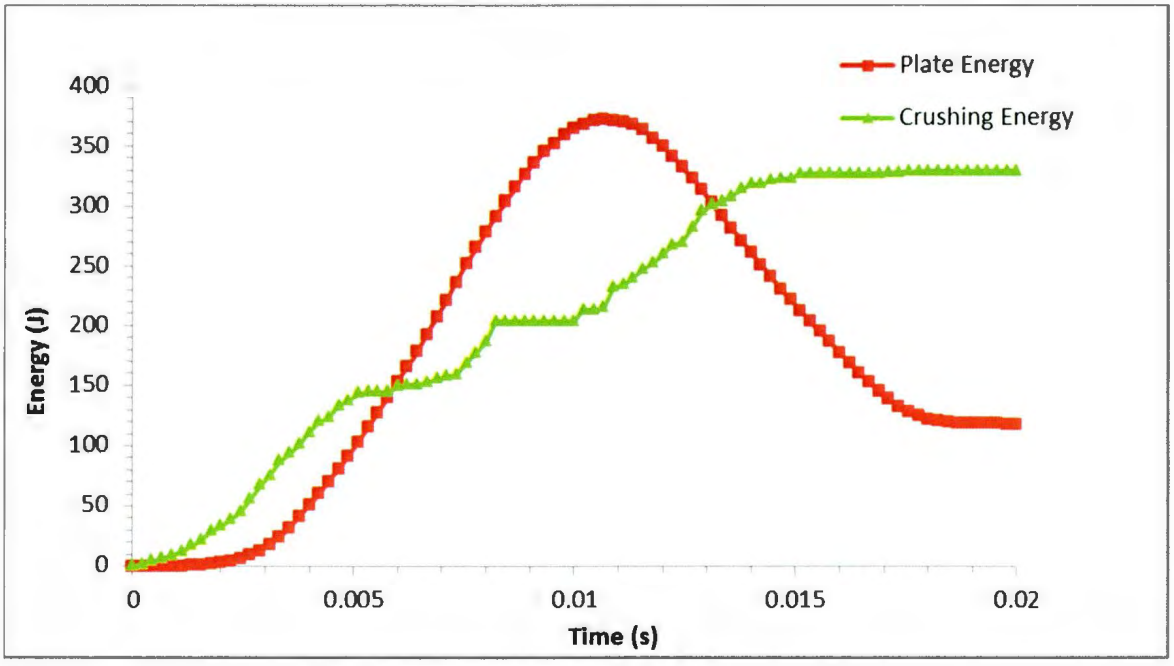


**Run 10: 40 Degree ice specimen impacted with 0.5" plate**

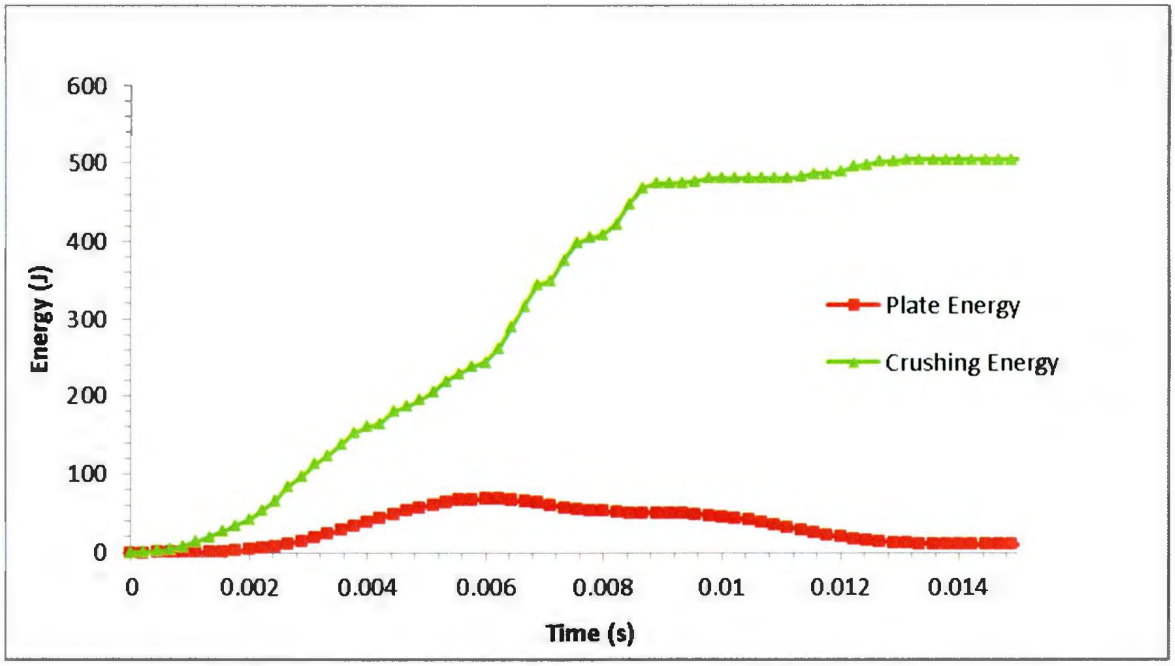


**Run 11: 40 Degree ice specimen impacted with 0.75" plate**

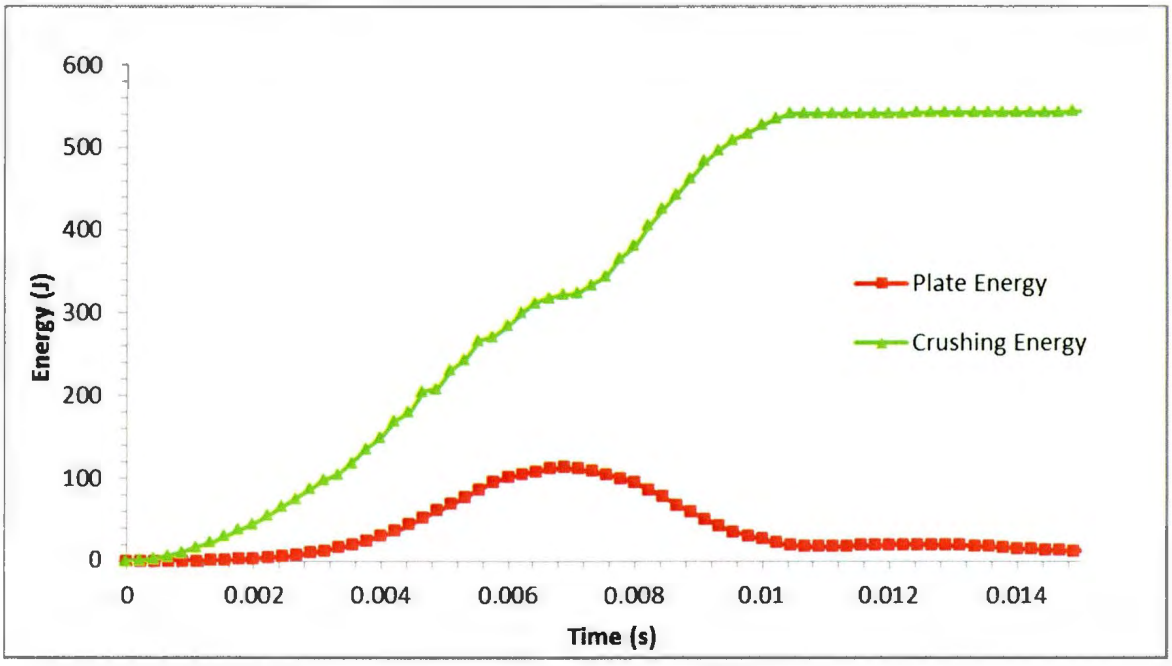


**Run 20: 40 Degree ice specimen impacted with 0.75" plate**